Nanobody constructs, targeting growth factors and their receptors, for PET imaging and cancer therapy

Maria Vosjan

The work described in this thesis was performed at the Section Tumor Biology, Department of Otolaryngology/Head and Neck Surgery, VU University Medical Center, Amsterdam, The Netherlands. The research presented in this thesis was financially supported by the Dutch Technology Foundation (STW, Grant 10074).

Printing of this thesis was financially supported by BV Cyclotron VU.

Cover: The cover was designed by Mike Vos

Printed by GVO drukkers & Vormgevers B.V.

ISBN: 978-90-6464-596-9

VRIJE UNIVERSITEIT

Nanobody constructs, targeting growth factors and their receptors, for PET imaging and cancer therapy

ACADEMISCH PROEFSCHRIFT

ter verkrijging van de graad Doctor aan
de Vrije Universiteit Amsterdam,
op gezag van de rector magnificus
prof.dr. L.M. Bouter,
in het openbaar te verdedigen
ten overstaan van de promotiecommissie
van de Faculteit der Geneeskunde
op donderdag 29 november 2012 om 13.45 uur
in de aula van de universiteit,
De Boelelaan 1105

door

Maria Jenneke Willemina Dorothea Vosjan

geboren te Ommen

promotor:	prof.dr. G.A.M.S. van Dongen
copromotoren:	dr. G.W.M. Visser
	dr. P.M.P. van Bergen en Henegouwen

Contents

1

Chapter 1:

General introduction

Guus AMS van Dongen
Maria JWD Vosjan

Adapted from:
Cancer Biotherapy and Radiopharmeuticals. (2010) 25:375-85

1. Monoclonal antibodies and antibody imaging: Immuno-PET

1.1 Characteristics of monoclonal antibodies

One hundred years ago, Paul Ehrlich, the founder of chemotherapy, received the Nobel Prize for Physiology or Medicine[1,2]. His postulate of creating 'magic bullets' for use in the fight against human diseases inspired generations of scientists to develop powerful molecular cancer therapeutics. Magic bullets being drugs that go straight to their disease-specific targets and not being harmful to healthy tissues. Researchers who followed in his footsteps indeed succeeded to identify specific receptors on the surface of tumor cells. One key achievement in realizing Ehrlich's vision was the development of the hybridoma technology for the production of monoclonal antibodies (mAbs) by Georges Köhler and César Milstein[3]. With this technology an unlimited range of murine mAbs can be obtained against any particular cellular antigen. During their initial use in the 1980s, therapeutic successes with murine mAbs were limited due to their immunogenicity and their restricted ability to induce immune effector mechanisms[4,5]. This prompted the development of chimeric and humanized antibodies that use a plethora of mechanisms to attack cancer cells, such as antibody-dependent cellular toxicity (ADCC), complement-dependent cytotoxicity (CDC), blockade of signal transduction, induction of apoptosis, and immunomodulation. Besides intact mAb molecules (molecular weight ~150 kDa), also mAb fragments and variants were engineered like $F(ab')_2$, F(ab'), Fab, single chain Fv (scFv), and the covalent dimers $scFv_2$, diabodies and minibodies (molecular weights ranging from 25-100 kDa), as well as several types of protein therapeutics based on nontraditional scaffolds such as domain antibodies[6], Affibodies[7], Nanobodies[8], and Anticalins[9].

Presently, 30 mAbs, have been approved by the U.S. Food and Drug Administration (FDA) for therapy, most of them for systemic treatment of cancer[10-13]. The yearly sales of mAbs have been estimated at $20 billion in 2006[14,15]. Moreover, despite the economic downturn the mAb market has grown till $48 billion in 2010[16]. The top 5 mAbs had sales over $5 billion each in 2010. The clinical phase for FDA approved anticancer mAbs took on average 90.8 months[10]. Over 200 new mAb candidates for treatment of cancer and immunological diseases are under clinical development by biotech and pharmaceutical firms worldwide, and also here most of them are full-size humanized and human IgG antibodies rather than antibody fragments or antibody-like scaffolds[17].

Despite these commercial successes, it is fair to state that the efficacy of current mAbs is still quite limited, with benefit for just a portion of patients, while approval of new

mAbs directed against novel targets is stagnating. Moreover, the costs of mAb therapy are excessive, and this issue has become subject of national discussions regarding the rights of cancer care[18,19]. The question is how to improve the efficiency of mAb development and the efficacy of mAb-based therapy and how to identify patients with the highest chance of benefit. In other words: when, how and for whom should antibody-based therapy be reserved? Stakeholders in this arena are physicians (who want to have patients treated in an optimal way), pharmaceutical companies (who want to have rapid and cheap drug development, and application of mAbs in appropriate patient groups), insurance companies and health care authorities (who want to have optimal efficacy of medicines, at minimum price) and first of all patients groups (who want to have highest probability for cure, at minimum morbidity). To answer these questions, better insight in the in vivo behavior of therapeutic mAbs and their interaction with critical disease targets in individual patients should be obtained. For this, Positron Emission Tomography (PET) imaging with radiolabeled mAbs (immuno-PET) is particularly attractive and better qualified than Single Photon Emission Computerized Tomography (SPECT) imaging, because it enables sensitive non-invasive whole body imaging of mAbs at superior spatial and temporal resolution[20].

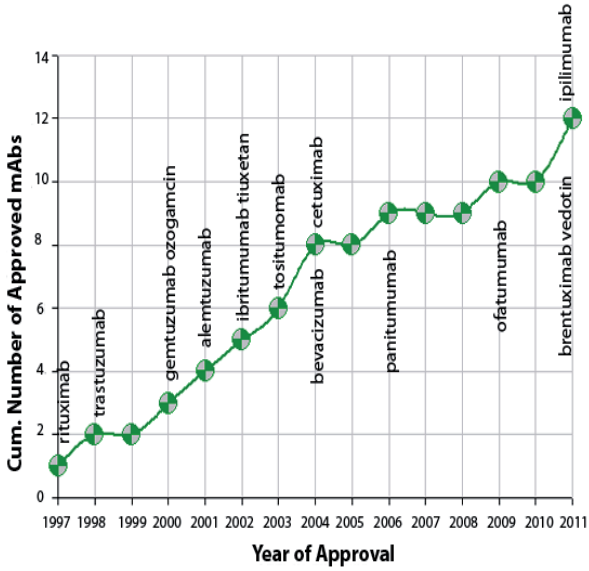

Figure 1. Number of approved mAbs for cancer treatment by the FDA. The first approved mAb was rituximab. Up to now 12 mAbs have been approved for cancer treatment.

1.2 Monoclonal antibodies and their targets

While intact mAbs typically achieve optimal tumor-to-non-tumor ratios 2-4 days after injection, for the smaller fragments this is mostly 1-6 hours after injection. Currently, twelve mAbs have been approved by the US Food and Drug Administration (FDA) for cancer therapy, all being intact mAbs (Table 1 and Figure 1). Seven of the mAbs have been approved for treatment of hematological malignancies: rituximab, gemtuzumab ozogamicin, alemtuzumab, ibritumomab tiuxetan, tositumomab, ofatumumab and brentuximab vedotin. Five mAbs have been approved for therapy of solid tumors: trastuzumab is used for treatment of metastatic breast cancer; cetuximab, bevacizumab and panitumumab have been approved for treatment of metastatic colorectal cancer; while cetuximab and bevacizumab have also been approved for the treatment of head and neck cancer and non-small cell lung cancer, respectively. Finally, ipilimumab was most recently approved for treatment of advanced melanoma. These "solid tumor mAbs" are most effective when combined with chemo- or radiotherapy. They interfere with signal transduction pathways by targeting growth factors or their receptors, the key drivers of

Table 1. Approved mAbs for cancer treatment

FDA Approved	Generic name (trade name)	Target	Type	Indication
1997	Rituximab (Rituxan)	CD20	Chimeric IgG1	Non-Hodgkin's lymphoma
1998	Trastuzumab (Herceptin)	HER2/neu	Humanized IgG1	Breast cancer
2000	Gemtuzumab ozogamicin (Myelotarg) [a]	CD33	Humanized IgG4 conjugated to calicheamicin	Acute myeloid leukemia
2001	Alemtuzumab (Campath-1H)	CD52	Humanized IgG1	Chronic lymphatic leukemia
2002	^{90}Y-Ibritumomab tiuxetan (Zevalin) [a]	CD20	^{90}Y-radiolabeled murine IgG1	Non-Hodgkin's lymphoma
2003	^{131}I-Tositumomab (Bexxar) [a]	CD20	^{131}I-radiolabeled murine IgG2a	Non-Hodgkin's lymphoma
2004 2006	Bevacizumab (Avastin)	VEGF	Humanized IgG1	Colorectal cancer Non-small cell lung cancer
2004 2006	Cetuximab (Erbitux)	EGFR	Chimeric IgG1	Colorectal cancer Head and neck cancer
2006	Panitumomab (Vectibix)	EGFR	Human IgG1	Colorectal cancer
2009	Ofatumumab (Arzerra)	CD20	Human IgG1	Chronic lymphocytic leukemia
2011	Ipilimumab (Yervoy)	CTLA-4	Human IgG1	Melanoma
2011	Brentuximab vedotin (Adcetris)[a]	CD30	Chimeric IgG1, conjugated to MMAE drug	Anaplastic large cell lymphoma, Hodgkin lymphoma

[a]Conjugated antibodies.

Abbreviations: FDA, U.S. Food and Drug Administration; CD, cluster of differentiation; HER2/neu, human epidermal growth factor receptor 2; VEGF, vascular endothelial growth factor, EGFR, epidermal growth factor receptor; CTLA, Cytotoxic T-Lymphocyte Antigen; MMAE, monomethyl auristatin E.

tumor growth and survival. In addition, most of the naked therapeutic mAbs can also act by other effector mechanisms like ADCC, CDC, or induction of apoptosis. To enhance its therapeutic potency, gemtuzumab has been armed with the supertoxic drug ozogamicin, brentuximab with monomethyl auristatin E (MMAE), while ibritumomab tiuxetan (Zevalin™) and tositumomab (Bexxar™) are radiolabeled mAbs containing the β^--emitters yttrium-90 (^{90}Y) and iodine-131 (^{131}I), respectively. Due to a 'cross-fire' effect, radionuclides are especially attractive as warheads to be used in radioimmunotherapy (RIT), since in order to be effective not all tumor cells have to be targeted by radiolabeled mAbs. Next to aforementioned mAbs, one naked mAb (Nimotuzumab) and one radioimmunoconjugate (^{131}I-ch-TNT) have been approved in China[11]. Clinical successes with aforementioned therapeutic mAbs have boosted research and development on new mAbs directed against validated and novel targets enormously[21].

In 2007 Reichert and Valge-Archer[11] reported on 206 unique therapeutic mAbs in clinical trials during the time period 1980 to 2005 by commercial companies worldwide for a variety of cancer indications. The 206 anti-cancer mAbs were specific for 76 targets. Of these 76, 43 were targets for only one mAb. Remarkably, 91 mAbs were specific for only 10 targets, and for most of these targets approved mAbs have become available in the mean time. Targets of highest interest included: epithelial cell adhesion molecule (EpCAM) (17 mAbs), epidermal growth factor receptor (EGFR) (12 mAbs), mucin-1 (MUC1/CanAg) (10 mAbs), cluster of differentiation 20 (CD20) (10 mAbs), carcino-embryonic antigen (CEA) and human epithelial receptor 2 (HER2) (9 mAbs each), and CD22, CD33, Lewis Y and prostate-specific membrane antigen (PSMA) (6 mAbs each). Taking into account the large number of mAbs directed against novel as well as validated targets under development, this raises the question about how to select the best mAbs in an efficient way.

1.3 Antibody imaging in a therapeutic setting

Two different approaches of immuno-PET imaging are followed to guide therapy with mAbs, being mostly slow kinetic intact mAbs designed to give durable blockade of growth factors or their receptors (see section 1.2). In a first approach, fast kinetic antibody-based PET probes are used for same-day imaging at low radiation burden for patients, to confirm target expression, as recently described by Wu et al[22,23]. This approach is potentially helpful for diagnostic purposes and as a scouting procedure for the selection of patients for therapy with intact mAbs. In a second approach, the therapeutic intact mAbs are radiolabeled themselves and imaged in a pretherapy scouting setting or early during the course of therapy to get a better insight in the in vivo behavior and efficacy of the mAbs

in individual patients.

For the first approach mAb fragments or small mAb-like molecules can be used. Since for immuno-PET the physical half-life ($t_{½}$) of the radionuclide should be matched to the biological half-life of the protein to which it is being conjugated, for this application gallium-68 (^{68}Ga, $t_{½}$ = 1.13 h), fluorine-18 (^{18}F, $t_{½}$ = 1.83 h), copper-64 (^{64}Cu, $t_{½}$ = 12.7 h), niobium-90 (^{90}Nb, $t_{½}$ = 14.6 h), yttrium-86 (^{86}Y, $t_{½}$ = 14.7 h) and bromine-76 (^{76}Br, $t_{½}$ = 16.2 h) are the positron emitters of choice. The short-lived positron emitter ^{68}Ga is of particular clinical interest, because it can be obtained from a commercially available long life-span ^{68}Ge/^{68}Ga generator ($t_{½}$ = 271 d), making it continuously available even for centers without a cyclotron, and at reasonable costs. Procedures for coupling these positron emitters to mAbs and preclinical results with short-lived positron emitters coupled to mAb fragments have been extensively examined[20,22-29]. Although excellent imaging results have been obtained with antibody-based PET probes in tumor-bearing mice, caution is needed when aiming the translation of these results to clinical applications. While mAb reactivity with human tumors is considered to be similar for xenografted nude mice and cancer patients, cross-reactivity with normal organs can be totally different. This was demonstrated in PET imaging studies with anti-EGFR mAbs in nude mice bearing EGFR (HER1)-positive human cancer xenografts. Most mAbs, cetuximab and panitumumab included, only bind to human EGFR and not to murine EGFR, and therefore showed predominantly high and selective tumor uptake[30-32]. However, Tolmachev et al[33], evaluated an 8 kDa Affibody recognizing human as well as murine EGFR, and observed a relatively high liver uptake and low tumor uptake. Liver uptake was particularly high at low Affibody dose and could be explained by the abundant EGFR expression in this organ, which is consistent with abundant EGFR expression in human livers. Indeed, initial clinical imaging studies with ^{111}In-labeled anti-EGFR mAb 225 also showed high liver uptake, while for imaging of EGFR expression in tumors relatively high mAb doses were required[34]. Also recent clinical immuno-PET studies with ^{89}Zr-trastuzumab demonstrated that a relatively high mAb dose of at least 50 mg is required to allow reliable HER2 imaging in breast cancer patients. At low mAb dosis rapid hepatic clearance of the probe was observed, most probably due to high levels of shed extracellular domain (ECD) of HER2 in the plasma (Figure 2)[35]. Aforementioned data indicate that tumor imaging with a low dose of fast kinetic mAb fragment or intact mAb will be difficult if not impossible, when there is a high level of target antigen present in well accessible normal organs (mAb sink).

In the second approach, therapeutic intact mAbs are radiolabeled with long-lived positron emitters like zirconium-89 (^{89}Zr, $t_{½}$ = 78.4 h) or iodine-124 (^{124}I, $t_{½}$ = 100.3 h) and

imaged prior or during the course of mAb therapy. For the latter purpose, a small part of the therapeutic dose of intact mAb can be radiolabeled, while cold and radiolabeled mAb can be administered simultaneously or immediately after each other. With this approach, the relation between targeting efficiency and therapeutic response can be studied.

We foresee that quantitative PET imaging of therapeutic intact mAbs can be of value at several stages of mAb development and application. Preclinical immuno-PET studies in xenograft bearing nude mice can learn about the efficiency of tumor targeting with a particular mAb and about regulation of target expression, while immuno-PET studies in non-human primates can be particularly attractive to assess cross-reactivity with normal tissues in relation to toxicity. From first-in-human clinical trials with new mAbs it is important to learn about the ideal mAb dosing for optimal tumor targeting (e.g. saturation of receptors), the uptake in critical normal organs to anticipate toxicity, and the interpatient variations in pharmacokinetics and tumor targeting. mAb imaging might provide this information in an efficient and safe way, with fewer patients treated at suboptimal dose. This approach is especially attractive when a novel type of antibody-like scaffold is evaluated or when the mAb of interest is directed against a novel tumor target that has not been validated in clinical trials before. As will be illustrated in a later section, quantitative mAb imaging might also be of value to guide optimal use of FDA approved mAbs, also when used in combination therapy.

1.4 Quality aspects of clinical immuno-PET

To translate immuno-PET from preclinical investigations to a phase I clinical trial, it is necessary to create a pharmaceutical quality formulation, manufactured under current good manufacturing practice (cGMP). In most cases the radionuclides used for radiolabeling are to be considered as active pharmaceutical ingredients (APIs), especially when the final preparation is released for use without further purification. Also chelates used for binding of radionuclides are to be considered as APIs. Quality aspects that must be documented for radionuclides and radiopharmaceuticals are: identification (e.g., half-life, gamma emission spectrum); (radio)chemical purity; stability data; storage conditions; expiry; batch identification, and impurity profile. During the last years procedures have been developed for the production of large batches of highly pure ^{89}Zr and ^{124}I in a cGMP compliant way, and both positron emitters are nowadays commercially available[36-38].

While ^{89}Zr is coupled via a chelate to the lysine residues of a mAb, ^{124}I can be coupled directly via tyrosine residues. With respect to the latter, procedures have been established for efficient coupling of carrier-added ^{124}I [38], while many preclinical proof

of concept ^{124}I-immuno-PET studies have been performed as described in some recent reviews[20,23]. For stable coupling of ^{89}Zr to mAbs, a multistep procedure has been developed by Verel et al. using a succinylated derivative of desferrioxamine B (N-sucDf) as bifunctional chelate[36]. The choice of desferrioxamine B is attractive because it is used clinically in a safe way for many years. In the mean time, several preclinical immuno-PET studies have been performed with ^{89}Zr-N-sucDf-mAb conjugates as prelude to clinical trials, e.g. with cmAb U36[36], DN30 (anti-c-Met)[39], G250 (anti-carbonic anhydrase IX)[40,41], cetuximab[30,32], ibritumomab tiuxetan[42], rituximab[43], bevacizumab[44], and trastuzumab[45]. A shortcoming of the N-sucDf-based labeling procedure, however, is that it is relatively time consuming and complicated, and therefore challenging with respect to cGMP compliancy.

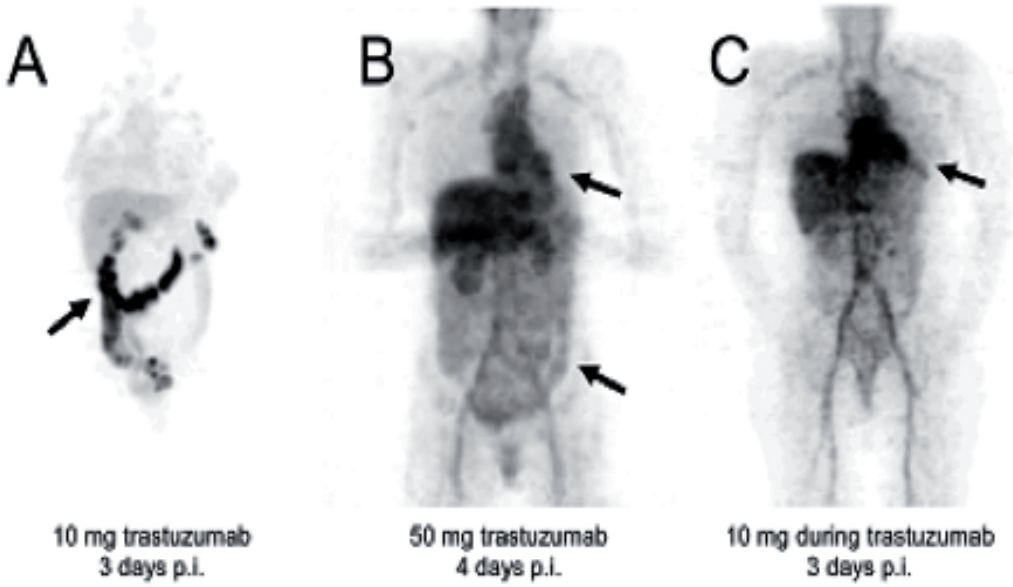

Figure 2. Dose-dependent biodistribution and blood clearance of ^{89}Zr-trastuzumab with 10 mg trastuzumab (A), 50 mg trastuzumab (B), or 10 mg trastuzumab (C) during trastuzumab therapy. Blood pool activity and intestinal excretion are indicated by arrows. (from Dijkers EC, et al,[35]).

Aforementioned achievements indicate that almost all reagents and procedures are in place to allow broad scale clinical application of immuno-PET with ^{89}Zr- and ^{124}I-labeled slow kinetic mAbs. However, improvement might be achieved when a more efficient and rapid method of coupling of ^{89}Zr to proteins would be developed.

While ^{89}Zr is particularly suitable for PET imaging of internalizing mAbs, ^{124}I is the radionuclide of choice in combination with non-internalizing mAbs. In contrast to directly labeled ^{124}I, ^{89}Zr is trapped inside the cell after internalization of the mAb (residualization)

[30,46]. Residualization also occurs to some extent in organs of mAb catabolism like liver, kidney and spleen. For mAb fragments ^{68}Ga can be the radionuclide of choice, since the half-life of the mAb fragments matches with the half life of this positron emitter. ^{68}Ga is also a residualizing PET isotope and might be coupled to a mAb fragment in the same way as ^{89}Zr.

Quality analyses to be performed after radiolabeling include tests to assess the chelate-to-mAb substitution ratio, radiochemical purity, mAb integrity and immunoreactivity, and apyrogenicity. When labeled according to aforementioned procedures, ^{124}I-mAbs can also be used as PET surrogates for scouting the biodistribution of therapeutic ^{131}I-mAb conjugates, while ^{89}Zr-mAbs can be used for scouting therapeutic ^{90}Y- and ^{177}Lu-mAb conjugates[30,38,42,46-48].

1.5 Potential of ^{89}Zr-trastuzumab PET: an example

In current practice, pathological analyses are often performed to confirm target expression and to select patients for mAb therapy. For example, patients with metastatic breast cancer are only eligible for therapy with the anti-HER2 mAb trastuzumab, when protein overexpression and gene amplification has been confirmed on a biopsy of the tumor by immunohistochemistry or fluorescence in situ hybridization (in 20-30% of patients). It is questionable, however, whether a representative overview of *in vivo* HER2 expression status can be obtained by analysis of just one single biopsy. It is possible that HER2 expression in primary tumor and metastatic lesions is heterogeneous, or does not remain stable during the course of the disease for example upon chemo- and/or hormonal therapy[49-52].

Taking multiple or repeated biopsies is not a solution, especially because lesions are often heterogeneous (resulting in non-representative biopsies) and difficult to access. It is of note that HER2 has also a functional role in normal tissues like the heart. This is probably the explanation for the cardiotoxicity induced by trastuzumab, especially when combined with anthracyclines. Interestingly, shortly after completion of anthracycline treatment, myocardial HER2 over-expression has been demonstrated in 50% of the patients[53]. Therefore, it seems worthwhile to evaluate the value of trastuzumab imaging for prediction of cardiotoxicity, especially when next generation anti-HER2 therapeutics like trastuzumab-DM1 (trastuzumab coupled to the supertoxic drug mertansine) are considered for therapy[53-55]. Cross-reactivity of such supertoxic conjugates with normal tissues might result in unacceptable toxicity, as was recently demonstrated for the anti-CD44v6 conjugate bivatuzumab-DM1[56].

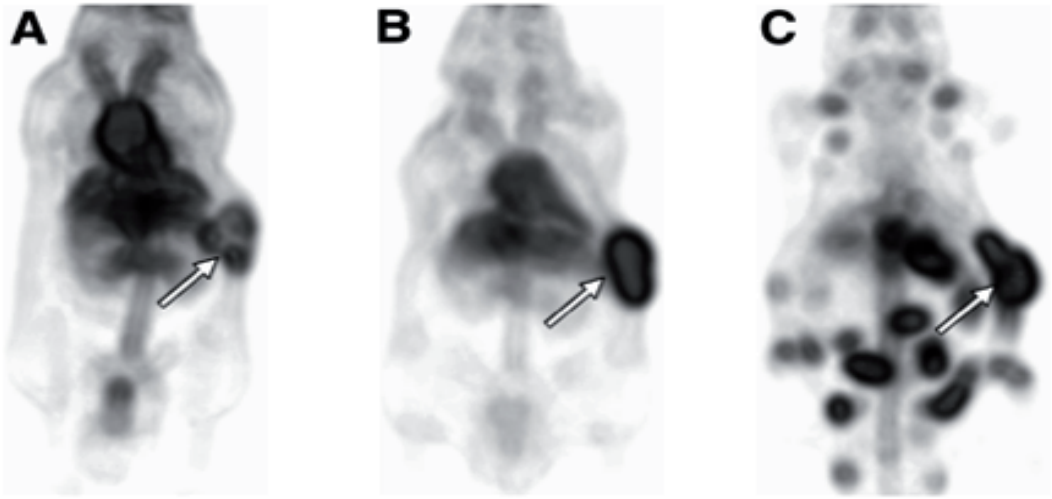

Figure 3. Examples of noninvasive small-animal PET images (dorsal presentation). ^{89}Zr-trastuzumab uptake in human SKOV-3 xenografts in 3 mice at 6 h (A), day 1 (B), and day 6 (C, metastasized tumor) after injection is shown. Primary tumors are indicated by arrows (from Dijkers EC, et al[45]).

Antibody imaging might have added value for patient selection, because it can be used to assess target expression and mAb accumulation in all tumor lesions and normal tissues, non-invasively, quantitatively, and even over time (4D). This information might be particularly relevant when mAb therapy is combined with other treatment modalities like chemo- and radiotherapy, to find routes to maximum synergism. Ideally, topographic information on tumor extension is obtained to enable assessment of homogeneity of mAb tumor accumulation.

Preclinical proof of concept studies have been performed using ^{89}Zr-trastuzumab as the PET imaging probe. ^{89}Zr-trastuzumab immuno-PET appeared capable of visualization of HER2-positive xenografts, primary tumors as well as small metastatic lesions, while HER2-negative lesions present in the same animals were not detected (Figure 3)[45]. Using the same ^{89}Zr-trastuzumab probe, downregulation of HER2 expression was visualized and quantified upon treatment of tumors with HSP90 inhibitors[57,58]. Since also EGFR and VEGF expression are downregulated by these HSP90 inhibitors, similar results can be obtained by imaging with radiolabeled cetuximab or bevacizumab[59,60]. These studies showed that immuno-PET probes like ^{89}Zr-trastuzumab have the potential to be used to measure the efficacy of treatment with HSP90 inhibitors, and that due to the longer half life of ^{89}Zr this probe is better qualified for HER2 expression imaging than previously described ^{68}Ga- and ^{64}Cu-trastuzumab probes[57,61-63].

1.6 Experience with clinical immuno-PET

^{124}I-labeled mAbs already have been used for clinical immuno-PET years ago, but the number of patients included in these studies was small[64,65]. Diagnostic results were far from optimal, among others because of the poor quality of the murine mAbs used, which were lacking the specificity of nowadays mAbs[66]. Currently, interest in ^{124}I-labeled mAbs has been renewed, partly due to the improved methods for production of ^{124}I and its coupling to mAbs. Two clinical applications attracted attention. Jayson et al.[67] used various doses of ^{124}I-HuMV833, a mAb binding to $VEGF_{121}$ and $VEGF_{165}$, to perform PET-imaging studies in 12 patients with various progressive solid tumors. Antibody distribution and clearance were markedly heterogeneous between and within patients and between and within individual

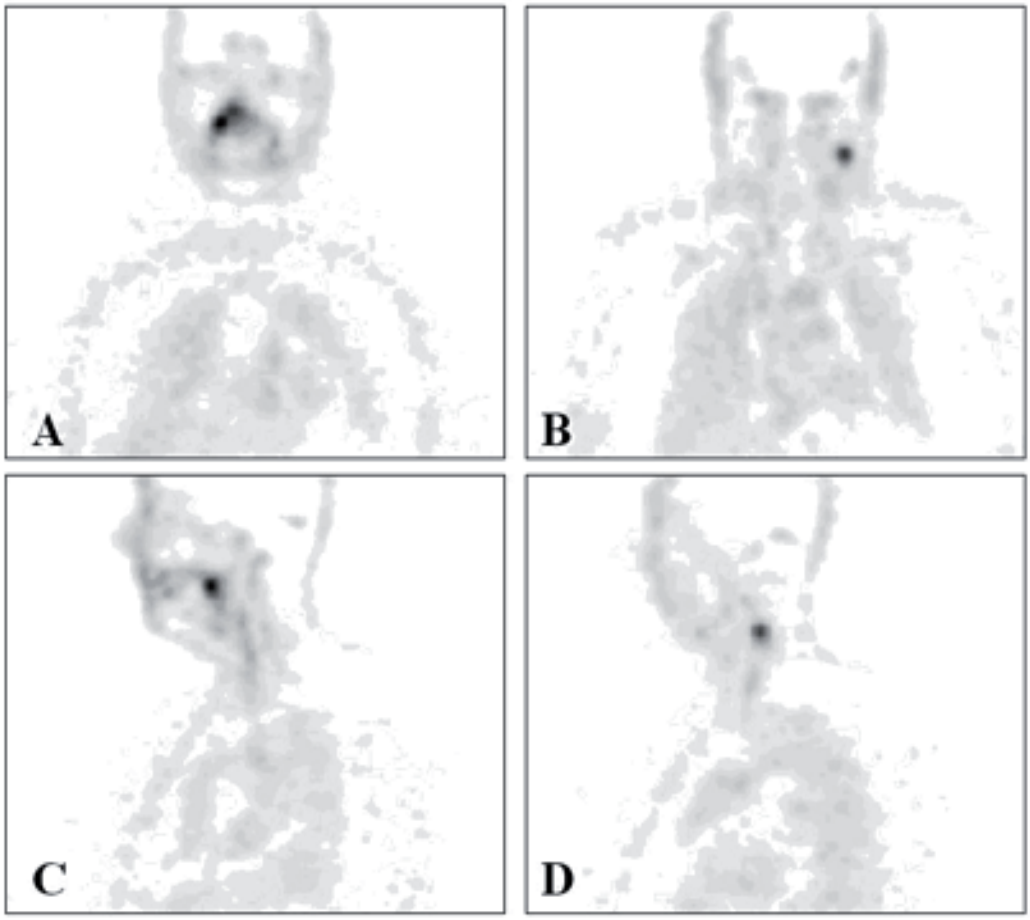

Figure 4. Immuno-PET images with ^{89}Zr-cmAb U36 of head and neck cancer patient with a tumor on the right side of the soft palate and a lymph node metastasis at the left side of the neck (level III). Images were obtained 72 hours post injection. A, coronal image of primary tumor; B, coronal image of lymph node metastasis in the neck; C, sagittal image of primary tumor; D, sagittal image of lymph node metastasis in the neck (from Börjesson PKE, et al.[70]).

tumors. These differences may represent the variation in available targets for the mAb, which could have implications for anti-VEGF therapy. In the mean time similar studies have been started using ^{89}Zr-bevacizumab as the imaging probe[44,60].

In the other clinical application ^{124}I-immuno-PET was used for *in vivo* profiling of renal cancer. Divgi et al.[68] used ^{124}I-cmAb G250 to predict the presence of clear cell renal carcinomas in 25 patients scheduled for surgical tumor resection. G250 is directed against carbonic anhydrase-IX, which is over-expressed in clear-cell renal carcinoma. It might be informative to know whom of the renal cancer patients have this aggressive tumor type because of treatment decisions, although opinions on this point deviate[69]. 15 of 16 clear-cell carcinomas were identified accurately by immuno-PET, and all nine non-clear-cell renal masses were negative for the tracer. This study illustrates how molecular imaging with specific probes can contribute to personalized medicine. Also here, ^{89}Zr-G250 conjugates are under development as alternative immuno-PET probes[40,41].

Since the introduction of ^{89}Zr-immuno-PET technology, several clinical trials have been started, for example using ^{89}Zr-labeled trastuzumab, bevacizumab, cetuximab, rituximab or ibritumumab tiuxetan as the PET probe, and a few have been reported in literature. A first-in-human ^{89}Zr-immuno-PET trial has been conducted with ^{89}Zr-cmAb U36, to see whether this imaging probe is safe and capable for imaging of CD44v6-positive tumors[70,71]. The aim was to determine the diagnostic value of immuno-PET with ^{89}Zr-cmAb U36 in patients with head and neck squamous cell carcinoma (HNSCC), who were at high risk of having neck lymph node metastases. Twenty HNSCC patients, scheduled to undergo resection of the primary tumor and uni- or bilateral neck dissection, underwent CT and/or MRI and ^{89}Zr-cmAb U36 immuno-PET prior to surgery. Immuno-PET detected all primary tumors (n = 17) as well as lymph node metastases in 18 of 25 positive neck levels. Missed lymph nodes were relatively small and contained just a small proportion of tumor tissue. Representative images are shown by Figure 4. It was concluded that immuno-PET with ^{89}Zr-cmAb U36 performs at least as good for detection of HNSCC lymph node metastases (and probably distant metastases) as CT/MRI, and that use of PET-CT might further support image interpretation.

In these studies also radiation dose estimates were made, while the potential for ^{89}Zr-cmAb U36 quantification was assessed[72]. PET quantification of blood-activity in the left ventricle of the heart showed good agreement with sampled blood activity (difference equals 0.2% ± 16.9%), except for heavy weight patients (> 100 kg). A good agreement was also found for assessment of mAb uptake in primary tumors (mean deviation: -8.4% ± 34.5%), indicating the potential of ^{89}Zr-immuno-PET for accurate non-invasive

quantification of mAb biodistribution. The mean radiation doses for patients receiving 74 MBq ^{89}Zr in this study was about 40 mSv, which is high and will limit repeated application of ^{89}Zr-immuno-PET. However, the introduction of the new-generation PET/CT scanners will allow better-quality immuno-PET images to be obtained with a lower ^{89}Zr activity dose. Indeed, recent PET/CT studies in which 37 MBq of ^{89}Zr-trastuzumab were used, showed excellent quality images at an effective dose of about 20 mSv[35].

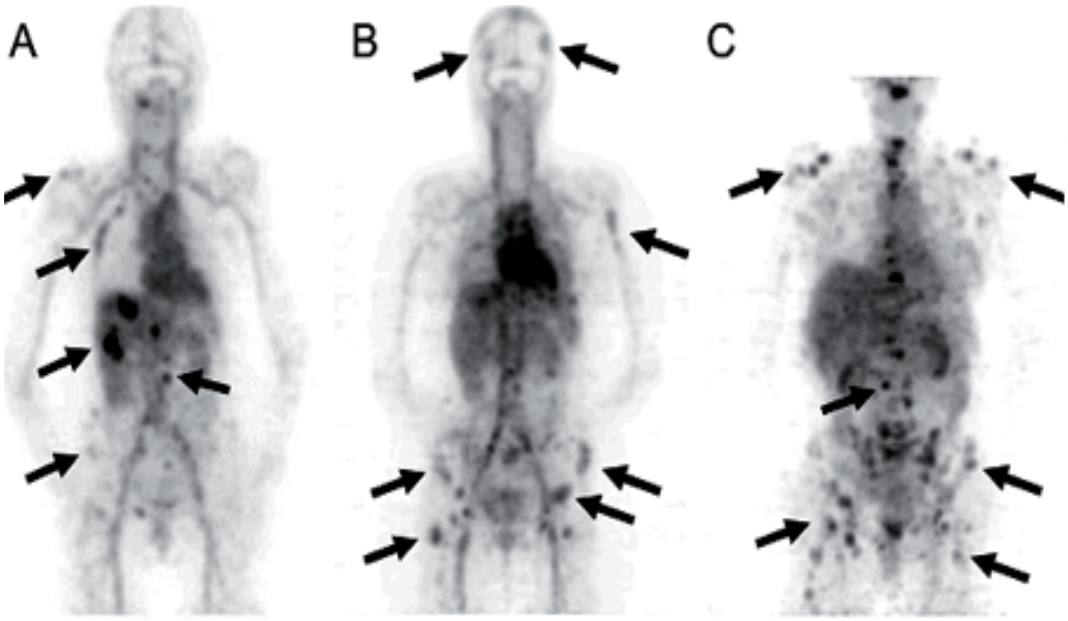

Figure 5. Examples of ^{89}Zr-trastuzumab uptake 5 days p.i. in a patient with liver and bone metastases (A) and two patients with multiple bone metastases (B+C). A number of lesions have been specifically indicated by the arrows (from Dijkers EC, et al.[35]).

The Groningen group determined the best conditions for PET imaging of HER2 expression with ^{89}Zr-trastuzumab[35]. For this purpose HER2-positive metastatic breast cancer patients received 37 MBq ^{89}Zr-trastuzumab at three trastuzumab protein doses, 10 or 50 mg or 100 mg while patients were on trastuzumab treatment. Fourteen patients were included. Several conclusions were drawn from these studies: at least 50 mg trastuzumab is needed to allow reliable visualization of mAb uptake in HER2-positive lesions; the best moment to assess ^{89}Zr-trastuzumab tumor uptake is 4-5 days post-injection; PET images showed a high spatial resolution, and a good signal-to-noise ratio, which resulted in an image quality unapproachable by previous ^{111}In-trastuzumab SPECT scans[73]. Excellent tumor uptake and visualization of metastatic liver, lung, bone and even brain HER2-positive lesions were obtained (Figure 5). ^{89}Zr-trastuzumab PET allowed quantification of conjugate uptake in HER2 positive lesions, and it became clear that for some patients

with extensive tumor load no HER2 saturation occurred during trastuzumab therapy[74]. This latter observation indicates that some breast cancer patients might be underdosed with current trastuzumab therapy regimens, and it therefore could be considered to use HER2-PET for applying a more patient tailored trastuzumab dosing schedule.

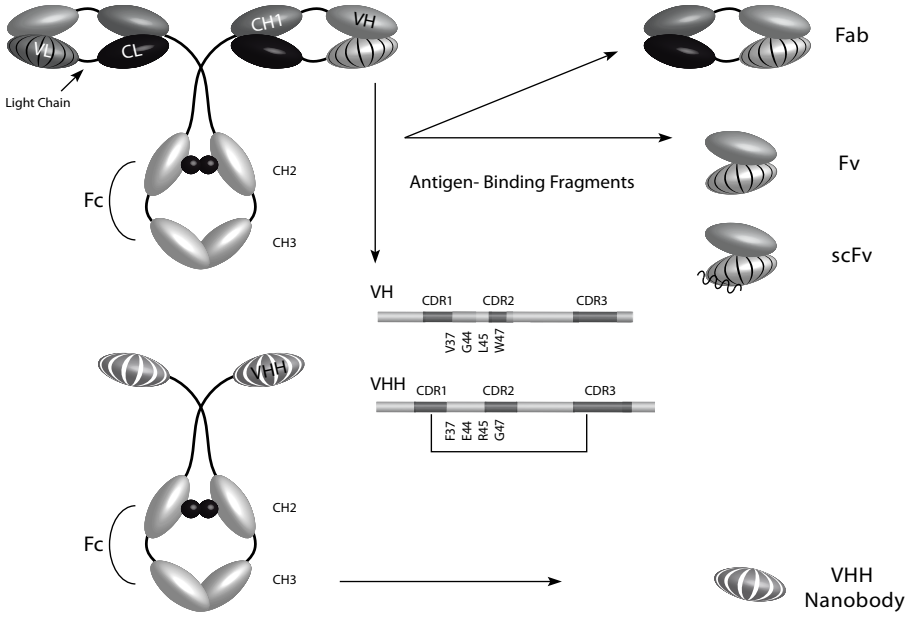

Figure 6. Schemetic representation of conventional antibodies and heavy-chain only antibodies present in camelid serum.

2 Nanobody, next generation antibody technology

2.1 Improvement of antibody therapy: multi-specificity

All approved antibodies for cancer treatment are intact mAbs, and most of them are directed against a growth factor or growth factor receptor. As mentioned in section 1.1, notwithstanding several clinical successes the efficacy of current mAbs is quite limited. This conclusion comes with very recent insights that selective targeting of just one single tumor target might be insufficient for optimal efficacy. Cancer cells have the inherent ability to use several growth factor (receptor) systems for growth advantage and survival, which means that other receptor systems can take over the signaling and therefore tumors are still able to survive after blockade of just one growth factor (receptor) system. The potential of dual-specificity antibody therapy has already been demonstrated in several studies in which mAbs or tyrosine kinase inhibitors affecting different anti-cancer targets,

e.g., EGFR, HER2, IGF-IR or VEGF-R2 were combined [75-82]. For example, Barnes et al.[83] demonstrated in a preclinical study that simultaneous administration of the human anti-IGF-IR antibody IMC-A12 and cetuximab (anti-EGFR) showed significant growth inhibition in head and neck cancer xenografts, while single agent therapies only showed minimal reduction. Moreover, in 2009 Tonra et al.[84] showed that targeting VEGF-R2 and EGFR was prioritized over other treatment strategies utilizing EGFR, IGF-1R and VEGF-R2 antibodies in nude mice bearing different xenografts. Several clinical trials have been started aiming at the simultaneous inhibition of EGFR and VEGF-2R, using tyrosine kinase inhibitors or mAbs [85].

A disadvantage of using combinations of traditional intact mAbs for cancer therapy, however, is the high costs. Moreover, due to their large size (~150 kDa) tumor penetration of intact mAbs is not optimal and therefore it is challenging to reach all tumor cells for effective growth inhibition. Besides mixtures of mAbs, also single molecule mAb-fragments that affect more than one target have been evaluated. Such mAb-formats would lead most easily to drug registration once anti-tumor activity has been proved. Lu et al.[86] developed an IgG-like bispecific antibody (bi-diabody) directed against the EGFR as well as IGF-1R and demonstrated that inhibition of both receptors, either by a mixture of monospecific antibodies or by the bispecific bi-diabody, resulted in broader and enhanced anti-tumor activity in tumor bearing mice. Although these results were fascinating, the question remained if bispecific versions of conventional mAbs are the most favorable format for dual-specificity targeting. In the studies of Lu et al.[86], in vivo instability was observed; while the production of the bi-diabody was rather complicated. In 2011, Dong and coworkers[87] described another IgG-like bispecific antibody that targets EGFR as well as IGF-1R. Improvement was made in the stability, whereas PEGylation was used to enhance the solubility and serum half-life. *In vitro* assays showed that this bispecific antibody improved inhibition of cell growth compared to the monospecific combination of mAbs. In animal studies in mice bearing different tumor xenografts, best tumor growth delays were seen in the group that received the bispecific mAb.

In an analysis in Nature Reviews Drug Discovery in 2011, Holmes[88] discussed the potency of bispecific antibodies based on immunoglobulin G (IgG) and it was stated that the development of bispecific antibodies is 'hot' at this moment. The clinical knowledge of monospecific mAbs has matured, and many pharmaceutical companies are keen on developing bispecific antibodies that have the potential to simultaneously affect two targets. Some bispecific antibodies are in phase II clinical trials like; MM-111, targeting HER2 and HER3; FBTA05, which targets CD20 and CD3; and blinatumomab which is used

for acute lymphoblastic leukemia. It uses a retargeting mode of action to bring $CD3^+$ T cells into close contact with B cells that express CD19.

2.2 Novel antibody formats

Nanobody technology might be better suited for blockade of growth factor (receptor) systems. Nanobodies are smaller than intact traditional IgG mAbs and can therefore better penetrate into a tumor. Besides this, Nanobody technology enables easy construction of so called “dual specific” or “multiple specific” Nanobodies (targeting more than one tumor target) in search for more effective cancer treatment. For preclinical and clinical evaluation of the targeting potential of such new antibody fragments immuno-PET can be of great help.

2.2.1 Nanobodies

Nanobodies are a novel class of antibody-based fragments which were initially discovered in 1993 in members of the Camelidae family (e.g., llama, camel and dromedary)[89]. Since these naturally occurring antibodies are devoid of light chains, the antigen-binding region is composed of only a single immuno globulin (Ig) fold, the VH, termed ‘VHH‘ (variable part of the heavy chain or heavy–chain antibodies). These Ig’s consists of two disulfide-linked heavy chains, each composed of one variable domain (VHH or Nanobody) linked to two constant domains (CH2 and CH3) via a hinge region (Figure 6). Similar types of heavy chain only antibodies have also been found in nurse sharks and spotted ratfish[90].

The small molecular size of Nanobodies offers several advantages and some potential disadvantages in comparison to the larger conventional antibodies. Major advantages are high solubility, intrinsic stability, easy cloning, modular nature, binding to cavities and difficult-to-access antigens, and easy production in bacteria or yeast. A drawback can be the small size of a Nanobody (~15 kDa) which is below the renal threshold, causing rapid excretion via the kidneys. To elongate the half-life of a Nanobody an albumin-specific Nanobody unit can be fused to the existing Nanobody[91,92]. The elongated life time Nanobodies have a life time comparable to conventional IgGs and can be used as therapeutics.

Nanobodies can easily be formatted into multiple-targeting molecules by fusing different Nanobody units within one molecule directed against different epitopes on the same growth factor or the same receptor (called; bi-paratopic Nanobodies) as such increasing the potency and enhancing therapeutic efficacy. Alternatively, Nanobody units can be combined within one molecule targeting different receptors or ligands (called; bi-

specific Nanobodies). These latter Nanobodies are able to block more than one receptor pathway, and therefore potentially improve therapeutic effectiveness.

2.3 Receptor tyrosine kinases

Cell membrane receptors can be classified into distinct families based on the ligands they recognize, the biological responses they induce and, more recently, according to their primary structure[93]. One large family of cell surface receptors provides intrinsic protein tyrosine kinase activity. These receptor tyrosine kinases (RTKs) play an important role in the control of most fundamental cellular processes like the cell cycle, cell migration, cell metabolism and survival, as well as cell proliferation and differentiation. In the following paragraphs the commonly upregulated, overexpressed and/or activated RTKs will be discussed in more detail. Moreover, their suitability for drug targeting in cancer therapy will be discussed.

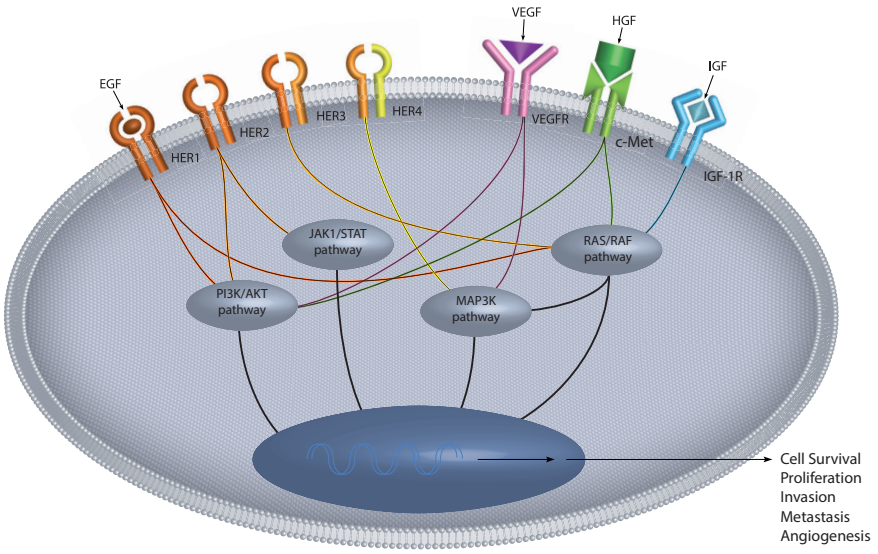

Figure 7. The MAPK and PI3K/AKT pathways are activated by various receptor kinases (EGFR, VEGF, c-Met, IGFR and others) by their cognate ligands (e.g., EGF, VEGF, HGF, and IGF) leading to proliferation of tumor cells.

2.3.1 Epidermal Growth Factor Receptor

The epidermal growth factor receptor (EGFR, also known as HER-1 or ErbB1) consists of four family members of related receptor tyrosine kinases (ErbB1-4; HER1-4)[94]. EGFR and its family members are implicated in the development and progression of different human cancers like head and neck, breast, lung, prostate, and colorectal cancer. When EGFR is overexpressed this frequently results in poor prognosis for patients.

Members of this receptor class have a common structural architecture (see Figure 7): an ecto-domain were different ligands can bind, a transmembrane region, and an intracellular domain containing the RTK, and the different tyrosine residues that are phosphorylated upon receptor activation[95]. The HER receptors can be stimulated by more than 20 different natural ligands. EGF or TGFα bind to EGFR and induces receptor dimerization. This can either be homodimerization (two of the same receptors) or heterodimerization (two different receptors), which leads to kinase activation and downstream signaling, with ultimately cell proliferation. No ligand is known for HER2, whereas HER3 contains an inactive tyrosine kinase. So, for the functioning of these two receptors heterodimerization is essential. Finally, Heregulin, Neuregulin and Betacellulin are known ligands for HER4.

Upon tyrosine kinase activation, 1-10 different tyrosine residues in the cytoplasmatic intracellular domain become phosphorylated. These phosphorylated tyrosine residues form binding sites for different signaling molecules. The ligand identity, as well as the dimer partner determines which tyrosines are phosphorylated, and hence which proteins are recruited and which (tumor-promoting) processes are initiated (e.g. proliferation, migration, metastasis, angiogenesis etc). As these processes are the hallmarks of cancer, HER receptors are considered to be the tumor 'Achilles heels' in therapeutic approaches, with EGFR and HER2 being most broadly exploited as targets for blocking of dimerization.

Several approaches are currently being undertaken to inhibit HER-signaling: 1) blocking of ligand binding to EGFR by monoclonal antibodies; 2) blocking of EGFR and HER2 dimerization by monoclonal antibodies; 3) blocking kinase activation by small molecule drugs like tyrosine kinase inhibitors; and 4) modulation of EGFR expression, either by inhibition of EGFR synthesis by siRNA or by stimulation of EGFR degradation[95].

As mentioned in section 1.1 mAbs Erbitux® (cetuximab) and Vectibix® (panitumumab) directed against HER1, and Herceptin® (trastuzumab) against HER2 have been approved as cancer therapeutics. Also the tyrosine kinase inhibitors (TKIs) Iressa® (gefitinib), Tarceva® (erlotinib) have been approved for HER1-cancer therapy, whereas Tykerb® (lapatinib) and Caprelsa® (vandetanib) have been approved for both EGFR and

HER2 therapy. Furthermore, many new mAbs and TKIs are under development.

2.3.2 Hepatocyte Growth Factor and c-Met Receptor

Hepatocycte Growth Factor (HGF), also known as scatter factor, is secreted as a single-chain, inactive polypeptide by mesenchymal cells, and is cleaved by serine proteases into a 69-kDa α-chain and 34-kDa β-chain. HGF is the only known ligand for the c-Met receptor[96-98]. The c-Met receptor is expressed during embryogenesis and adulthood in epithelial cells of many organs like liver, prostate, pancreas, muscle, kidney, and bone marrow. In tumor cells, c-Met activation triggers diverse series of signaling cascades resulting, like the HER receptor, in cell growth, proliferation, invasion, metastasis formation and escape from apoptosis[98]. Overexpression of HGF and c-Met is associated with increased aggressiveness of tumors and poor prognostic outcome of cancer patients (www.vai.org/vari/metandcancer and ref [99]). HGF and c-Met expression have been observed in most solid tumors. Blocking HGF might be a more beneficial strategy over blocking the c-Met receptor, as HGF is expected to be highly expressed in the tumor only [82].

The last decades, several pharmaceutical companies have been actively involved in the development of therapeutic mAbs and TKIs that antagonize c-Met activation. At least 16 agents have been or are being evaluated in the clinic at the moment, as reviewed by Liu et al.[100]. To their and our knowledge, three anti-HGF mAbs are under clinical development at the moment, including AMG102 (rilotumumab), a humanized anti-human HGF IgG2 mAb from Amgen, AV-299 from Schering/Aveo, and TAK-701 from Milennium.

Furthermore, the HGF/c-Met pathway has been found to have a relationship with other important pathways, like EGFR, HER2, RON, CD44 and FAS[100]. Resistance to EGFR targeted therapy is e.g. known to include activation of a parallel pathway like c-Met. c-Met amplification has shown to be responsible for acquired resistance to the EGFR-TKI gefitinib in non-small-cell lung cancer (NSCLC). Resistance there was mediated by c-Met-ErbB3 transactivation, leading to restored signaling via the PI3K/AKT pathway [101].

2.3.3 Insulin-like Growth Factor Receptor type 1 (IGF-1R)

The receptor tyrosine kinases (RTK) from the insulin-like growth factor (IGF) signaling system also play a prominent role in tumor growth[102]. The IGF system consists of the ligands insulin, IGF-I and IGF-II, and the cell-surface receptors that mediate their biological effects. The latter include the insulin receptor (IR), the IGF-I receptor (IGF-IR) and the IGF-II receptor (IGF-IIR). The IGF receptors belong, like EGFR, to the family of receptor tyrosine kinases, and are present in the plasma membrane as heterotetramers containing two α

and two β-subunits. Ligand binding involves the simultaneous interaction of the ligand with both α-subunits and this cross-linking triggers receptor activation. Phosphorylation of the intracellular domain of the receptor results in molecular signaling leading to cell proliferation. Insulin is essential for glucose homeostasis, whereas both IGF ligands are involved in normal growth and development.

Comparable to the EGFR system, overexpression of receptors from the IGF system has been frequently observed in different tumors. Therefore, this receptor class is considered to be a promising anti-cancer target for mAbs and small molecules. Similar to what has been performed for the ErbB family of receptors; antagonistic mAbs that inhibit both ligand binding and receptor activation have been generated against the IGF receptor system. Because of the shared signaling pathways (Figure 7), it can be expected that EGFR and IGF-1(R) signaling affect each other ("cross-talk"); (1) stimulation of the IGF system enhanced signaling of other growth factor systems such as EGF, (2) IGF caused resistance against growth inhibition and cell death induced by anti-EGFR mAb cetuximab, and (3) IGF-1R/EGFR heterodimerization counteracted the anti-tumor action of the TKI erlotinib. These data provide a strong rationale for combined EGFR and IGF-1(R) targeting and inhibition[81].

2.3.4 Vascular Endothelial Growth Factor (VEGF)

Angiogenesis is a process by which new blood vessels are formed from existing capillaries. The newly formed blood vessels supply the blood and oxygen that is essential for a solid tumor to grow beyond a certain size (1-2 mm^3). The angiogenic process is induced by the activation of vascular endothelial cells through binding of vascular endothelial growth factors (VEGFs) to different cell surface receptors. These growth factors are produced by macrophages, but also by tumor cells themselves.

There are seven VEGF members, among which VEGF-A plays a major role in tumor blood vessel formation[103]. The receptor family for the VEGFs comprises three tyrosine kinase receptors (VEGFR1-3) and two co-receptors (neuropilin-1 and 2) of which VEGF-R1 and R2 are primarily involved in tumor angiogenesis[103].

By now, many compounds with anti-angiogenic activity have been described, however, with exception of drugs targeting VEGF ligands or receptors, the vast majority have failed to confirm the encouraging preclinical results when tested in clinical trials[104,105]. Furthermore, the initial concept to radically ''starve'' the tumor by stripping the blood supply had to be modified as aggressive angiogenesis inhibition may aggravate tumor metabolism and promote metastatic spread.

Many of the mechanisms responsible for increased tumor growth related to EGF(R), c-Met, IGF-I(R), and VEGF(R) are distinct. For this reason, simultaneous blockade of receptor systems would probably result in improved efficacy of tumor therapy. While several anti-VEGF-R2 mAbs are under development, antibodies that bind (neutralize) the VEGF-R2 ligand (VEGF) also show tumor inhibitory effects (e.g. bevacizumab)[106]. High VEGF expression was found to be strongly correlated with high VEGF-R2 expression, and this co-expression was associated with higher tumor proliferation and worse survival. These results suggest the existence of an autocrine VEGF-loop and provide a strong rationale for anti-VEGF therapy. Also for the HER family and VEGF-R2, signaling cross-talk has become apparent (Figure 7): while EGFR induces the expression of VEGF, EGFR/HER2 hetero-dimers induce VEGF expression and promote angiogenesis even more potently[107]. Inhibition of EGFR with cetuximab was shown to result in anti-angiogenic effects like a decrease in VEGF synthesis[108]. Moreover, VEGF expression was elevated in anti-EGFR-resistant colon cancer[109]. Therefore, it seems logical to combine anti-EGFR and anti-VEGF therapy.

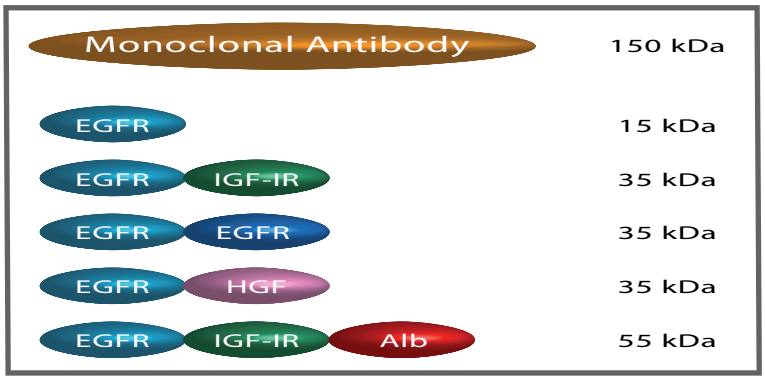

Figure 8. Flexibility of the Nanobody technology toolbox for generation of multi-valent and/or multi-specific single molecule formats. Theoretical design showing the size relationship between Nanobodies and classical intact mAbs. It has to be assessed how many "beads in the chain" can be exploited. For practical reasons, this will most probably be between 3 and 5 units.

2.4 The potential of Nanobodies for dual-specificity therapy

Up till now, only two formats of single domain antibody fragments are known: domain antibodies based on human VH segments and the naturally occurring camelid VHH fragments, called Nanobodies (Figure 6). The domain antibodies based on human VH segments have the disadvantage that genetic engineering is needed to compensate for the absence of – and therefore loss of - contact to the VL domain. This part of VH segments naturally contains a hydrophobic interface, which needs to be mutated to ensure the stability of the single domain[8,110]. In contrast, Nanobodies are naturally occurring as single

domain structures and are therefore inherently more stable as monomer. More important, Nanobody technology allows for immunization of Camelidae with the antigen of interest and the subsequent cloning of the full repertoire of affinity matured Nanobody genes. For domain antibodies based on human VH gene segment, only (semi) synthetic "single pot" libraries can be made, usually leading to low affinity lead molecules, which subsequently need affinity maturation.

Due to the single domain character of Nanobody fragments, standard molecular biology techniques such as polymerase chain reaction (PCR) allow for the facile purification and selection of appropriate Nanobody candidates from the full antibody repertoire of immunized camelids. Unique features of the Nanobody platform compared to conventional mAb technology are: (1) easy and rapid drug development, (2) adjustable serum half life time, by using half-life extension technology; combining targeting Nanobodies with anti-albumin Nanobody units (3) easy and cheap production in bacteria and yeast, and (4) high flexibility of drug format. The relatively small size of the gene (360-400 nt) permits Nanobody genes to be fused as separate building blocks into proteins as dimers (~35 kDa), trimers (~50 kDa) or multimers (Figure 8). Nanobody studies in cynomolgous monkeys point to low immunogenicity. Because of their small size they are well capable of tumor penetration. The aforementioned Nanobody technology seems very promising for development of next generation dual-specificity mAbs[91,111].

First clinical trials with Nanobodies were performed with Nanobody ALX-0081, against the von Willebrand factor (vWF). vWF acts at a very early stage in the blood clotting cascade by controlling the platelet adhesion and aggregation, and it represents a potential novel anti-thrombotic target in cardiovascular disease. In 2009, a phase II clinical trial with Nanobody ALX-0081 in high risk patients with Acute Coronary Syndrome (ACS) undergoing a percutaneous coronary intervention (PCI) was started. In this study ALX-0081 is compared with ReoPro® (abciximab) as adjunctive therapy to a PCI procedure. Results of this study are expected soon. Before this clinical trial a study was performed to assess the *in vitro* efficacy of ALX-0081 in human blood[112]. In this study, nine patients who were scheduled for a PCI procedure and 11 healthy volunteers were included. Blood was drawn 24 h before and 1 h after start of the PCI procedure, and was subsequently spiked with different concentrations of ALX-0081 or buffer. In all *in vitro* experiments, ALX-0081 led to complete inhibition of platelet adhesion and aggregation.

Other Nanobodies are entering phase I clinical trials (e.g., anti-TNFα, anti-RANKL, anti-IL-6R, anti-CXCR4).

3. Aim and outline of the thesis

In this thesis, novel antibody technology to improve imaging and blockade of growth factors and their receptors in cancer is described. For this purpose, PET and Nanobody technology were explored using binding units directed against EGFR, HGF and serum albumin as an example. Next to these, also Nanobodies directed against IGF-1R, HER2 and VEGF were developed within the framework of the STW-project and the collaboration with Ablynx, but not evaluated during the course of this promotion period.

For stable coupling of ^{89}Zr to mAbs, a multistep procedure was developed by Verel et al. using a succinylated derivative of desferrioxamine B (N-sucDf) as bifunctional chelate. This multistep procedure is used in clinical settings in a safe way for many years; however, a more rapid and less laborious procedure is desirable. In chapter 2 the newly developed chelate p-isothiocyanotobenzyl-desferrioxamine is described. This novel chelate was developed to enable rapid coupling of the long-lived positron emitter ^{89}Zr to slow kinetic mAbs and antibody-like scaffolds, opening avenues towards accurate quantitative assessment of biodistribution and PET imaging of these molecules. In chapter 3 a convenient protocol is provided for conjugation of ^{89}Zr to slow kinetic mAbs or antibody-like scaffolds (like Nanobodies). In chapter 4 the newly developed desferal-chelate was also investigated for its suitability to couple the short-lived positron emitter ^{68}Ga to fast kinetic Nanobodies. As an example the monovalent anti-EGFR Nanobody 7D12 was used. Chapter 5 presents the results with a trivalent anti-EGFR-Nanobody in a preclinical therapy study using mice bearing EGFR-positive human xenografts. In this study, the efficacy of the trivalent Nanobody 7D12-9G8-Alb1 was compared with the already registered mAb cetuximab. Nanobody 7D12-9G8-Alb1 is a biparatopic Nanobody targeting two different epitopes on EGFR fused with an anti-albumin unit (Alb1) that causes half-life extension in blood. In chapter 6 we present the first preclinical data with two bivalent anti-HGF-Nanobodies 1E2-Alb8 and 6E10-Alb8. To this end, biodistribution studies using ^{89}Zr-labeled anti-HGF-Nanobodies and therapy studies with anti-HGF-Nanobodies were performed. The effectiveness of these Nanobodies in comparison to other mAbs under clinical development is discussed. In chapter 7, a general discussion of the results presented in this thesis is provided.

References

1 Himmelweit F. The collected papers of Paul Ehrlich. London: Pergamon Press 1956.

2 Strebhardt K, Ullrich A. Paul Ehrlich's magic bullet concept: 100 years of progress. Nat. Rev. Cancer 2008; 8: 473-80.

3 Kohler G, Milstein C. Continuous cultures of fused cells secreting antibody of predefined specificity. Nature 1975; 256: 495-7.

4 Khazaeli MB, Conry RM, LoBuglio AF. Human immune response to monoclonal antibodies. J. Immunother. Emphasis. Tumor Immunol. 1994; 15: 42-52.

5 DeNardo GL, Bradt BM, Mirick GR, DeNardo SJ. Human antiglobulin response to foreign antibodies: therapeutic benefit? Cancer Immunol. Immunother. 2003; 52: 309-16.

6 Ward ES, Gussow D, Griffiths AD, Jones PT, Winter G. Binding activities of a repertoire of single immunoglobulin variable domains secreted from Escherichia coli. Nature 1989; 341: 544-6.

7 Nord K, Gunneriusson E, Ringdahl J, Stahl S, Uhlen M, Nygren PA. Binding proteins selected from combinatorial libraries of an alpha-helical bacterial receptor domain. Nat. Biotechnol. 1997; 15: 772-7.

8 Roovers RC, van Dongen GAMS, en Henegouwen PMP. Nanobodies in therapeutic applications. Curr. Opin. Mol. Ther. 2007; 9: 327-35.

9 Beste G, Schmidt FS, Stibora T, Skerra A. Small antibody-like proteins with prescribed ligand specificities derived from the lipocalin fold. Proc. Natl. Acad. Sci. U. S. A 1999; 96: 1898-903.

10 Reichert JM. Monoclonal antibodies as innovative therapeutics. Curr. Pharm. Biotechnol. 2008; 9: 423-30.

11 Reichert JM, Valge-Archer VE. Development trends for monoclonal antibody cancer therapeutics. Nat. Rev. Drug Discov. 2007; 6: 349-56.

12 Scolnik PA. mAbs: a business perspective. MAbs. 2009; 1: 179-84.

13 Reichert JM. Antibody-based therapeutics to watch in 2011. MAbs. 2011; 3: 76-99.

14 Maggon K. Monoclonal antibody "gold rush". Curr. Med. Chem. 2007; 14: 1978-87.

15 Lawrence S. Billion dollar babies--biotech drugs as blockbusters. Nat. Biotechnol. 2007; 25: 380-2.

16 Maggon K. Top Ten Monoclonal Antibodies. Knol 2012.

17 Nelson AL, Reichert JM. Development trends for therapeutic antibody fragments. Nat. Biotechnol. 2009; 27: 331-7.

18 Mano M. The burden of scientific progress: growing inequalities in the delivery of cancer care. Acta Oncol. 2006; 45: 84-6.

19 Neyt M, Albrecht J, Cocquyt V. An economic evaluation of Herceptin in adjuvant setting: the Breast Cancer International Research Group 006 trial. Ann. Oncol. 2006; 17: 381-90.

20 Verel I, Visser GWM, van Dongen GA. The promise of immuno-PET in radioimmunotherapy. J. Nucl. Med. 2005; 46 Suppl 1: 164S-71S.

21 Zafir-Lavie I, Michaeli Y, Reiter Y. Novel antibodies as anticancer agents. Oncogene 2007; 26: 3714-33.

22 Olafsen T, Wu AM. Antibody vectors for imaging. Semin. Nucl. Med. 2010; 40: 167-81.

23 McCabe K, Wu AM. Positive progress in immunoPET - Not just a coincidence. Cancer Biother. Radiopharm. 2010; 25:253-61.

24 van Dongen GAMS, Visser GWM, Lub-de Hooge MN, de Vries EG, Perk LR. Immuno-PET: a navigator in monoclonal antibody development and applications. Oncologist. 2007; 12: 1379-89.

25 Boswell CA, Brechbiel MW. Development of radioimmunotherapeutic and diagnostic antibodies: an inside-out view. Nucl. Med. Biol. 2007; 34: 757-78.

26 Wu AM, Olafsen T. Antibodies for molecular imaging of cancer. Cancer J. 2008; 14: 191-7.

27 Nayak TK, Brechbiel MW. Radioimmunoimaging with longer-lived positron-emitting radionuclides: potentials and challenges. Bioconjug. Chem. 2009.

28 Holland JP, Williamson MJ, Lewis JS. Unconventional nuclides for radiopharmaceuticals. Mol. Imaging 2010; 9: 1-20.

29 Reddy S, Robinson MK. Immuno-positron emission tomography in cancer models. Semin. Nucl. Med. 2010; 40: 182-9.

30 Perk LR, Visser GWM, Vosjan MJWD et al. ^{89}Zr as a PET surrogate radioisotope for scouting biodistribution of the therapeutic radiometals ^{90}Y and ^{177}Lu in tumor-bearing nude mice after coupling to the internalizing antibody cetuximab. J. Nucl. Med. 2005; 46: 1898-906.

31 Cai W, Chen K, He L, Cao Q, Koong A, Chen X. Quantitative PET of EGFR expression in xenograft-bearing mice using ^{64}Cu-labeled cetuximab, a chimeric anti-EGFR monoclonal antibody. Eur. J. Nucl. Med. Mol. Imaging 2007; 34: 850-8.

32 Aerts HJWL, Dubois L, Perk L et al. Disparity between in vivo EGFR expression and ^{89}Zr-labeled cetuximab uptake assessed with PET. J. Nucl. Med. 2009; 50: 123-31.

33 Tolmachev V, Friedman M, Sandstrom M et al. Affibody molecules for epidermal growth factor receptor targeting in vivo: aspects of dimerization and labeling chemistry. J. Nucl. Med. 2009; 50: 274-83.

34 Divgi CR, Welt S, Kris M et al. Phase I and imaging trial of indium 111-labeled anti-epidermal growth factor receptor monoclonal antibody 225 in patients with squamous cell lung carcinoma. J. Natl. Cancer Inst. 1991; 83: 97-104.

35 Dijkers EC, Oude Munnink TH, Kosterink JG et al. Biodistribution of ^{89}Zr-trastuzumab and PET imaging of HER2-positive lesions in patients with metastatic breast cancer. Clin. Pharmacol. Ther. 2010; 87: 586-92.

36 Verel I, Visser GWM, Boellaard R, Stigter-van Walsum M, Snow GB, van Dongen GAMS. ^{89}Zr immuno-PET: comprehensive procedures for the production of ^{89}Zr-labeled monoclonal antibodies. J. Nucl. Med. 2003; 44: 1271-81.

37 Holland JP, Sheh Y, Lewis JS. Standardized methods for the production of high specific-activity zirconium-89. Nucl. Med. Biol. 2009; 36: 729-39.

38 Tijink BM, Perk LR, Budde M et al. ^{124}I-L19-SIP for immuno-PET imaging of tumour vasculature and guidance of ^{131}I-L19-SIP radioimmunotherapy. Eur. J. Nucl. Med. Mol. Imaging 2009; 36: 1235-44.

39 Perk LR, Stigter-van Walsum M, Visser GWM et al. Quantitative PET imaging of Met-expressing human cancer xenografts with ^{89}Zr-labelled monoclonal antibody DN30. Eur. J. Nucl. Med. Mol. Imaging 2008; 35: 1857-67.

40 Brouwers A, Verel I, Van Eerd J et al. PET radioimmunoscintigraphy of renal cell cancer using ^{89}Zr-labeled cG250 monoclonal antibody in nude rats. Cancer Biother. Radiopharm. 2004; 19: 155-63.

41 Hoeben BAW, Kaanders JHAM, Franssen GM. PET imaging of hypoxia with ^{89}Zr-labeled cG250-f(ab')2 in head and neck tumors. J. Nucl. Med. 2010.

42 Perk LR, Visser OJ, Stigter-van Walsum M et al. Preparation and evaluation of ^{89}Zr-Zevalin for monitoring of ^{90}Y-Zevalin biodistribution with positron emission tomography. Eur. J. Nucl. Med. Mol. Imaging 2006; 33: 1337-45.

43 Muylle K, Azerad MA, Perk LR. Immuno-PET/CT imaging with Zr-89-rituximab as a prelude for radioimmunotherpy with Y-90-rituximab in patients with relapsed CD20^{+}B cell non-Hodkin's lymphoma. Ann. Oncol. 2008.

44 Nagengast WB, de Vries EG, Hospers GA et al. In vivo VEGF imaging with radiolabeled bevacizumab in a human ovarian tumor xenograft. J. Nucl. Med. 2007; 48: 1313-9.

45 Dijkers ECF, Kosterink JGW, Rademaker AP et al. Development and characterization of clinical-grade ^{89}Zr-trastuzumab for HER2/neu immunoPET imaging. J. Nucl. Med. 2009; 50: 974-81.

46 Verel I, Visser GWM, Boerman OC et al. Long-lived positron emitters zirconium-89 and iodine-124 for scouting of therapeutic radioimmunoconjugates with PET. Cancer Biother. Radiopharm. 2003; 18: 655-61.

47 Verel I, Visser GWM, Boellaard R et al. Quantitative ^{89}Zr immuno-PET for in vivo scouting of ^{90}Y-labeled monoclonal antibodies in xenograft-bearing nude mice. J. Nucl. Med. 2003; 44: 1663-70.

48 Verel I, Visser GWM, Vosjan MJWD, Finn R, Boellaard R, van Dongen GAMS. High-quality ^{124}I-labelled monoclonal antibodies for use as PET scouting agents prior to ^{131}I-radioimmunotherapy. Eur. J. Nucl. Med. Mol. Imaging 2004; 31: 1645-52.

49 Rasbridge SA, Gillett CE, Seymour AM et al. The effects of chemotherapy on morphology, cellular proliferation, apoptosis and oncoprotein expression in primary breast carcinoma. Br. J. Cancer 1994; 70: 335-41.

50 Gancberg D, Di Leo A, Cardoso F et al. Comparison of HER-2 status between primary breast cancer and corresponding distant metastatic sites. Ann. Oncol. 2002; 13: 1036-43.

51 Zidan J, Dashkovsky I, Stayerman C, Basher W, Cozacov C, Hadary A. Comparison of HER-2 overexpression in primary breast cancer and metastatic sites and its effect on biological targeting therapy of metastatic disease. Br. J. Cancer 2005; 93: 552-6.

52 Gong Y, Booser DJ, Sneige N. Comparison of HER-2 status determined by fluorescence in situ hybridization in primary and metastatic breast carcinoma. Cancer 2005; 103: 1763-9.

53 de Korte MA, de Vries EGE, Lub-de Hooge MN et al. ^{111}Indium-trastuzumab visualises myocardial human epidermal growth factor receptor 2 expression shortly after anthracycline treatment but not during heart failure: a clue to uncover the mechanisms of trastuzumab-related cardiotoxicity. Eur. J. Cancer 2007; 43: 2046-51.

54 Behr TM, Behe M, Wormann B. Trastuzumab and breast cancer. N. Engl. J. Med. 2001; 345: 995-6.

55 Lewis Phillips GD, Li G, Dugger DL et al. Targeting HER2-positive breast cancer with trastuzumab-DM1, an antibody-cytotoxic drug conjugate. Cancer Res. 2008; 68: 9280-90.

56 Tijink BM, Buter J, de Bree R et al. A phase I dose escalation study with anti-CD44v6 bivatuzumab mertansine in patients with incurable squamous cell carcinoma of the head and neck or esophagus. Clin. Cancer Res. 2006; 12: 6064-72.

57 Holland JP, Caldas-Lopes E, Divilov V et al. Measuring the pharmacodynamic effects of a novel Hsp90 inhibitor on

HER2/neu expression in mice using Zr-DFO-trastuzumab. PLoS.One. 2010; 5: e8859.

58 Oude Munnink TH, Korte MA, Nagengast WB et al. ^{89}Zr-trastuzumab PET visualises HER2 downregulation by the HSP90 inhibitor NVP-AUY922 in a human tumour xenograft. Eur. J. Cancer 2010; 46: 678-84.

59 Niu G, Cai W, Chen K, Chen X. Non-invasive PET imaging of EGFR degradation induced by a heat shock protein 90 inhibitor. Mol. Imaging Biol. 2008; 10: 99-106.

60 Nagengast WB, de Korte MA, Oude Munnink TH et al. ^{89}Zr-bevacizumab PET of early antiangiogenic tumor response to treatment with HSP90 inhibitor NVP-AUY922. J. Nucl. Med. 2010; 51: 761-7.

61 Smith-Jones PM, Solit DB, Akhurst T, Afroze F, Rosen N, Larson SM. Imaging the pharmacodynamics of HER2 degradation in response to Hsp90 inhibitors. Nat. Biotechnol. 2004; 22: 701-6.

62 Smith-Jones PM, Solit D, Afroze F, Rosen N, Larson SM. Early tumor response to Hsp90 therapy using HER2 PET: comparison with ^{18}F-FDG PET. J. Nucl. Med. 2006; 47: 793-6.

63 Niu G, Li Z, Cao Q, Chen X. Monitoring therapeutic response of human ovarian cancer to 17-DMAG by noninvasive PET imaging with ^{64}Cu-DOTA-trastuzumab. Eur. J. Nucl. Med. Mol. Imaging 2009; 36: 1510-9.

64 Wilson CB, Snook DE, Dhokia B et al. Quantitative measurement of monoclonal antibody distribution and blood flow using positron emission tomography and 124-iodine in patients with breast cancer. Int. J. Cancer 1991; 47: 344-7.

65 Larson SM, Pentlow KS, Volkow ND et al. PET scanning of iodine-124-3F9 as an approach to tumor dosimetry during treatment planning for radioimmunotherapy in a child with neuroblastoma. J. Nucl. Med. 1992; 33: 2020-3.

66 Zuckier LS, DeNardo GL. Trials and tribulations: oncological antibody imaging comes to the fore. Semin. Nucl. Med. 1997; 27: 10-29.

67 Jayson GC, Zweit J, Jackson A et al. Molecular imaging and biological evaluation of HuMV833 anti-VEGF antibody: implications for trial design of antiangiogenic antibodies. J. Natl. Cancer Inst. 2002; 94: 1484-93.

68 Divgi CR, Pandit-Taskar N, Jungbluth AA et al. Preoperative characterisation of clear-cell renal carcinoma using iodine-124-labelled antibody chimeric G250 (^{124}I-cG250) and PET in patients with renal masses: a phase I trial. Lancet Oncol. 2007; 8: 304-10.

69 Powles T, Ell PJ. Does PET imaging have a role in renal cancers after all? Lancet Oncol. 2007; 8: 279-81.

70 Börjesson PKE, Jauw YWS, Boellaard R et al. Performance of immuno-positron emission tomography with zirconium-89-labeled chimeric monoclonal antibody U36 in the detection of lymph node metastases in head and neck cancer patients. Clin. Cancer Res. 2006; 12: 2133-40.

71 Zalutsky MR. Potential of immuno-positron emission tomography for tumor imaging and immunotherapy planning. Clin. Cancer Res. 2006; 12: 1958-60.

72 Börjesson PKE, Jauw YWS, de Bree R et al. Radiation dosimetry of ^{89}Zr-labeled chimeric monoclonal antibody U36 as used for immuno-PET in head and neck cancer patients. J. Nucl. Med. 2009; 50: 1828-36.

73 Perik PJ, Lub-de Hooge MN, Gietema JA et al. Indium-111-labeled trastuzumab scintigraphy in patients with human epidermal growth factor receptor 2-positive metastatic breast cancer. J. Clin. Oncol. 2006; 24: 2276-82.

74 Oude Munnink TH, Dijkers E, Netters SJ. Trastuzumab pharmacokinetics influenced by extent HER2 positive tumor load. J. Clin. Oncol. 2010;28:e355-6.

75 Tonra JR, Deevi DS, Corcoran E et al. Synergistic antitumor effects of combined epidermal growth factor receptor and vascular endothelial growth factor receptor-2 targeted therapy. Clin. Cancer Res. 2006; 12: 2197-207.

76 Goetsch L, Gonzalez A, Leger O et al. A recombinant humanized anti-insulin-like growth factor receptor type I antibody (h7C10) enhances the antitumor activity of vinorelbine and anti-epidermal growth factor receptor therapy against human cancer xenografts. Int. J. Cancer 2005; 113: 316-28.

77 Jung YD, Mansfield PF, Akagi M et al. Effects of combination anti-vascular endothelial growth factor receptor and anti-epidermal growth factor receptor therapies on the growth of gastric cancer in a nude mouse model. Eur. J. Cancer 2002; 38: 1133-40.

78 Shaheen RM, Ahmad SA, Liu W et al. Inhibited growth of colon cancer carcinomatosis by antibodies to vascular endothelial and epidermal growth factor receptors. Br. J. Cancer 2001; 85: 584-9.

79 Reid A, Vidal L, Shaw H, de Bono J. Dual inhibition of ErbB1 (EGFR/HER1) and ErbB2 (HER2/neu). Eur. J. Cancer 2007; 43: 481-9.

80 Larbouret C, Robert B, Navarro-Teulon I et al. In vivo therapeutic synergism of anti-epidermal growth factor receptor and anti-HER2 monoclonal antibodies against pancreatic carcinomas. Clin. Cancer Res. 2007; 13: 3356-62.

81 van der Veeken J, Oliveira S, Schiffelers RM, Storm G, van Bergen En Henegouwen PMP, Roovers RC. Crosstalk between epidermal growth factor receptor- and insulin-like growth factor-1 receptor signaling: implications for cancer therapy. Curr. Cancer Drug Targets. 2009; 9: 748-60.

82 Xu H, Stabile LP, Gubish CT, Gooding WE, Grandis JR, Siegfried JM. Dual blockade of EGFR and c-Met abrogates redundant signaling and proliferation in head and neck carcinoma cells. Clin. Cancer Res. 2011.

83 Barnes CJ, Ohshiro K, Rayala SK, El-Naggar AK, Kumar R. Insulin-like growth factor receptor as a therapeutic target in head and neck cancer. Clin. Cancer Res. 2007; 13: 4291-9.

84 Tonra JR, Corcoran E, Deevi DS et al. Prioritization of EGFR/IGF-IR/VEGFR2 combination targeted therapies utilizing cancer models. Anticancer Res. 2009; 29: 1999-2007.

85 Ciardiello F, Troiani T, Bianco R et al. Interaction between the epidermal growth factor receptor (EGFR) and the vascular endothelial growth factor (VEGF) pathways: a rational approach for multi-target anticancer therapy. Ann. Oncol. 2006; 17 Suppl 7: vii109-vii114.

86 Lu D, Zhang H, Koo H et al. A fully human recombinant IgG-like bispecific antibody to both the epidermal growth factor receptor and the insulin-like growth factor receptor for enhanced antitumor activity. J. Biol. Chem. 2005; 280: 19665-72.

87 Dong J, Sereno A, Aivazian D et al. A stable IgG-like bispecific antibody targeting the epidermal growth factor receptor and the type I insulin-like growth factor receptor demonstrates superior anti-tumor activity. MAbs. 2011; 3: 273-88.

88 Holmes D. Buy buy bispecific antibodies. Nat. Rev. Drug Discov 2011; 10: 798-800.

89 Hamers-Casterman C, Atarhouch T, Muyldermans S et al. Naturally occurring antibodies devoid of light chains. Nature 1993; 363: 446-8.

90 Holliger P, Hudson PJ. Engineered antibody fragments and the rise of single domains. Nat. Biotechnol. 2005; 23: 1126-36.

91 Tijink BM, Laeremans T, Budde M et al. Improved tumor targeting of anti-epidermal growth factor receptor Nanobodies through albumin binding: taking advantage of modular Nanobody technology. Mol. Cancer Ther. 2008;

7: 2288-97.

92 Coppieters K, Dreier T, Silence K et al. Formatted anti-tumor necrosis factor alpha VHH proteins derived from camelids show superior potency and targeting to inflamed joints in a murine model of collagen-induced arthritis. Arthritis Rheum. 2006; 54: 1856-66.

93 Schlessinger J. Cell signaling by receptor tyrosine kinases. Cell 2000; 103: 211-25.

94 Yarden Y, Sliwkowski MX. Untangling the ErbB signalling network. Nat. Rev. Mol. Cell Biol. 2001; 2: 127-37.

95 Harari PM. Epidermal growth factor receptor inhibition strategies in oncology. Endocr. Relat Cancer 2004; 11: 689-708.

96 Cooper CS, Park M, Blair DG et al. Molecular cloning of a new transforming gene from a chemically transformed human cell line. Nature 1984; 311: 29-33.

97 Bottaro DP, Rubin JS, Faletto DL et al. Identification of the hepatocyte growth factor receptor as the c-met proto-oncogene product. Science 1991; 251: 802-4.

98 Birchmeier C, Birchmeier W, Gherardi E, Vande Woude GF. Met, metastasis, motility and more. Nat. Rev. Mol. Cell Biol. 2003; 4: 915-25.

99 Boccaccio C, Comoglio PM. Invasive growth: a MET-driven genetic programme for cancer and stem cells. Nat. Rev. Cancer 2006; 6: 637-45.

100 Liu X, Newton RC, Scherle PA. Development of c-MET pathway inhibitors. Expert. Opin. Investig. Drugs 2011; 20: 1225-41.

101 Engelman JA, Zejnullahu K, Mitsudomi T et al. MET amplification leads to gefitinib resistance in lung cancer by activating ERBB3 signaling. Science 2007; 316: 1039-43.

102 Larsson O, Girnita A, Girnita L. Role of insulin-like growth factor 1 receptor signalling in cancer. Br. J. Cancer 2005; 92: 2097-101.

103 Yamazaki Y, Morita T. Molecular and functional diversity of vascular endothelial growth factors. Mol. Divers. 2006; 10: 515-27.

104 Kerbel R, Folkman J. Clinical translation of angiogenesis inhibitors. Nat. Rev. Cancer 2002; 2: 727-39.

105 Carmeliet P, Jain RK. Molecular mechanisms and clinical applications of angiogenesis. Nature 2011; 473: 298-307.

106 Willett CG, Boucher Y, di Tomaso E et al. Direct evidence that the VEGF-specific antibody bevacizumab has antivascular effects in human rectal cancer. Nat. Med. 2004; 10: 145-7.

107 Yen L, Benlimame N, Nie ZR et al. Differential regulation of tumor angiogenesis by distinct ErbB homo- and heterodimers. Mol. Biol. Cell 2002; 13: 4029-44.

108 van Cruijsen H, Giaccone G, Hoekman K. Epidermal growth factor receptor and angiogenesis: Opportunities for combined anticancer strategies. Int. J. Cancer 2005; 117: 883-8.

109 Bianco R, Rosa R, Damiano V et al. Vascular endothelial growth factor receptor-1 contributes to resistance to anti-epidermal growth factor receptor drugs in human cancer cells. Clin. Cancer Res. 2008; 14: 5069-80.

110 Revets H, De Baetselier P, Muyldermans S. Nanobodies as novel agents for cancer therapy. Expert. Opin. Biol. Ther.

2005; 5: 111-24.

111 Roovers RC, Laeremans T, Huang L et al. Efficient inhibition of EGFR signaling and of tumour growth by antagonistic anti-EGFR Nanobodies. Cancer Immunol. Immunother. 2007; 56: 303-17.

112 van Loon JE, de Jaegere PPT, Ulrichts H et al. The in vitro effect of the new antithrombotic drug candidate ALX-0081 on blood samples of patients undergoing percutaneous coronary intervention. Thromb. Haemost. 2011; 106: 165-71.

Chapter 2:

p-Isothiocyanatobenzyl-desferrioxamine: a new bifunctional chelate for facile radiolabeling of monoclonal antibodies with zirconium-89 for immuno-PET imaging

2

Lars R. Perk*
Maria J.W.D. Vosjan*
Gerard W.M. Visser
Marianne Budde
Paul Jurek
Garry E. Kiefer
Guus A.M.S. van Dongen

*Both authors contributed equally to this article

European Journal of Nuclear Medicine and Molecular Imaging (2010) 37:250-59

Abstract

Purpose Immuno-PET is an emerging imaging tool for the selection of high potential antibodies (mAbs) for imaging and therapy. The positron emitter zirconium-89 (^{89}Zr) has attractive characteristics for immuno-PET with intact mAbs. Previously, we have described a multi-step procedure for stable coupling of ^{89}Zr to mAbs via the bifunctional chelate (BFC) tetrafluorophenol-N-succinyldesferal (TFP-N-sucDf). To enable widespread use of ^{89}Zr-immuno-PET, we now introduce the novel BFC p-isothiocyanatobenzyl-desferrioxamine B (Df-Bz-NCS) and compare its performance in ^{89}Zr-immuno-PET with the reference BFC TFP-N-sucDf. Methods Three mAbs were premodified with Df-Bz-NCS and labeled with ^{89}Zr at different pHs to assess the reaction kinetics and robustness of the radiolabeling. Stability of both ^{89}Zr-Df-Bz-NCS- and ^{89}Zr-N-sucDf-conjugates was evaluated in different buffers and human serum. Comparative biodistribution and PET studies in tumor bearing mice were undertaken. Results The selected conjugation conditions resulted in a chelate:mAb substitution ratio of about 1.5:1. Under optimal radiolabelling conditions (pH between 6.8–7.2), the radiochemical yield was >85% after 60 min incubation at room temperature, resulting in radioimmunoconjugates with preserved integrity and immunoreactivity. The new radioimmunoconjugate was very stable in serum for up to 7 days at 37°C, with <5% ^{89}Zr release, and was equally stable compared to the reference conjugate when stored in the appropriate buffer at 4°C. In biodistribution and imaging experiments the novel and the reference radioimmunoconjugates showed high and similar accumulation in tumours in nude mice. Conclusions The novel Df-Bz-NCS BFC allows efficient and easy preparation of optimally performing ^{89}Zr-labelled mAbs, facilitating further exploration of ^{89}Zr-immuno-PET as an imaging tool.

Introduction

Presently, hundreds of monoclonal antibodies (mAbs) and mAb fragments are under clinical development because of their excellent potential for diagnosis and systemic treatment of cancer and other pathological conditions [1]. Positron emission tomography (PET) offers an attractive imaging option to confirm and quantify selective tumor uptake of such targeting molecules [2-4].

To enable PET imaging of intact mAbs and mAb-fragments (immuno-PET), an appropriate positron emitter, with a half-life ($t_{1/2}$) that is compatible with the time needed to achieve optimal tumor-to-nontumor ratios (typically 2-4 days for intact mAbs, and 2-4 hours for mAb-fragments), has to be securely coupled to the targeting molecule. Among others, the following positron emitters for immuno-PET are under investigation at the moment: gallium-68 (^{68}Ga; $t_{½}$: 1.13 h), fluorine-18 (^{18}F; $t_{½}$: 1.83 h), copper-64 (^{64}Cu; $t_{½}$: 12.7 h), yttrium-86 (^{86}Y; $t_{½}$: 14.7 h), bromine-76 (^{76}Br; $t_{½}$: 16.2 h), zirconium-89 (^{89}Zr; $t_{½}$: 78.4 h), and iodine-124 (^{124}I; $t_{½}$: 100.3 h). Another important consideration in the choice of a positron emitter is whether the mAb or mAb fragment becomes internalized after binding to the target antigen. In that case, a positron emitter is needed that residualizes in the target cell after internalization, like ^{68}Ga, ^{64}Cu, ^{86}Y, and ^{89}Zr, to enable imaging at optimal contrast. These radionuclides have to be attached via chelating agents to mAbs and mAb-fragments.

For the imaging of intact mAbs with PET, we recently described the large scale production of ^{89}Zr and a strategy for labeling mAbs with ^{89}Zr via a multi-step synthesis using a succinylated-derivative of desferrioxamine B (N-sucDf) as bifunctional chelate [5]. The utility of this approach was clearly demonstrated through high-quality ^{89}Zr-mAb-PET images reported in preclinical and clinical studies [6-13]. The choice of desferrioxamine B is attractive because it is used clinically in a safe way for many years. The upcoming commercialization of ^{89}Zr will make this radionuclide broadly available for research and clinical applications.A shortcoming of the aforementioned labeling approach is that the multi-step procedure is relatively complicated and time-consuming, and therefore challenging with respect to Good Manufacturing Practice (GMP) compliancy. We now introduce a newly developed p-isothiocyanatobenzyl-derivative of desferrioxamine B (Df-Bz-NCS; Macrocyclics, TX) that enables an efficient and rapid preparation of ^{89}Zr-labeled mAbs.

The chemical characterization of Df-Bz-NCS, its subsequent coupling to mAbs, and the radiolabeling of Df-Bz-NCS conjugated mAbs with ^{89}Zr, are described. The in vitro stability of ^{89}Zr-Df-Bz-NCS-mAb conjugates is compared with the corresponding ^{89}Zr-N-

sucDf-mAb conjugates. In addition, comparative biodistribution and animal-PET studies are presented.

Materials and methods

Materials, monoclonal antibodies, cell lines, and radioactivity

All reagents were obtained from Sigma-Aldrich (St. Louis, MO) unless otherwise stated. No special measures were taken regarding working under strict metal-free conditions. Deionized water (18 MΩ) was used in all reactions. Df-Bz-NCS was obtained from Macrocyclics (cat. no. B-705 world patent application WO 2008/124467 A1 for the synthetic details). MAb cetuximab (Erbitux; 2.0 mg/mL) directed against the epidermal growth factor receptor (EGFR) was purchased from Merck (Darmstadt, Germany) [14]. Selection, production, and characterization of chimeric mAb U36 (cU36; 11.53 mg/mL) directed against CD44v6 has been described elsewhere [15]. MAb rituximab (MabThera; 10 mg/mL) directed against CD20 was purchased from Roche Nederland BV (Woerden, The Netherlands).

The human epidermoid cervical carcinoma cell line A431 and the CD20+ B-cell lymphoma cell line Ramos were both obtained from the American Type Culture Collection (www.atcc.com, ATCC number: CRL-1555 and CRL-1596, respectively). The head and neck squamous cell carcinoma (HNSCC) cell line FaDu was obtained from Karl-Heinz Heider (Boehringer Ingelheim, Vienna, Austria)[16], and the HNSCC cell line UM-SCC-11B was obtained from Dr. T.E. Carey (Ann Arbor, MI)[17].

^{89}Zr ($T_{1/2}$ = 78.4 h, β^+ = 22.6%; ~2.7 GBq/mL in 1 M oxalic acid) was produced by BV Cyclotron VU (Amsterdam, The Netherlands) by a (p,n) reaction on natural yttrium-89 (^{89}Y) and isolated with a hydroxamate column [5].

Characterization of p-Isothiocyanatobenzyl-desferrioxamine (Df-Bz-NCS)

Synthesis of the new ligand 1-(4-isothiocyanatophenyl)-3-[6,17-dihydroxy-7,10,18,21-tetroxo-27-[N-acetylhydroxyamino)-6,11,17,22-tetraazaheptaeicosane)thiourea (p-isothiocyanato-benzyl desferrioxamine; Df-Bz-NCS) was performed by Macrocyclics (Dallas, TX). In short, Desferrioxamine B mesylate (Df; Desferal, Novartis, Basel) was dissolved in isopropanol/water while gently stirring. A chloroform solution of 1,4-phenylendiisothiocyanate and triethyl amine was then added and the reaction progress was monitored by reverse phase HPLC. Upon completion, the reaction mixture was extracted with 0.1 M HCl. The lower organic layer was concentrated in vacuo to

remove the chloroform but not the isopropanol. The remaining organic solution was purified by reverse-phase preparative HPLC using a water/acetonitrile gradient [Detector: UV/VIS at 275 nm. Column: Phenomenex Luna C18(2) (250x50 mm, 10 µm). Sample prep: Direct injection of the isopropanol solution. Mobile phase: 0-10 min 40/60 A/B; 10–15 min ramp 40/60 to 90/10 A/B; 15-25 min 90/10 A/B; A = CH_3CN, B = H_2O. Flow rate = 100ml/min. Retention time of product was ~10min. Desired fractions were placed at -20°C to precipitate the product. The final product was isolated by filtration as a white solid (41% yield).

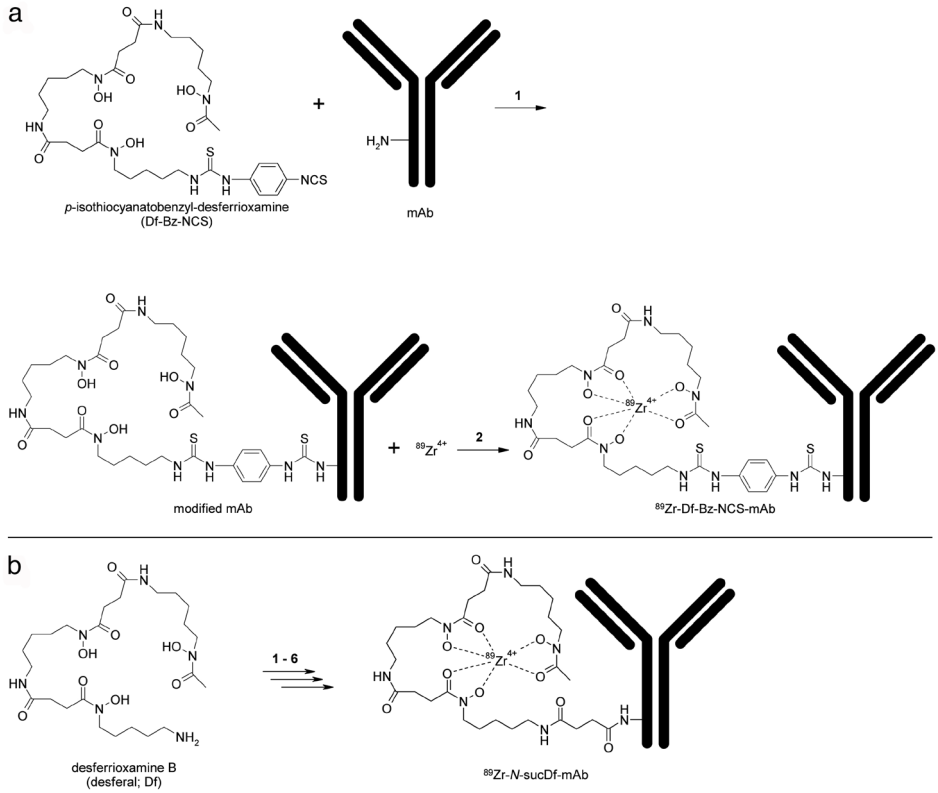

Figure 1. Schematic representation of mAb modification with the new bifunctional chelate Df-Bz-NCS (1) and subsequent labeling with ^{89}Zr (2) (a). The multi-step reference procedure using desferrioxamine B as starting ligand (b).

Analytical data final product: ^1H NMR (D_6-DMSO): δ 1.21 (m, -CH_2, 6H), 1.38 (m, -CH_2, 4H), 1.95 (s, -CH_3, 3H), 2.27 (m, -CH_2, 4H), 2.99 (m, CH_2, 4H), 3.45 (m, CH_2, 8H), 7.35 (d, 2,6-ArH, J = 8.9 Hz, 2H), 7.75 (d, 3,5=ArH, J=8.9 Hz, 2H), 7.75 (m, N-H, 2H), 7.88 (bs, N-H, 1H), 9.59 (m, N-OH, 4H). ^{13}C NMR: δ 19.18 (CH_3), 22.34, 22.35, 22.44, 24.88, 24.90, 24.94, 24.96, 24.98, 26.42, 26.88, 27.66, 28.78, 28.79, 28.83, 37.28, 37.92, 42.57, 42.60, 42.63, 45.67, 45.97, 121.92, 123.50, 124.98, 131.58, 138.17 (N=C=S), 169.00 (C=O), 170.20 (C=O), 170.84 (C=O), 179.02 (C=S). Elemental analysis calculated (%) for $C_{33}H_{52}N_8O_8S_2$: C 52.64,

H 6.96, N 14.88, S 8.52, found C 52.43, H 7.08, N 14.81, S 8.59. m/z: (ESI+); 775 (100% $[M + Na]^+$), (ESI-); 751 (100% $[M-H]^-$). Chromatographic purity: > 98% Detector: UV/VIS at 225 nm. Column: Restek Ultra IBD (100x4.6 mm, 3 µm, 100 A). Sample prep: a 1.0 mg/ml solution prepared in DMSO. Mobile phase: 0-10 min ramp 5/95 to 95/5 A/B; 10-15 min 95/5 A/B; A = 0.1% TFA in CH_3CN, B = 0.1% TFA in H_2O.

Preparation of ^{89}Zr-labeled Df-Bz-NCS-mAb

cU36, cetuximab, or rituximab were premodified with Df-Bz-NCS (Fig. 1a). In short, while gently shaking, a three-fold molar excess of Df-Bz-NCS (in 20 µL DMSO) was added to the mAb (2 – 10 mg in 1 mL 0.1 M $NaHCO_3$ buffer, pH 9.0), and incubated for 30 min at 37°C. Nonconjugated chelate was removed by size exclusion chromatography using a PD10 column (GE Healthcare Life Sciences) and 0.9% sodium chloride/gentisic acid 5 mg/ml (pH 5.0) as eluent. Subsequently, Df-Bz-NCS-mAb was labeled with ^{89}Zr at room temperature in a volume of 2 mL for 60 min; to 200 µl ^{89}Zr (37-250 MBq) solution 90 µl 2 M Na_2CO_3 were added, after 3 min 300 µl 0.5 M HEPES buffer (pH 7.0), 710 µl Df-Bz-NCS-mAb (1 - 2 mg) and 700 µl 0.5 M HEPES (pH 7.0) were added. Other pH values were obtained by adjusting the HEPES buffer to chosen pH values. Finally, ^{89}Zr-Df-Bz-NCS-mAb was purified by size exclusion chromatography (PD10 column) using 0.25 M sodium acetate/gentisic acid 5 mg/ml buffer (pH 5.5) or 0.9% sodium chloride/gentisic acid 5 mg/ml (pH 5.0) as the mobile phase.

Preparation of ^{89}Zr-labeled N-sucDf-mAb

As reference to the new method for ^{89}Zr labeling, Df was also coupled to mAbs via the multi-step procedure as previously described by Verel et al. [5] (Figure 1b). In short, the chelate Df was succinylated (N-sucDf), temporarily filled with stable iron [Fe(III)], and coupled to the lysine residues of the mAb (cU36 or cetuximab) by means of a tetrafluorophenol-N-sucDf ester. After removal of Fe(III) by transchelation to EDTA at 35°C, the premodified mAb was purified on a PD10 column. Approximately 1 N-sucDf moiety was coupled per mAb molecule. Subsequently, N-sucDf-mAb was labeled with ^{89}Zr in 0.25 M HEPES buffer at pH 7.0; to 200 µl ^{89}Zr (37-185 MBq) solution 90 µl 2 M Na_2CO_3 were added, after 3 min 300 µl 0.5 M HEPES buffer (pH 7.0), 710 µl N-SucDf-mAb (1 - 2 mg) and 700 µl 0.5 M HEPES (pH 7.0) were added. Finally, ^{89}Zr-N-sucDf-mAb was purified on a PD10 column using 0.9% sodium chloride/gentisic acid 5 mg/ml (pH 5.0) or 0.25 M sodium acetate/gentisic acid 5 mg/ml buffer (pH 5.5) as the mobile phase.

Analyses

After each preparation of ^{89}Zr-labeled Df-Bz-NCS-mAb or N-sucDf-mAb, the conjugates were analyzed by instant thin-layer chromatography (ITLC) for radiolabeling efficiency and radiochemical purity, and by high performance liquid chromatography (HPLC) and sodium dodecyl sulfate-polyacrylamide gel electrophoresis (SDS-PAGE) followed by phosphor imager analyses for integrity, and by a cell-binding assay for immunoreactivity.

ITLC analyses of ^{89}Zr-labelled N-sucDf-mAb or Df-Bz-NCS-mAb was performed on silica gel impregnated glass fiber sheets (Pall Corp., East Hills, NY). As the mobile phase, 0.02 M citrate buffer (pH 5.0) was used.

HPLC monitoring of the final products was performed on a Jasco HPLC system using a Superdex™ 200 10/300 GL size exclusion column (GE Healthcare Life Sciences). As eluent, a mixture of 0.05 M sodium phosphate and 0.15 M sodium chloride (pH 6.8) was used at a flow rate of 0.5 ml/min. Electrophoresis was performed on a Phastgel System (GE Healthcare Life Sciences) using preformed 7.5% SDS-PAGE gels under non-reducing conditions.

The immunoreactivity was determined by measuring binding of ^{89}Zr-cU36, ^{89}Zr-cetuximab, or ^{89}Zr-rituximab (10.000 cpm/ml) to a serial dilution of 0.2% glutaraldehyde-fixed UM-SCC-11B cells or 2% paraformaldehyde-fixed A431, or Ramos cells, respectively, essentially as described by Lindmo et al. [18].

Determination of chelate-to-mAb ratio

The Df-Bz-NCS to mAb molar ratio was determined following a general method as described by Meares et al. [19]. In short, conjugates were labeled according to the aforementioned procedure with a known nanomolar excess of zirconium oxalate solution spiked with ^{89}Zr.

In vitro stability

For assessment of the in vitro stability of ^{89}Zr-Df-Bz-NCS-mAb in comparison with the reference conjugate ^{89}Zr-N-sucDf-mAb, two sets of experiments were performed. In a first set, labeled mAbs were stored at 4°C (storage and transportation conditions) and room temperature in 0.9% NaCl/gentisic acid 5 mg/ml or 0.25 M sodium acetate/gentisic acid 5 mg/ml. Final activity concentration was between 30 – 40 MBq/ml, specific activity was between 67 - 86 MBq/mg mAb. At various time points, aliquots were taken and analyzed by ITLC, SDS-PAGE and HPLC.

In a second set, purified radiolabeled mAbs were added to freshly prepared human serum (1:4 v/v dilution; sodium azide added to 0.02%) at a final concentration of the

radiolabeled conjugates of ~1.3 nmol/ml and ~45 MBq/ml. The samples were incubated at 37°C in a CO_2-enriched atmosphere (5% CO_2). At various time points, aliquots were taken and analyzed by ITLC, SDS-PAGE, and HPLC.

Evaluation of in vivo biodistribution

For assessment of biodistribution and the in vivo stability of the new ^{89}Zr-Df-Bz-NCS-mAb conjugate in comparison with the established ^{89}Zr-N-sucDf–mAb conjugate, two sets of experiments were performed with nude mice bearing subcutaneously implanted human xenografts of the HNSCC line FaDu or the vulvar tumor line A431 at two lateral sides. In one experiment, the moderately internalizing cU36 mAb was tested, in the other the extensively internalizing mAb cetuximab [20]. Female mice (HSD:Athymic Nude-Foxn1^{nu}, 21-31 g; Harlan) were 8 to 10 weeks old at the time of the experiments. All animal experiments were done according to NIH Principles of Laboratory Animal Care and Dutch national law ("Wet op de dierproeven", Stb 1985, 336).

In a first experiment, mice bearing FaDu xenografts (two groups of n=8) were injected intravenously (i.v.) with either ^{89}Zr-Df-Bz-NCS-cU36 (0.38 ± 0.01 MBq) or the reference compound ^{89}Zr-N-sucDf-cU36 (0.38 ± 0.01 MBq). Unlabeled mAb cU36 was added to the injection mixture to bring the total mAb dose to 100 µg per mouse. At 72 and 144 h post injection, four mice of each group were anesthetized, bled, killed, and dissected. After blood, tumor, and normal tissues had been weighed, the amount of radioactivity in each sample was measured in a gamma counter. Radioactivity uptake was calculated as the percentage of the injected dose per gram of tissue (%ID/g).

In a second experiment, mice bearing A431 xenografts (two groups of n=16) were injected i.v. with either ^{89}Zr-Df-Bz-NCS-cetuximab (0.24 ± 0.01 MBq) or the reference compound ^{89}Zr-N-sucDf-cetuximab (0.24 ± 0.01 MBq). Unlabelled cetuximab was added to the injection mixture to bring the total mAb dose to 500 µg per mouse. At 24, 48, 72, and 120 h post injection, four mice of each group were anesthetized, bled, killed, and dissected, with further processing according to the above procedure.

PET study

PET imaging was performed on a double-crystal-layer HRRT PET scanner (Siemens/CTI), a dedicated small animal and human brain scanner, as described earlier [7,21]. FaDu xenograft-bearing nude mice (two groups of n=3) were anesthetized by inhalation of 2% isoflurane, injected with either 4.12 ± 0.04 MBq ^{89}Zr-Df-Bz-NCS-cU36 (~200 µg mAb) or 4.03 ± 0.09 MBq ^{89}Zr-N-sucDf-cU36 (~200 µg mAb) via the retroorbital plexus, and scanned

at 72h post-injection.

Transmission scans for attenuation and scatter correction were routinely obtained with each scan in two-dimensional mode using a single point ^{137}Cs source. Three-dimensional emission scans were acquired in 64-bit list mode during 60 min using a 400-650 keV window. The 64-bit list mode file was first converted into a single-frame histogram using a span of 9, and subsequently reconstructed using a 3D ANW-OSEM reconstruction algorithm with 2 iterations and 16 subsets and a matrix size of 256x256, including corrections for normalization, decay and dead time. For visualization of the images, Amide's A Medical Imaging Data Examiner (AMIDE) was used, freely available for download online [22]. Immediately after the PET scan the animals were killed, blood, tumors, major organs and tissues were collected, weighed, and counted in a gamma-counter.

Statistical analyses

Differences in tissue uptake between injected conjugates were statistically analyzed for each time point with SPSS 15.0 software using Student t-test for unpaired data. Two-sided significance levels were calculated and $P < 0.01$ was considered statistically significant.

Results

Preparation of ^{89}Zr-Df-Bz-NCS-mAb

^{89}Zr-Df-Bz-NCS-mAb was prepared according to the chemical route as shown in Figure 1a. First, Df-Bz-NCS is coupled to the lysine groups of a mAb. Conjugation conditions selected for this step comprised the addition of a three-fold molar excess of Df-Bz-NCS to the mAb solution (13 - 66 nmol mAb), a reaction pH of 9.0, and incubation for 30 min at 37°C. These conditions resulted in a reproducible chelate:mAb substitution ratio of about 1.5:1, irrespective cU36, cetuximab or rituximab was used, as assessed by trace labeling with ^{89}Zr in a standard solution of Zr-oxalate.

In the next step, Df-Bz-NCS-mAbs were labeled with ^{89}Zr in HEPES buffer (final concentration 0.25 M). After 60 min incubation at room temperature at pH 6.8 – 7.2, the amount of ^{89}Zr trans-chelated from oxalate to Df-Bz-NCS-mAb was always more than 85% (mean, 91.9±4.6%). The time courses of ^{89}Zr-complexation of mAb cU36 conjugated with Df-Bz-NCS at different pHs are shown in Figure 2. Labeling efficiency was distinctly higher at pH 6.8 and 7.2 than at pH 6.0, 6.2 and 7.4.

Labeling of mAb cU36, cetuximab or rituximab modified with Df-Bz-NCS resulted

in overall yields after purification of always >80% (mean, 87.0±4.6%). The radiochemical purity was always >95% (mean, 97.5±0.7%; determined with ITLC and confirmed by HPLC). The immunoreactive fraction of the different ^{89}Zr-Df-Bz-NCS-mAb preparations ranged from 84.1% to 96.8% at the highest cell concentration, and was similar to those of their ^{131}I-labelled counterparts (data not shown). HPLC and SDS-PAGE analyses revealed optimal integrity of the different mAbs after modification and labeling with ^{89}Zr (data not shown).

Evaluation of in vitro stability

^{89}Zr-labeled Df-Bz-NCS-mAb and N-sucDf-mAb conjugates were both stored in 0.9% NaCl/gentisic acid 5 mg/ml and in 0.25 M sodium acetate/gentisic acid 5 mg/ml at 4°C over several days to evaluate the in vitro stability. To anticipate effects of insufficient cooling, the conjugates were also analyzed after storage at room temperature (21°C). Storing the ^{89}Zr-Df-Bz-NCS-mAb conjugates in 0.25 M sodium acetate/gentisic acid 5 mg/ml buffer (pH 5.5) at 4°C gave the best results; only 0.9±0.4% of the initially bound ^{89}Zr was dissociated from the mAb after 48 h, and 4.1±1.3% after 144 h. Upon storage in the same buffer at room temperature (21°C), 6.1±1.4% and 10.5 ± 2.1% was dissociated after 48 h and 144 h, respectively. Also upon storage in 0.9% NaCl/gentisic acid 5 mg/ml (pH 5.0) at 4°C the radioimmunoconjugates remained reasonably stable, showing 13.2±2.8% dissociation after 144 h. However, storage in the same buffer at room temperature resulted in rapid release of radioactivity from the conjugate, 48.4±5.7%. The corresponding ^{89}Zr-N-SucDf-mAb conjugates remained very stable, showing less than 5% release after 144 h under all conditions investigated.

The in vitro stability data for the ^{89}Zr-Df-Bz-NCS-cU36 and ^{89}Zr-N-sucDf-cU36 conjugates, when incubated in freshly prepared human serum at 37°C, showed that loss of ^{89}Zr from both conjugates over a 7 day period was very small. The percentages dissociated at day 3 were 2.3±0.1% for the Df-Bz-NCS conjugate and 3.4±0.6% for the N-sucDf conjugate, and at day 7 were 4.0±0.6% for the Df-Bz-NCS conjugate and 4.7±0.5% for the N-sucDf conjugate, respectively.

Evaluation of the in vivo biodistribution

Two sets of biodistribution studies were performed. In the first experiment, ^{89}Zr-Df-Bz-NCS-cU36 and the reference compound ^{89}Zr-N-sucDf-cU36 were injected into FaDu-bearing nude mice. At 72 and 144 h after injection, the average %ID/g of tumor, blood, normal tissue, and gastrointestinal contents was determined (Figure 3). No significant differences in the biodistribution of both conjugates were found.

Only a minor proportion of mAb cU36 internalizes after binding to its target

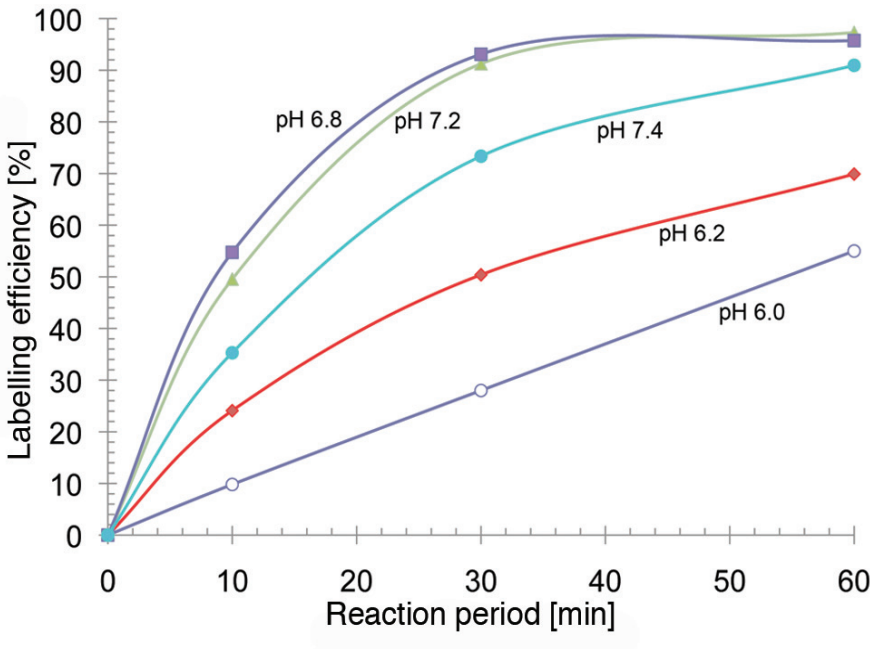

Figure 2. Time course of ^{89}Zr complexation of mAb cU36 conjugated with Df-Bz-NCS at different pH and at room temperature.

antigen, therefore in the second biodistribution study the anti-EGFR mAb cetuximab was chosen because of the high rate of internalization. ^{89}Zr-Df-Bz-NCS-cetuximab and the reference compound ^{89}Zr-N-sucDf-cetuximab were injected into A431-bearing nude mice. At 24, 48, 72, and 120 h after injection, the average %ID/g of tumor, blood, normal tissue, and gastrointestinal contents was determined (Figure 4). The overall biodistribution of the two radioimmunoconjugates was very similar, showing no significant differences except for blood levels at 24 and 120 h after injection (Figure 4; significant differences ($P<0.01$) are indicated with an asterisk). The ^{89}Zr-Df-Bz-NCS-cetuximab tumor accumulation ranged from 15.6±4.4 %ID/g to 23.1±7.1 %ID/g and the ^{89}Zr-N-sucDf-cetuximab accumulation from 12.3±3.2 %ID/g to 25.3±6.1 %ID/g, in the time period between 24 and 120 h post injection.

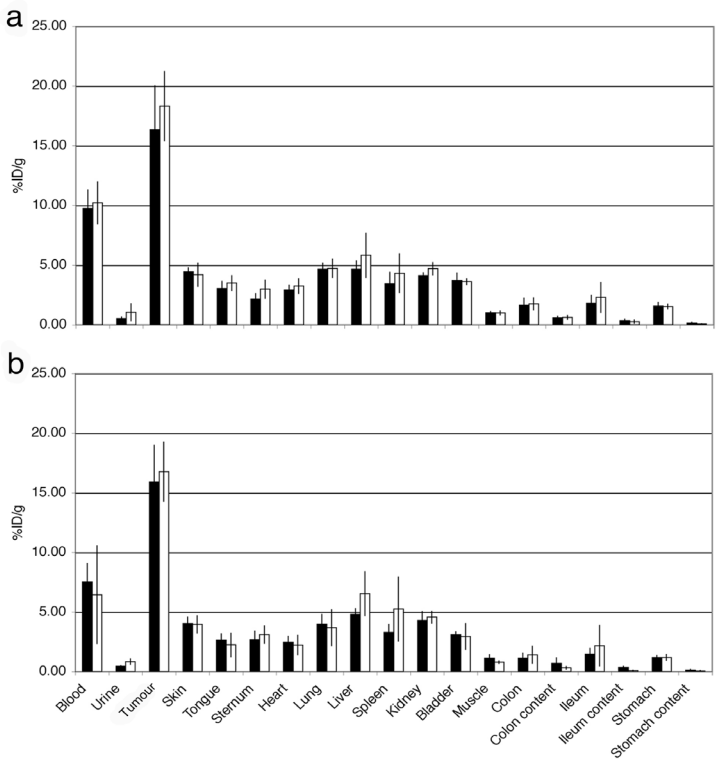

Figure 3. Biodistribution of ^{89}Zr-Df-Bz-NCS-cU36 (*black bars*) amd ^{89}Zr-*N*-sucDf-cU36 (*white bars*) in FaDu tumor-bearing nude mice at 72 h (**a**) and 114 h (**b**) after injection. Total administered mAb dose: 100 µg. Mean (%ID/g) ±SD at each time point after injection (n=4 animals per time point for each conjugate)

PET study

To exclude ^{89}Zr uptake in tissues not evaluated in the biodistribution experiments, a PET imaging study was performed. Representative PET images of FaDu xenograft-bearing nude mice at 72 h after injection with ^{89}Zr-Df-Bz-NCS-cU36 or ^{89}Zr-N-sucDf-cU36 are shown in Figure 5a and 5b, respectively. Immuno-PET with both radioimmunoconjugates revealed clear delineation of the tumors (arrows), whereas no prominent uptake of radioactivity was observed in other tissues, except for the liver in which ^{89}Zr residualizes after catabolism of the conjugates.

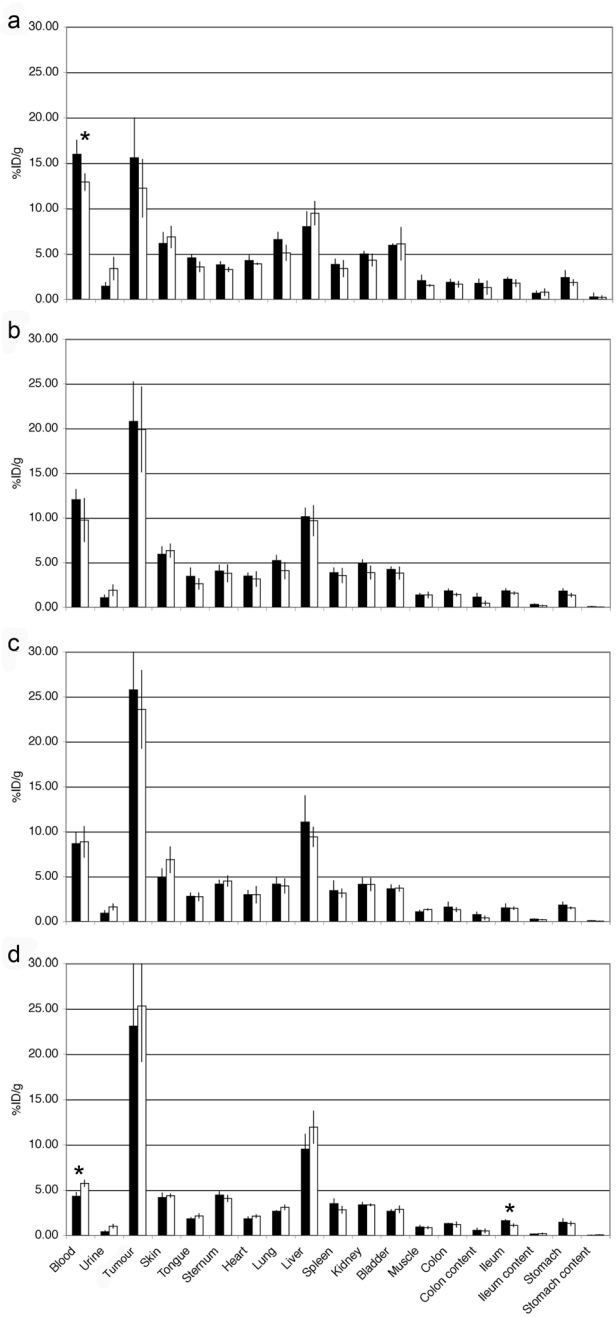

Figure 4. Biodistribution of ^{89}Zr-Df-Bz-NCS-cetuximab (black bars) and ^{89}Zr-*N*-sucDe-cetuximab (white bars) in A431 tumor-bearing nude mice at 24 h (**a**), 48 h (**b**), 72 h (**c**), and 120 h (**d**) after injection. Total administered mAb dose: 500 µg. Mean (%ID/g) ±SD at each time point after injection (n=4 animals per time point for each conjugate). Significant differnces (P<0.01) in biodistribuition between both radrioimmunoconjugates are marked with an *asterisk*.

Discussion

Immuno-PET, the tracking and quantification of mAbs and mAb-fragments with PET in vivo, is an emerging novel option to improve diagnostics and to guide mAb-based therapy [2-4]. Availability of positron emitters with a proper half-life, simple and robust radiochemistry, and advanced animal as well as clinical PET and PET-CT scanners, is crucial in these developments.

In the present report, we have described a method for labeling mAbs with the long-lived positron emitter ^{89}Zr using the novel bifunctional chelate Df-Bz-NCS. ^{89}Zr has attractive characteristics for immuno-PET with intact mAbs, especially when these mAbs become internalized upon binding to their cellular target. Radioimmunoconjugates produced by this method were stable in storage buffer as well as in human serum in vitro. Biodistribution and imaging experiments showed high and selective accumulation in tumors in nude mice.

The chelate Df has frequently been used for radiolabeling of mAbs in the past, but these conjugates have never been evaluated clinically [23-26]. More recently, Verel et al. [5] developed a sophisticated method for stable coupling of ^{89}Zr to mAbs using a succinylated-derivative of Df, which was used as the reference method in the present study (Figure 1b). ^{89}Zr-labelled mAbs prepared according to this method have been successfully tested preclinically and clinically [6-13]. In the past and ongoing clinical studies, neither adverse reactions nor significant changes in blood and urine values were observed after injection of these conjugates. Moreover, no antibody responses directed against the Df chelate were observed indicating that its immunogenicity is low [8]. These data illustrate that ^{89}Zr-labeled Df-mAbs can be used safely in patients. However, a shortcoming of the aforementioned method is that the multi-step procedure is relatively complicated and time consuming, and therefore challenging with respect to GMP compliance.

Now we introduce p-isothiocyanatobenzyl-derivative of Df (Df-Bz-NCS) that might provide an efficient and rapid preparation of ^{89}Zr-labelled mAbs. Bifunctional chelates bearing isothiocyanate as the reactive group for conjugation to mAbs or other biologicals are frequently used [27]. The isothiocyanate group of the bifunctional chelate forms a thiourea bond with a primary amine of the protein or mAb.

Coupling of Df-Bz-NCS to mAbs was very efficient. A reproducible chelate:mAb substitution ratio of 1.5:1 was obtained in a typical conjugation reaction with several different mAbs using only a three-fold molar excess of Df-Bz-NCS. The chelate:mAb substitution ratio was chosen to be kept below 2, to avoid alteration of the pharmacokinetics

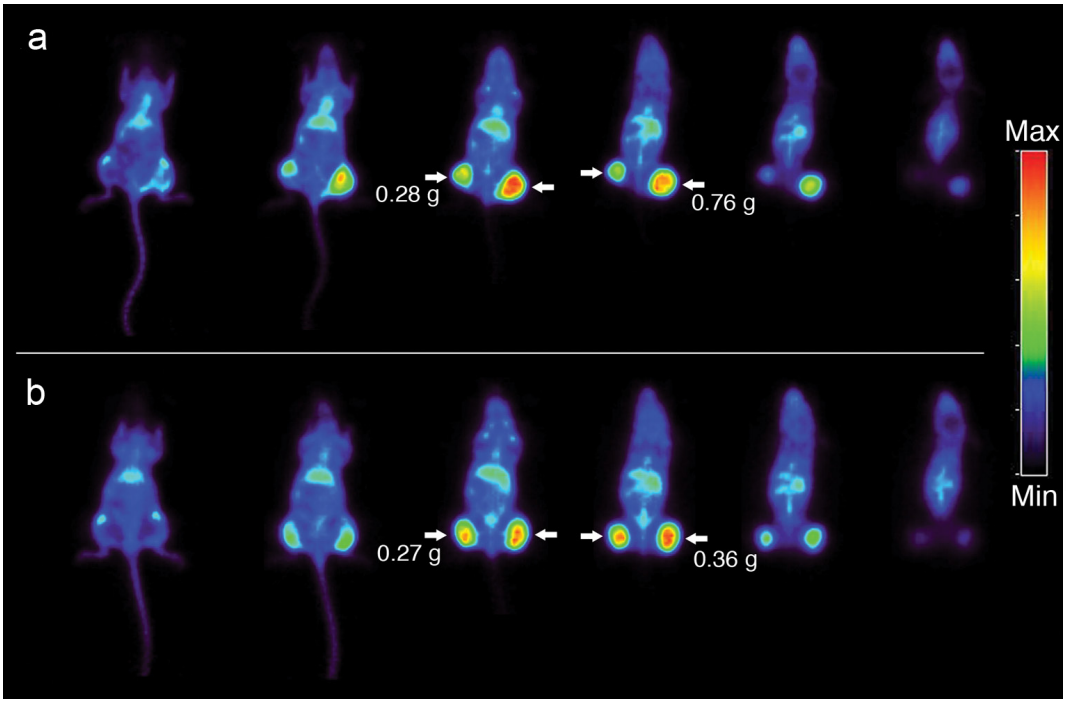

Figure 5. HRRT PET images (coronal slices) of two different FaDu xenograft-bearing nude mice at 72 h after injection with ^{89}Zr-Df-Bz-NCS-cU36 (**a**) or with ^{89}Zr-*N*-sucDf-cU36 (**b**). Slices from ventral (*left*) to dorsal (*right*). Images demonstrate high level of radiolabeled antibody accumulating in the tumor (arrows point to flank tumors) and low levels of tracer uptake in nontarget tissues

and immunoreactivity of the mAb [28, 29].

The rate of complexation of ^{89}Zr into the Df-Bz-NCS conjugate was very similar as compared to the reference N-sucDf conjugate reported by Verel et al. [5], indicating that the different chemical linkages (e.g. =S instead of =O group in the side chain which might be involved in $^{89}Zr^{4+}$ coordination) have no influence on the complexation rate. At the pH-optimum, almost quantitative complexation was reached after 30 minutes at room temperature. The resulting radioimmunoconjugates showed no impairment of immunoreactivity and integrity of the mAbs.

Radioimmunoconjugates were stored in various media to find the optimal conditions for storage and transportation over several days. The ^{89}Zr-Df-Bz-NCS-mAb can best be stored at 4°C in sodium acetate buffer in presence of the antioxidant gentisic acid. Under these conditions, only a minor portion of the initially bound ^{89}Zr was dissociated from the mAb after 144 h. The need for protection of the radioimmunoconjugate against radiation damage during storage has been shown in previous studies [5, 30]. The presence

of the antioxidant ascorbic acid during storage of high-dose ^{90}Y- or ^{131}I-labelled mAbs proved to be beneficial, however, ascorbic acid cannot be used during storage of ^{89}Zr-labelled Df-mAbs, because this reagent causes detachment of ^{89}Zr from Df by reducing Zr^{4+} to Zr^{2+} [5].

Under certain storage conditions, the new ^{89}Zr-Df-Bz-NCS conjugate is slightly less stable than the reference radioimmunoconjugate, and it is important to be aware of this. Especially, the presence of Cl^--ions in the storage buffer impaired the integrity of the radioimmunoconjugates, most likely due to the radiation-induced formation of OCl^--ions reacting with the SH-group of the enolised thiourea-unit. The thus formed intermediary sulphenyl chloride bonds, and sulphonyl chloride bonds arising upon further oxidation, are known to undergo a series of reactions, among which are coupling reactions and cleavage of methionyl peptide bonds. ITLC data also indicated that most of the deterioration is not detachment of ^{89}Zr from the Df-chelate itself, but disruption of the Zr-Df unit.

The in vitro stability of the ^{89}Zr-Df-Bz-NCS conjugate and the ^{89}Zr-N-sucDf conjugate was also compared in freshly prepared human serum at 37°C. The stability of both conjugates under these conditions was very comparable and high, showing less than 4.7% release after a 7 days incubation period. Serum acts as an oxidisable scavenger and protects against directs hits to the mAb molecule, minimizing the radiation-induced deterioration of the mAb. Comparable in vitro stability data of ^{89}Zr-N-sucDf conjugates were previously reported by our group [20].

To investigate whether the new linker used for coupling of Df to the mAbs affects the biodistribution properties in mice, two sets of biodistribution experiments were performed. In the first experiment, the biodistribution of ^{89}Zr-Df-Bz-NCS-cU36 and the reference compound ^{89}Zr-N-sucDf-cU36 was compared in FaDu-bearing nude mice. In this model, no significant differences in the biodistribution between both conjugates were found. However, only a minor proportion of mAb cU36 internalizes after binding to its target antigen, therefore in the second biodistribution study the anti-EGFR mAb cetuximab was chosen because of the high rate of internalization [20]. Also in this model, a very similar biodistribution was found. Although, some significant differences were found, e.g. blood levels at 24 and 120 h after injection. Overall, both studies indicate that the different linkers used do not affect the biodistribution properties in nude mice. Moreover, none of the normal organs showed an adverse high uptake. The aforementioned results were confirmed in comparative immuno-PET studies with both chelates. PET images did not show accumulation of radioactivity in bone, which would have been indicative of free ^{89}Zr.

Conclusions

In the present study we evaluated the newly developed bifunctional chelate Df-Bz-NCS for radiolabeling of mAbs with ^{89}Zr for PET-imaging. The two-step procedure allows efficient and rapid preparation of ^{89}Zr-labeled mAbs. Resulting ^{89}Zr-Df-Bz-NCS-mAb conjugates appeared optimal with respect to radiochemical purity, integrity, and immunoreactivity. Furthermore, the radioimmunoconjugates were stable in serum in vitro and comparative biodistribution and imaging experiments showed high and selective accumulation in tumors in nude mice. Special emphasis should be given to the storage conditions. The recent commercialization of ^{89}Zr and the availability of an easy-to-use radiolabeling strategy using Df-Bz-NCS allow further exploration of ^{89}Zr-immuno-PET as an imaging tool for the selection of high potential candidate mAbs for therapy as well as for the selection of patients with the highest chance of benefit from mAb-based therapy [2].

Acknowledgments

This project was financially supported by the Dutch Technology Foundation (STW, grants VBC.6120 and 10074) and partly supported by the European Union FP7, ADAMANT. The publication reflects only the authors' view. The European Commission is not liable for any use that may be made of the information contained. The authors thank the technical staff of BV Cyclotron VU and the Radionuclide Centre for supply and processing of ^{89}Zr, Marc Huisman for PET analyses, and Marijke Stigter-van Walsum for technical assistance with animal studies.

References

1. Carter PJ. Potent antibody therapeutics by design. Nat Rev Immunol 2006;6:343-57.

2. van Dongen GAMS, Visser GWM, Lub-de Hooge MN, de Vries EG, Perk LR. Immuno-PET: a navigator in monoclonal antibody development and applications. Oncologist 2007 ;12:1379-89.

3. Wu AM. Antibodies and antimatter: the resurgence of immuno-PET. J Nucl Med 2009;50:2-5.

4. Nayak TK, Brechbiel MW. Radioimmunoimaging with longer-lived positron-emitting radionuclides: Potentials and Challenges. Bioconjug Chem 2009.

5. Verel I, Visser GWM, Boellaard R, Stigter-van Walsum M, Snow GB, van Dongen GAMS. ^{89}Zr immuno-PET: comprehensive procedures for the production of ^{89}Zr-labeled monoclonal antibodies. J Nucl Med 2003;44:1271-1281.

6. Dijkers E, Lub-de Hooge MN, Kosterink JG et al. Characterization of ^{89}Zr-trastuzumab for clinical HER2 immunoPET imaging. J Clin Oncol (meeting abstracts) 2007;25:3508.

7. Perk LR, Stigter-van Walsum M, Visser GWM et al. Quantitative PET imaging of Met-expressing human cancer xenografts with ^{89}Zr-labelled monoclonal antibody DN30. Eur J Nucl Med Mol Imaging 2008;35:1857-67.

8. Borjesson PKE, Jauw YWS, Boellaard R et al. Performance of immuno-positron emission tomography with zirconium-89-labeled chimeric monoclonal antibody U36 in the detection of lymph node metastases in head and neck cancer patients. Clin Cancer Res 2006;12:2133-40.

9. Nagengast WB, de Vries EG, Hospers GA et al. In vivo VEGF imaging with radiolabeled bevacizumab in a human ovarian tumor xenograft. J Nucl Med 2007;48:1313-19.

10. Verel I, Visser GWM, Boerman OC et al. Long-lived positron emitters zirconium-89 and iodine-124 for scouting of therapeutic radioimmunoconjugates with PET. Cancer Biother Radiopharm 2003;18:655-61.

11. Verel I, Visser GWM, Boellaard R et al. Quantitative ^{89}Zr immuno-PET for in vivo scouting of ^{90}Y-labeled monoclonal antibodies in xenograft-bearing nude mice. J Nucl Med 2003;44:1663-70.

12. Brouwers A, Verel I, Van Eerd J et al. PET radioimmunoscintigraphy of renal cell cancer using ^{89}Zr-labeled cG250 monoclonal antibody in nude rats. Cancer Biother Radiopharm 2004;19:155-63.

13. Perk LR, Visser OJ, Stigter-van Walsum M et al. Preparation and evaluation of ^{89}Zr-Zevalin for monitoring of ^{90}Y-Zevalin biodistribution with positron emission tomography. Eur J Nucl Med Mol Imaging 2006;33:1337-45.

14. Mendelsohn J, Baselga J. Epidermal growth factor receptor targeting in cancer. Semin Oncol 2006;33:369-85.

15. Schrijvers AH, Quak JJ, Uyterlinde AM et al. MAb U36, a novel monoclonal antibody successful in immunotargeting of squamous cell carcinoma of the head and neck. Cancer Res 1993;53:4383-90.

16. Rangan SR. A new human cell line (FaDu) from a hypopharyngeal carcinoma. Cancer 1972;29:117-21.

17. Welters MJ, Fichtinger-Schepman AM, Baan RA et al. Relationship between the parameters cellular differentiation, doubling time and platinum accumulation and cisplatin sensitivity in a panel of head and neck cancer cell lines. Int J Cancer 1997;71:410-15.

18. Lindmo T, Boven E, Cuttitta F, Fedoroko J, Bunn PA Jr. Determination of the immunoreactive fraction of radiolabeled monoclonal antibodies by linear extrapolation to binding at infinite antigen excess. J Immunol Methods 1984;72:77-89.

19. Meares CF, McCall MJ, Reardan DT, Goodwin DA, Diamanti CI, McTique M. Conjugation of antibodies with bifunctional chelating agents: isothiocyanate and bromoacetamide reagents, methods of analysis, and subsequent addition of metal ions. Anal Biochem 1984;142:68-78.

20. Perk LR, Visser GWM, Vosjan MJWD et al. ^{89}Zr as a PET surrogate radioisotope for scouting biodistribution of the therapeutic radiometals ^{90}Y and ^{177}Lu in tumor-bearing nude mice after coupling to the internalizing antibody cetuximab. J Nucl Med 2005;46:1898-06.

21. de Jong HWAM, van Velden FHP, Kloet RW, Buijs FL, Boellaard R, Lammertsma AA. Performance evaluation of the ECAT HRRT: an LSO-LYSO double layer high resolution, high sensitivity scanner. Phys Med Biol 2007;52:1505-26.

22. Loening AM, Gambhir SS. AMIDE: a free software tool for multimodality medical image analysis. Mol Imaging 2003;2:131-37.

23. Yokoyama A, Ohmomo Y, Horiuchi K et al. Deferoxamine, a promising bifunctional chelating agent for labeling proteins with gallium: Ga-67 DF-HSA: concise communication. J Nucl Med 1982;23:909-14.

24. Koizumi M, Endo K, Kunimatsu M et al. ^{67}Ga-labeled antibodies for immunoscintigraphy and evaluation of tumor targeting of drug-antibody conjugates in mice. Cancer Res 1988;48:1189-94.

25. Pochon S, Buchegger F, Pelegrin A et al. A novel derivative of the chelon desferrioxamine for site-specific conjugation to antibodies. Int J Cancer 1989;43:1188-94.

26. Meijs WE, Haisma HJ, Klok RP et al. Zirconium-labeled monoclonal antibodies and their distribution in tumor-bearing nude mice. J Nucl Med 1997;38:112-18.

27. Liu S. Bifunctional coupling agents for radiolabeling of biomolecules and target-specific delivery of metallic radionuclides. Adv Drug Deliv Rev 2008;60:1347-70.

28. van Gog FB, Visser GWM, Klok RP, van der Schors R, Snow GB, van Dongen GAMS. Monoclonal antibodies labeled with rhenium-186 using the MAG3 chelate: relationship between the number of chelated groups and biodistribution characteristics. J Nucl Med 1996;37:352-62.

29. Kukis DL, DeNardo GL, DeNardo SJ et al. Effect of the extent of chelate substitution on the immunoreactivity and biodistribution of 2IT-BAT-Lym-1 immunoconjugates. Cancer Res 1995;55:878-84.

30. Chakrabarti MC, Le N, Paik CH, De Graff WG, Carrasquillo JA . Prevention of radiolysis of monoclonal antibody during labeling. J Nucl Med 1996;37:1384-88.

Chapter 3:

3

Conjugation and radiolabeling of monoclonal antibodies with zirconium-89 for PET imaging using the bifunctional chelate p-isothiocyanatobenzyl-desferrioxamine

Maria J.W.D. Vosjan
Lars R. Perk
Gerard W.M. Visser
Marianne Budde
Paul Jurek
Garry E. Kiefer
Guus A.M.S. van Dongen

Nature Protocols (2010) 4:739-743

Abstract

The positron emitter zirconium-89 (^{89}Zr) has very attractive properties for positron emission tomography (PET) imaging of intact monoclonal antibodies (mAbs) using immuno-PET. This protocol describes the step-by-step procedure for the facile radiolabeling of mAbs or other proteins with ^{89}Zr using p-isothiocyanatobenzyl-desferrioxamine (Df-Bz-NCS). First, Df-Bz-NCS is coupled to the lysine–NH_2 groups of a mAb at pH9.0 (pre-modification), followed by purification using gel filtration. Next, the premodified mAb is labeled at room temperature by addition of a [^{89}Zr]Zr-oxalic acid solution followed by purification using gel filtration. The entire process of premodification, radiolabeling and purification steps will take about 2.5 h.

Introduction

At present, hundreds of monoclonal antibodies (mAbs) and mAb fragments are under clinical development because of their excellent potential for the systemic treatment of cancer and other pathological conditions[1,2]. Positron emission tomography (PET) offers an attractive imaging option: (1) to confirm and quantify tumor uptake of such targeting molecules; (2) to learn about uptake in critical normal organs to anticipate toxicity; and (3) to elucidate the inter-patient variations in pharmacokinetics and tumor targeting[3-6].

For PET imaging of mAbs (immuno-PET), an appropriate positron emitter, with a half-life ($t_{½}$) that is compatible with the time needed to achieve optimal tumor-to-non tumor ratios (typically 2-4 days for intact mAbs), has to be securely coupled to the targeting molecule. Therefore, zirconium-89 (^{89}Zr; $t_{½}$: 78.4 h) was selected. Other positron emitters for immuno-PET are under investigation at the moment: gallium-68 (^{68}Ga; $t_{½}$:1.13 h), fluorine-18 (^{18}F; $t_{½}$:1.83 h), copper-64 (^{64}Cu; $t_{½}$:12.7 h), yttrium-86 (^{86}Y; $t_{½}$:14.7 h), bromine-76 (^{76}Br; $t_{½}$:16.2 h), and iodine-124 (^{124}I; $t_{½}$:100.3 h)[3-6].

We recently described the large scale production of radionuclidic pure ^{89}Zr (specific activity ≥0.15 GBq nmol^{-1}) with a small cyclotron (^{89}Y-target; E_p 14 MeV), and a strategy for labeling mAbs with ^{89}Zr via a multi-step synthesis using a succinylated-derivative of desferrioxamine B (Df) as bifunctional chelate[7]. The utility of this approach was demonstrated through high quality ^{89}Zr-mAb-PET images and quantification results reported in preclinical[8-12] and clinical studies[5-11]. In these studies, typically 370 kBq and 37-74 MBq ^{89}Zr-mAb was used for immuno-PET in mice and humans, respectively. In both preclinical and clinical studies neither pharmacokinetic changes nor aspecific accumulation in non-target organs were observed, except for uptake in catabolic organs like liver and kidneys. The only concern is the high radiation dose to the patient, which is inherent to the use of long-lived positron emitters like ^{89}Zr and ^{124}I, and might limit repeated application of ^{89}Zr-immuno-PET[15]. Df is an attractive chelate because it is used clinically in a safe way for many years[13,15-17]. The recent commercialization of ^{89}Zr makes this radionuclide generally available for research and clinical development. (see Materials).

A shortcoming of the aforementioned approach is that the multi-step procedure, extensively described by Verel et al.[7], is relatively complicated and time consuming. In this protocol we present an efficient and more rapid preparation of ^{89}Zr-labeled mAbs using the newly developed p-isothiocyanatobenzyl-derivative of Df (Df-Bz-NCS; Macrocyclics)[18]. First, Df-Bz-NCS is coupled to the lysine-NH_2 groups of a protein at pH 9.0, followed by purification using gel filtration. Next, the pre-modified mAb is labeled at room temperature by addition of a [^{89}Zr]Zr-oxalic acid solution followed by purification using gel filtration. For

this preparation there is no need to work under strict metal-free conditions and neither is it necessary to remove trace metal ions from the solutions like in other chelate chemistry (e.g., DOTA and DTPA). When mAb fragments instead of complete antibodies are used, this protocol can still be used, maintaining the same molar ratios of reagents as described herein.

There is an earlier version of this protocol (ref number, http://www.natureprotocols.com/2008/01/24/facile_radiolabeling_of_monocl.php) present in the community generated section of our site (http://protocols.nature.com/user/login). Since then, this method has been used in published primary research (Perk et al.[18]), and this version has been peer-reviewed.

Df-Bz-NCS is also a very convenient bifunctional chelate for labeling of proteins at room temperature with gallium-68 (^{68}Ga; $t_{½}$: 1.13 h) (M.J.W.D.V. and G.A.M.S.v.D., unpublished observations). ^{68}Ga is especially attractive for PET imaging of fast kinetic targeting proteins like mAb fragments, but this is not part of the present protocol.

The procedure described is for mAbs and mAb fragments like Nanobodies[19] (www.ablynx.com) but can also be used for other proteins in the mass range 2-10 mg, provided the same molar ratios of reagents are applied. A schematic representation of the procedure is shown in Figure 1.

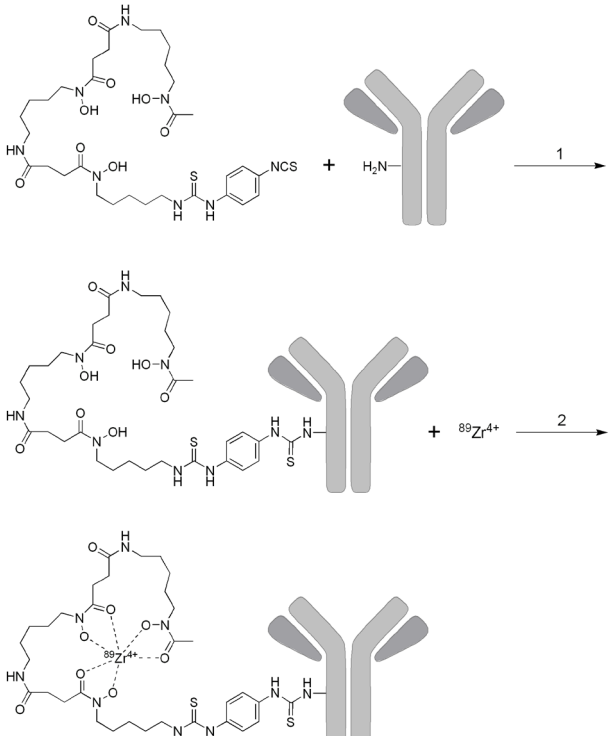

Figure 1. Schematic representation of monoclonal antibody (mAb) modification with Df-Bz-NCS (1) and subsequent labeling with ^{89}Zr (2).

Materials

REAGENTS

CRITICIAL Special actions need not to be taken regarding working under metal-free conditions. Trace metal ions need not to be removed from the solutions.

- Antibody or protein to be conjugated (typically 2-10 mg)
- Df-Bz-NCS (molecular weight=752.9 g mol^{-1}; Macrocyclics, cat. no. B-705)
- Distilled, deionized water (Milli-Q; greater than 18 MΩ*cm resistance)
- DMSO (Aldrich, cat. no. 494429)
- Sodium carbonate; 0.1 M and 2.0 M solutions in water (Aldrich, cat. no. 204420)
- Normal (0.9%) saline (B.Braun, cat. no. 5/12251178/1197)
- Gentisic acid (Fluka, cat. no. 37550)
- Oxalic acid; 1.0 M solution in water (Fluka, cat. no. 75688)
- HEPES buffer solution (Invitrogen, cat. no. 15630-049; see REAGENT SETUP)
- Sodium hydroxide (NaOH); 1.0 M solution in water (Riedel-de Haën, cat. no. 30620)
- Sulfuric acid solution (Merck, cat. no. 1.00714.1000)
- Citric acid monohydrate (Fluka, cat. no. 27491)
- Sodium acetate trihydrate (Fluka, cat. no. 71190)
- Gentisic acid 5 mg ml^{-1} in 0.25 M sodium acetate (pH5.4-5.6)
  (see REAGENT SETUP) CRITICAL: prepare fresh on the day of use
- Sodium dihydrogen phosphate monohydrate (Merck, cat. no. 1.06346.0500)
- Disodium hydrogen phosphate anhydrous (Merck, cat. no. 1.06566.0100)
- Sodium chloride (Merck, cat. no. 1.06404.0500)
- Sodium azide (Merck, cat. no. 1.06688.0100) CAUTION Highly toxic
- Instant Thin Layer Chromatography strips (ITLC) eluent (see REAGENT SETUP)
- High-Performance Liquid Chromatograph (HPLC) eluent (see REAGENT SETUP)
- [^{89}Zr]Zr-oxalate in 1.0 M oxalic acid (≥ 0.15 GBq $nmol^{-1}$) (IBA Molecular)

CAUTION: ^{89}Zr emits positrons and gamma rays. It is imperative that researchers follow the guidelines set forth by their institution and the Nuclear Regulatory Commission, and ALARA (As Low As Reasonably Achievable) protocols to minimize exposure to emitted radiation. Proper protective equipment, shielding, ring and body dosimetry badges and a contamination monitor are required when handling any radioactive materials.

EQUIPMENT

- Calibrated pH meter, with Biotrode (Hamilton, cat. no. 238140)
- Eppendorf tubes, Protein LoBind Tubes, 1.5 ml (Eppendorf, cat. no. 0030 108.116)

- Shaker
- Disposable PD-10 desalting columns (GE Healthcare Life Sciences, cat. no. 17-0851-01)
- Thermomixer comfort (Eppendorf, cat. no. 5355 000.011)
- Sterile/clean glass reaction vials, 20 ml
- ITLC strips (Biodex, cat. no. 150-771)
- HPLC with a UV and a g-detector connected in series
- HPLC column: size exclusion Superdex™ 200 10/300 GL (GE Healthcare Life Sciences, cat. no. 17-5175-01)
- 0.45 µm filter for HPLC eluent (Millipore, cat. no. HVLP04700)
- SDS-PAGE system, Phastgel system; (GE Healthcare Life Sciences, cat. no 18-1200-10)

REAGENT SETUP

Gentisic acid 5 mg ml^{-1} in 0.25 M sodium acetate buffer (pH 5.4-5.6) Dissolve 3.4 g sodium acetate trihydrate and 0.5 g gentisic acid in 100 ml Milli-Q. Mix well and check the pH. Acceptance range: pH 5.4-5.6.

0.5 M HEPES buffer (pH 7.1-7.3) Add 18 ml of Milli-Q to 20 ml 1 M HEPES solution. Check pH. If pH < 7.1 adjust pH with 1 M NaOH, if pH > 7.3 adjust pH with 1 M H_2SO_4. Adjust volume to 40 ml with Milli-Q.

ITLC eluent (pH 4.9-5.1) Dissolve 420 mg citric acid monohydrate in 100 ml Milli-Q water, add 0.98 ml 2.0 M sodium carbonate. Mix well and check the pH. Acceptance range: pH 4.9-5.1.

HPLC eluent (pH 6.2-7.0) Dissolve 13.8 g of sodium dihydrogen phosphate monohydrate, 14.2 g of disodium hydrogen phosphate, 17.4 g of sodium chloride, and 1.3 g of sodium azide in 2 l of water. Mix well and check the pH. Acceptance range: pH 6.2-7.0. Pass the eluent through a Millipore filter and degas before use.

EQUIPMENT SETUP

HPLC method for quality control Turn the UV detector on and equilibrate the HPLC-column using the described HPLC eluent, flow 0.5 ml min^{-1} for at least 30 min prior to injection of the sample. The blank run is an injection with PD-10 column eluent (5 mg ml^{-1} gentisic acid in 0.25 M sodium acetate pH 5.4 -5.6).

A typical quality control run for a labeled ^{89}Zr-mAb is 20 µl injection on Superdex™ 200 10/300 GL column, flow 0.5 ml min^{-1}; R_t mAb =~25 min; R_t unbound ^{89}Zr =~45min.

Procedure

Coupling of the bifunctional chelate (TIMING 50 min)

1. Pipette the required amount of mAb solution (max. 1 ml; by preference between 2 and 10 mg ml^{-1} mAb) into an Eppendorf tube. Adjust the reaction mixture to a total volume of 1 ml by adding a sufficient amount of normal saline into the tube.

CRITICAL STEP Concentrations lower than 2 mg ml^{-1} will decrease the efficiency of the conjugation reaction, resulting in lower Df-mAb molar ratio.

2. Adjust pH of the mAb solution to pH 8.9 – 9.1 with 0.1 M Na_2CO_3 (max. 0.1 ml).
CRITICAL STEP Alternatively, the desired pH for the reaction can be obtained by performing a buffer exchange of the mAb stock solution against 0.1 M sodium bicarbonate buffer (pH9.0).

3. Dissolve Df-Bz-NCS in DMSO at a concentration between 2 and 5 mM (1.5-3.8 mg ml^{-1}) depending on the amount of mAb used. Add this to the protein solution to give a three-fold molar excess of the chelator over the molar amount of mAb and mix immediately. Keep the DMSO concentration below 2% in the reaction mixture.
CRITICAL STEP Typically, 20 µl (in steps of 5 µl) 2-10 mM Df-Bz-NCS (40-200 nmol) in DMSO is added to 2-10 mg intact antibody (13.2-66 nmol). In those cases, between 0.3-0.9 Df moieties will be coupled per antibody molecule[18].

4. Incubate the reaction for 30 min at 37°C using a Thermomixer at 550 rpm.

5. In the mean time rinse a PD-10 column with 20 ml 5 mg ml^{-1} gentisic acid in 0.25 M sodium acetate (pH 5.4-5.6).

6. Pipette the conjugation reaction mixture onto the PD-10 column and discard the flow-through.

7. Pipette 1.5 ml 5 mg ml^{-1} gentisic acid in 0.25 M sodium acetate (pH 5.4-5.6) onto the PD-10 column and discard the flow-through.

8. Pipette 2 ml 5 mg ml^{-1} gentisic acid in 0.25 M sodium acetate (pH 5.4-5.6) onto the PD-10 column and collect the Df-protein.

PAUSE POINT The Df-Bz-NCS-mAb can be stored at -20 °C until the day of radiolabeling for at least 2 weeks.

Radiolabeling (TIMING 1 h 45 min)
9. Pipette the required volume (=a) of [^{89}Zr]Zr-oxalic acid solution (max. 200 µl, typically 37 -185 MBq) into a glass 'reaction vial'.
CAUTION Follow appropriate radiation safety measures for Steps 9 – 17.

10. While gently shaking, add 200 µl – a µl (see Step 9) 1 M oxalic acid into the reaction vial. Subsequently, pipette 90 µl 2 M Na_2CO_3 into the reaction vial and incubate for 3 minutes at room temperature.

11. While gently shaking, pipette successively 0.30 ml 0.5 M HEPES (pH7.1-7.3), 0.71 ml of premodified mAb (typically 0.7-3.0 mg), and 0.70 ml 0.5 M HEPES (pH7.1-7.3) into the reaction vial.
CRITICAL STEP The pH of the labeling reaction should be in the range of 6.8-7.2 for optimal labeling efficiency.

$$\textit{Radiolabeling efficiency} = \frac{\text{CPM } R_f \text{ 0.0 - 0.1 (CPM radiolabeled mAb)}}{\text{CPM } R_f \text{ 0.0 - 1.0 (CPM total)}} \times 100\%$$

12. Incubate for 1 h at room temperature while gently shaking the reaction vial. Radiolabeling efficiency (typically >85%) can be determined by instant thin-layer chromatography (ITLC) using chromatography strips and 20 mM citric acid (pH 4.9-5.1) (ITLC eluent) as solvent. A 0.5-2.0 µl aliquot of the reaction solution can be directly applied to the ITLC strip. Radiolabeled mAb (R_f = 0.0 - 0.1). Any radioactivity R_f >0.1 represents radioactivity not bound to the mAb.

$$\frac{\text{MBq } ^{89}\text{Zr product vial (see Step 16)}}{\text{MBq } ^{89}\text{Zr starting activity (see Step 9)}} \times 100\%$$

13. Meanwhile, rinse a PD-10 column with 20 ml 5 mg ml^{-1} gentisic acid in 0.25 M sodium acetate (pH 5.4-5.6).

14. After 1 h incubation, pipette the reaction mixture onto the PD-10 column and discard the flow-through.

15. Pipette 1.5 ml 5 mg ml^{-1} gentisic acid in 0.25 M sodium acetate (pH 5.4-5.6) onto the PD-10 column and discard the flow-through.

16. Pipette 2 ml 5 mg ml^{-1} gentisic acid in 0.25 M sodium acetate (pH 5.4-5.6) onto the PD-10 column and collect the purified radiolabeled mAb.

17. Calculate the overall labeling yield:
and analyze the purified radiolabeled mAb by ITLC, HPLC and SDS-PAGE (EQUIPMENT SETUP). When the radiochemical purity is greater than 95% it is ready for storage at 4 °C or dilution in 5 mg ml^{-1} gentisic acid in 0.25 M sodium acetate (pH 5.4-5.6) for in vitro or in vivo studies. When the purity is <95% the PD-10 column purification should be repeated. The radiolabeled mAb is stable upon storage for 48 h (0.9% ± 0.4 % dissociation of the initial bound ^{89}Zr in a 37 MBq ml^{-1} ^{89}Zr-mAb solution at t = 48 h, but presence of chloride ions should be avoided).

Table 1 Troubleshooting table

PROBLEM	POSSIBLE REASONS	SOLUTION
Low labeling yield	Low premodification efficiency; insufficient removal of unreacted hydrolysed Df-Bz-NCS; incorrect pH during labeling	A higher molar excess of Df-Bz-NCS can be chosen in the conjugation reaction; repeat the PD-10 purification, or apply the alternative given below
mAb aggregation	Inhomogenic Df/mAb ratio due to high local DMSO concentration resulting in excessive local reaction (deviating from Poisson distribution); radiolysis	Ensure efficient shaking of the reaction mixture upon adding the chelate; pre-modification can be performed at room temperature; ensure that gentisic acid is added to the reaction buffers when indicated
Low radiochemical purity	Insufficient purification	Repeat PD-10 purification or, alternatively ultrafiltration or dialysis can be applied in the purification steps

CRITICAL STEP Gentisic acid is introduced during labeling and storage to minimize deterioration of the mAb integrity by radiation. The use of Cl^- ions should be avoided since radiation and subsequent radiolysis of water molecules form OCl^- ions which very specifically react with the SH-group of the enolized thiourea unit. The thus formed intermediary sulphenyl chloride bonds, and the sulphonyl chloride bonds arising upon

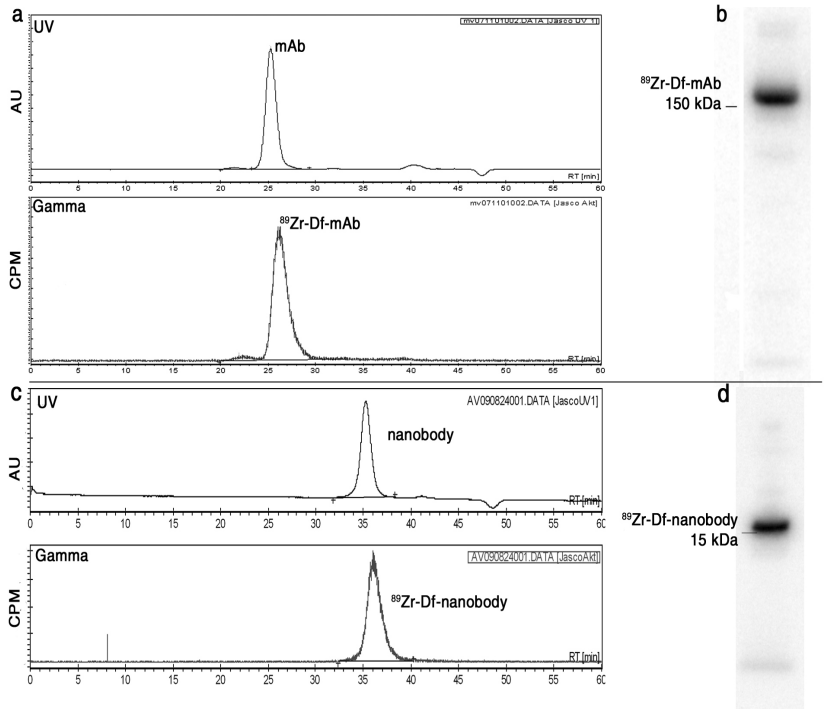

Figure 2. Representative HPLC chromatograms and SDS-PAGE gels. a and b show zirconium-89 (^{89}Zr)-labeled cmAb U36, and c and d show ^{89}Zr-labeled anti-EGFR nanobody (www.ablynx.com). SDS-PAGE was performed on a Phastgel System (GE Healthcare Life Sciences) using preformed 7.5% (b) or high density (d) SDS-PAGE gels under non-reducing conditions.

further oxidation, are known to undertake a series of reactions, among which are coupling reactions and cleavage of methionyl peptide bonds. Therefore, the use of a 0.25 M sodium acetate buffer is strongly recommended.

Timing

Steps 1-8, Coupling of the bifunctional chelate: 50 min

Steps 9-17: Radiolabeling: 1 h 45 min

Troubleshooting

Troubleshooting advice can be found in Table 1.

Anticipated results

Typically, 0.3-0.9 Df moieties are coupled per antibody molecule[18]. Labeling of the Df-conjugated mAb with ^{89}Zr will result in overall radiolabeling yields of >85%. Resulting ^{89}Zr-mAb conjugates are optimal with respect to radiochemical purity (>95% according to ITLC,

analytical HPLC and SDS-PAGE), immunoreactivity, and in vivo stability. Representative HPLC chromatograms and SDS-PAGE gels of ^{89}Zr-labeled cmAb U36 (150 kDa), and of a ^{89}Zr-labeled anti-EGFR nanobody[19] (15 kDa), are shown in Figure 2.

The positron emitter ^{89}Zr can be applied to assess normal biodistribution, and confirm and quantify selective tumor uptake of mAbs, mAb-fragments, non-traditional antibody-like scaffolds or other proteins of interest in animal and clinical studies using PET-imaging. A representative ^{89}Zr-immuno-PET image is shown in Figure 3.

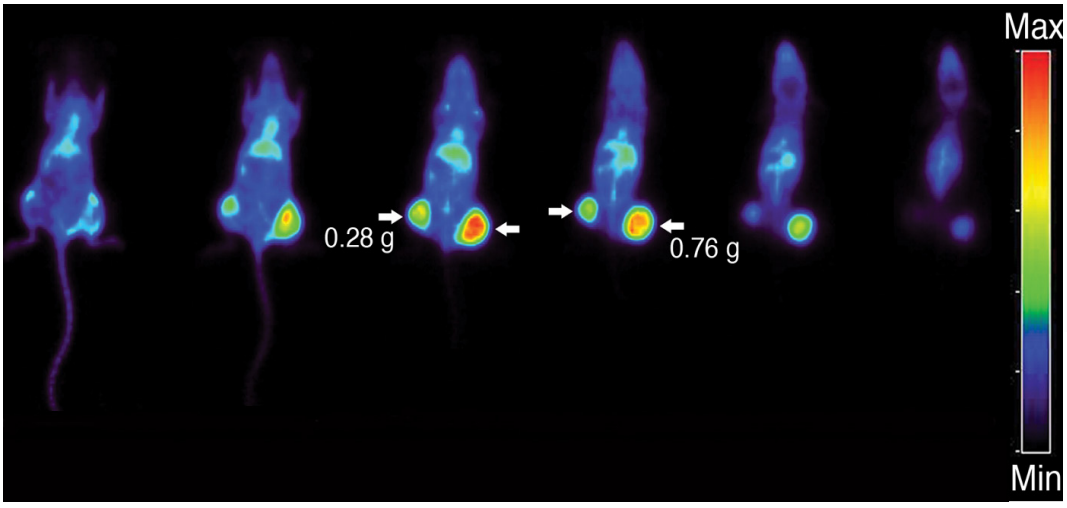

Figure 3. Positron emission tomography (PET) images of a nude mouse bearing two head and neck cancer FaDu xenografts, obtained at 72 h after i.v. injection of the anti-CD44v6 conjugate ^{89}Zr-Df-Bz-NCS-cmAb U36 (3.7 MBq, 200 µg mAb) with a double-crystal-layer high resolution research tomograph PET scanner (HRRT PET scanner, Siemens/CTI). Coronal slices from ventral (left) to dorsal (right). Tumors are indicated by arrows.

Acknowledgements

This project was financially supported by the Dutch Technology Foundation (STW, grants VBC.6120 and 10074) and partly supported by the European Union FP7, ADAMANT and partly performed within the framework of CTMM, the Center for Translational Molecular Medicine (www.ctmm.nl), project AIRFORCE number 030-103. The authors thank the technical staff of BV Cyclotron VU and the Radionuclide Centre for supply and processing of ^{89}Zr.

References

1. Carter, P.J. Potent antibody therapeutics by design. Nat. Rev. Immunol. 6, 343-357 (2006).

2. Reichert, J.M. & Valge-Archer, V.E. Development trends for monoclonal antibody cancer therapeutics. Nat. Rev. Drug. Discov. 6, 349-356 (2007).

3. Wu, A.M. Antibodies and antimatter: the resurgence of immuno-PET. J. Nucl. Med. 50, 2-5 (2009).

4. Nayak, T.K. & Brechbiel, M.W. Radioimmunoimaging with longer-lived positron-emitting radionuclides: Potentials and Challenges. Bioconjug. Chem. 20, 825-841 (2009).

5. Verel, I, Visser, G.W.M. & Van Dongen GAMS. The promise of immuno-PET in radioimmunotherapy. J. Nucl. Med. 46, 164S-171S (2005).

6. Van Dongen, G.A.M.S. et al. Immuno-PET: a navigator in monoclonal antibody development and applications. Oncologist 12, 1379-1389 (2007).

7. Verel, I. et al. ^{89}Zr immuno-PET: comprehensive procedures for the production of ^{89}Zr-labeled monoclonal antibodies. J. Nucl. Med. 44, 1271-1281 (2003).

8. Verel, I. et al. Quantitative ^{89}Zr immuno-PET for in vivo scouting of ^{90}Y-labeled monoclonal antibodies in xenograft-bearing nude mice. J. Nucl. Med. 44, 1663-1670 (2003).

9. Verel, I. et al. Long-lived positron emitters zirconium-89 and iodine-124 for scouting of therapeutic radioimmunoconjugates with PET. Cancer Biother. Radiopharm. 18, 655-661 (2003).

10. Brouwers, A. et al. PET radioimmunoscintigraphy of renal cell cancer using ^{89}Zr-labeled cG250 monoclonal antibody in nude rats. Cancer Biother. Radiopharm. 19, 155-163 (2004).

11. Nagengast, W.B. et al. In vivo VEGF imaging with radiolabeled bevacizumab in a human ovarian tumor xenograft. J. Nucl. Med. 48, 1313-1319 (2007).

12. Aerts, H.J.L.W. et al. Disparity between in vivo EGFR expression and zirconium-89-labeled cetuximab uptake assessed by PET. J. Nucl. Med. 50, 123-131 (2008).

13. Borjesson, P.K. et al. Performance of immuno-positron emission tomography with zirconium-89-labeled chimeric monoclonal antibody U36 in the detection of lymph node metastases in head and neck cancer patients. Clin. Cancer Res. 12, 2133-2140 (2006).

14. Zalutsky, M.R. Potential of immuno-positron emission tomography for tumor imaging and immunotherapy planning. Clin. Cancer Res. 12, 1958-1960 (2006).

15. Börjesson, P.K.E. et al. Radiation dosimetry of zirconium-89-labeled chimeric monoclonal antibody U36 as used for immuno-PET in head and neck cancer patients. J. Nucl. Med. 50, 1828-1836 (2009).

16. Dijkers, E. et al. Development and characterization of clinical-grade ^{89}Zr-trastuzumab for HER2/neu immunoPET imaging. J. Nucl. Med. 50, 974-981 (2009).

17. Perk, L.R. et al. Preparation and evaluation of ^{89}Zr-Zevalin for monitoring of ^{90}Y-Zevalin biodistribution with positron emission tomography. Eur. J. Nucl. Med. Mol. Imaging 33, 1337-1345 (2006).

18. Perk, L.R. et al. p-Isothiocyanatobenzyl-deferrioxamine : a new bifunctional chelate for facile radiolabeling of monoclonal antibodies with zirconium-89 for immuno-PET imaging. Eur. J. Nucl. Med. Mol. Imaging 37, 250-259 (2010).

19. Tijink,B.M. et al. Improved tumor targeting of anti-epidermal growth factor receptor Nanobodies through albumin binding: taking advantage of modular Nanobody technology. Mol Cancer Ther. 7,2288-2297 (2008).

Chapter 4:

Facile labelling of an anti-epidermal growth factor receptor Nanobody with Gallium-68 via a novel bifunctional desferal chelate for immuno-PET

4

Maria J.W.D. Vosjan
Lars R. Perk
Rob C. Roovers
Gerard W. M. Visser
Marijke Stigter-van Walsum
Paul M.P. van Bergen en Henegouwen
Guus A.M.S. van Dongen

European Journal of Nuclear Medicine and Molecular Imaging (2011) 38:753-63

Abstract

Purpose The ~15 kDa variable domains of camelid heavy-chain-only antibodies (called Nanobodies®) have the flexibility to be formatted as monovalent, monospecific, multivalent or multispecific single chain proteins with either fast or slow pharmacokinetics. We report the evaluation of the fast kinetic anti-epidermal growth factor receptor (EGFR) Nanobody 7D12, labelled with ^{68}Ga via the novel bifunctional chelate (BFC) p-isothiocyanatobenzyl-desferrioxamine (Df-Bz-NCS). Df-Bz-NCS has recently been introduced as the chelate of choice for ^{89}Zr-immuno-positron emission tomography (PET).

Methods Nanobody 7D12 was premodified with Df-Bz-NCS at pH 9. Radiolabelling with purified ^{68}Ga was performed at pH 5.0 – 6.5 for 5 min at room temperature. For in vitro stability measurements in storage buffer (0.25 M NaOAc with 5 mg ml^{-1} gentisic acid, pH 5.5) at 4°C or in human serum at 37°C, a mixture of ^{67}Ga and ^{68}Ga was used. Biodistribution and immuno-PET studies of ^{68}Ga-Df-Bz-NCS-7D12 were performed in nude mice bearing A431 xenografts using ^{89}Zr-Df-Bz-NCS-7D12 as the reference conjugate.

Results The Df-Bz-NCS chelate was conjugated to Nanobody 7D12 with a chelate-to-Nanobody molar substitution ratio of 0.2:1. The overall ^{68}Ga radiochemical yield was 55-70% (not corrected for decay); specific activity 100-500 MBq/mg. Radiochemical purity of the conjugate was >96%, while the integrity and immunoreactivity were preserved. $^{68/67}$Ga-Df-Bz-NCS-7D12 was stable in storage buffer as well as in human serum during a 5-h incubation period (< 2% radioactivity loss). In biodistribution studies the ^{68}Ga-labelled Nanobody 7D12 showed high uptake in A431 tumours (ranging from 6.1±1.3 to 7.2±1.5 %ID/g at 1-3 h after injection) and high tumour to blood ratios, which increased from 8.2 to 14.4 and 25.7 at 1, 2 and 3 h after injection, respectively. High uptake was also observed in the kidneys. Biodistribution was similar to that of the reference conjugate ^{89}Zr-Df-Bz-NCS-7D12. Tumours were clearly visualized in a PET imaging study.

Conclusions Via a rapid procedure under mild conditions a ^{68}Ga-Nanobody was obtained that exhibited high tumour uptake and tumour to normal tissue ratios in nude mice bearing A431 xenografts. Fast kinetic ^{68}Ga-Nanobody conjugates can be promising tools for tumour detection and imaging of target expression.

Introduction

The epidermal growth factor receptor (EGFR, HER1, ERb1) is a transmembrane protein of the tyrosine kinase receptor family. Activation of EGFR causes signalling that may lead to cell division, increased motility, angiogenesis, and suppression of apoptosis [1]. EGFR over-expression or constitutive activation has been shown to be associated with poor survival and recurrences in many human malignancies [2]. Detection of EGFR expression via nuclear medicine visualization may provide advantages over immunohistochemical staining of tumour biopsies, since evaluation of both the primary tumour as well as the metastases can be achieved. In addition, such confirmation of EGFR expression can be of value as a scouting procedure to select patients for anti-EGFR therapy with approved monoclonal antibodies (mAbs) like cetuximab or panitumumab or small molecular tyrosine kinase inhibitors. On this latter topic several studies with intact anti-EGFR (αEGFR) mAbs or mAb fragments labelled with single photon emission computed tomography (SPECT) (^{111}In, ^{99m}Tc) or positron emission tomography (PET) (^{64}Cu, ^{89}Zr) radionuclides have been reported [3-9].

Nanobody technology provides new perspectives for mono- as well as multitarget tumour detection and therapy [10-12]. Nanobodies are derived from a unique antibody format that is present in species from the family of Camelidae, including llama, camel and dromedary. These animals contain, besides their conventional antibody repertoire, an antibody class consisting of heavy chains only [10, 13]. The variable region of the heavy chain only antibodies (VHH) represents the complete binding unit of the antibody. Because of the small size of these VHH fragments (~15 kDa), this binding unit is also called Nanobody®. Although being smaller than a scFv fragment, a Nanobody has full antigen-binding potential and does not show aggregation problems, because of hydrophilic instead of hydrophobic patches in the V_H and V_L domains. Due to their single domain character, standard molecular biology techniques such as polymerase chain reaction (PCR) allow for the facile purification and selection of appropriate Nanobody candidates from the full antibody repertoire of immunized animals [14]. Unique features of the Nanobody technology platform in comparison to conventional mAb technology are easy and rapid drug development, and the easy and cheap production in bacteria and yeast [10, 15].

For a proof of concept we used the Nanobody technology platform to construct two αEGFR Nanobodies [11]. The biodistribution of a ^{177}Lu-labeled bivalent αEGFR Nanobody (αEGFR-αEGFR) in A431 tumor bearing nude mice showed a tumor uptake of 5.0±1.4 percentage of the injected dose per gram of tissue (%ID/g) at 6 h after injection

and high tumour to normal tissue ratios (e.g. tumour to blood ratio >80) due to rapid blood clearance. Simple fusion of an anti-albumin Nanobody building block gave a 50-kDa single-chain construct (αEGFR-αEGFR-αAlb) that showed pharmacokinetics and tumour uptake (up to 35.2±7.5 %ID/g) comparable to cetuximab, but faster and deeper tumour penetration. Therefore, such Nanobody formats might be ideal for imaging and therapeutic purposes, respectively.

In the present study we evaluated the in vivo diagnostic potential of fast kinetic αEGFR Nanobody 7D12 within the immuno-PET approach. For this purpose the short-lived positron emitter gallium-68 (^{68}Ga, $t_{½}$ = 68 min, $E_{β+max}$ 1.92 MeV) was chosen. ^{68}Ga is an attractive positron emitting radionuclide since it is cyclotron-independently available via the ^{68}Ge/^{68}Ga generator system.

In aqueous solutions the three-valent gallium forms a complex with many bifunctional chelates (BFC's) containing oxygen and nitrogen as donor atoms. The only clinically used BFC for ^{68}Ga is 1,4,7,10-tetraazacyclododecane-N,N',N'',N'''-tetraacetic acid (DOTA), but fast complex formation requires high temperature [16-19]. More recently, several new chelates have been described for labelling of ^{68}Ga to heat-labile proteins at ambient temperature including 1.4.7-triazacyclononane-1,4,7-triacetic acid (NOTA) and N,N'-bis [2-hydroxy-5-(carboxyethyl)benzyl]ethylenediamine-N,N´-diacetic acid HBED-CC) [19-21]. However, this new generation BFCs is not yet available for clinical immuno-PET applications.

For coupling of the long-lived positron emitter zirconium-89 (^{89}Zr; $t_{½}$ = 78.4 h, $E_{β+max}$ 0.9 MeV) (23%) to intact mAbs, we recently introduced the novel BFC p-isothiocyanatobenzyl derivative of desferrioxamine B (Df-Bz-NCS) [22, 23]. The choice of desferrioxamine B is attractive because it has been used safely in the clinical setting for many years. Since the hydroxamate function in desferrioxamine B has also been used for coupling of gallium-67 (^{67}Ga) in the past [24-27], we investigated whether this same Df-Bz-NCS can be used for labelling of ^{68}Ga under mild conditions. If so, a similar kind of GMP-compliant radiochemistry can be used for labelling of slow kinetic mAbs with ^{89}Zr, and fast kinetic mAb fragments with ^{68}Ga.

In this study, after establishing optimal ^{68}Ga labelling procedures by using a control intact IgG mAb, the bifunctional chelate Df-Bz-NCS was conjugated to αEGFR Nanobody 7D12 and subsequently radiolabelled with ^{68}Ga. The resulting ^{68}Ga-Df-Bz-NCS-7D12 conjugate was analysed for stability at 4°C in storage buffer and at 37°C in serum, whereas its in vivo behaviour was investigated via biodistribution and animal PET studies, using ^{89}Zr-Df-Bz-NCS-7D12 as the reference.

Materials and Methods

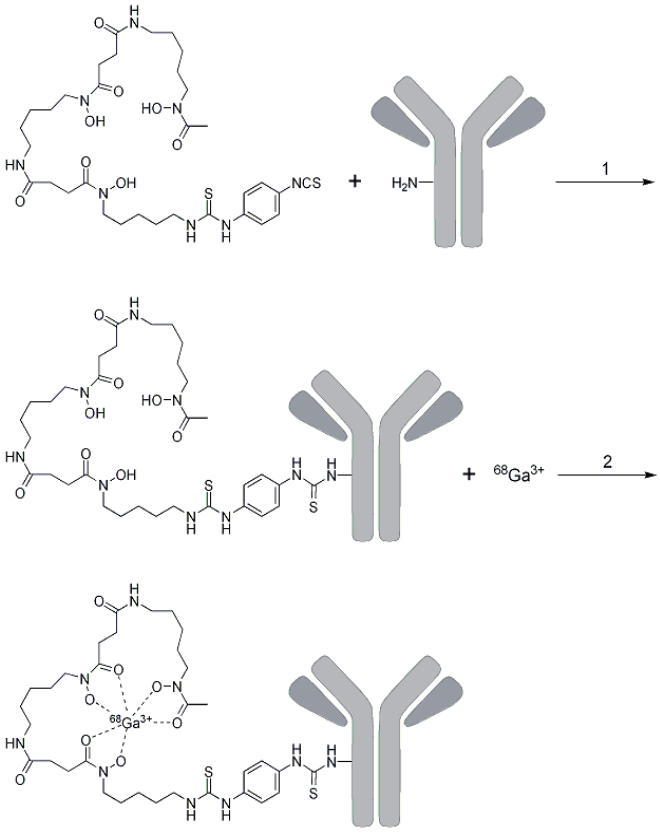

Figure 1. Two step synthesis of ^{68}Ga-Df-Bz-NCS-mAb with the bifunctional chelate Df-Bz-NCS.

Materials

All reagents were purchased from Sigma-Aldrich (St. Louis, MO) unless otherwise stated. Deionised water (18 MΩ*cm) and ultra pure HCl (Ga content 0.02 ng ^{nat}Ga/g) was used. No other special measures were taken regarding working under strict metal-free conditions. Df-Bz-NCS was purchased from Macrocyclics (catalog No. B705). Nanobody 7D12 was generated by Ablynx NV (Ghent, Belgium) as described previously [14] and kindly provided to us. The selection, production, and characterization of chimeric mAb U36 (cmAb U36 11.53 mg/ml) directed against CD44v6 has been described elsewhere [28]. The human epidermoid cervical carcinoma cell line A431 was obtained from the American Type Culture Collection (www.atcc.com), ATCC number: CRL-1555. The head and neck squamous cell carcinoma (HNSCC) cell line UM-SCC-11B was obtained from Dr. T.E. Carey (Ann Arbor, MI) [29]. ^{68}Ga was obtained from a commercial ^{68}Ge/^{68}Ga generator based on a TiO_2 bedding

with 1.85 GBq ^{68}Ge-loaded activity (IGG100; Eckert & Ziegler, Berlin, Germany). ^{67}Ga was purchased as ^{67}Ga-citrate (74 MBq/ml) from Covidien (Mansfield, MA). [^{89}Zr]Zr-oxalate in 1.0 M oxalic acid (≥ 0.15 GBq/nmol) was from IBA Molecular (www.iba.be/molecular).

Purification and concentration of ^{68}Ga and ^{67}Ga

The ^{68}Ga was eluted from the ^{68}Ge/^{68}Ga generator as described by Velikyan et al. [16]. In short, the generator was eluted according to the manufacturer's protocol with 3.5 ml ultra pure 0.1 M HCl solution. To that solution 3.5 ml ultra pure 8 M HCl was added under stirring, to give a final concentration of ~ 4 M HCl. The solution was passed through a pre-treated (1 ml 100% ethanol, 1 ml deionized water, 1 ml 4 M HCl) anion-exchange column [Chromafix, PS-HCO3 (s), Macherey-Nagel, Düren, Germany], the column was washed with 2 ml of 4 M HCl, flushed with air, and then the ^{68}Ga was eluted from the chromafix column with 200 µl deionized water (elution efficiency >85%). The use of ultra pure HCl implies that this procedure attributes at most 1.1 pmol ^{nat}Ga to this eluate.

$^{67}GaCl_3$ was obtained from ^{67}Ga-citrate. To this end, ^{67}Ga-citrate was mixed with an equal volume of ultra pure 8 M HCl. This solution was passed through a pre-treated Chromafix column and eluted as described for ^{68}Ga.

In all preparations for in vitro evaluation $^{68/67}$Ga was used, while for in vivo evaluation only ^{68}Ga was applied.

Preparation of $^{68/67}$Ga-Df-Bz-NCS-cmAb U36

For development of labelling procedures, the 150-kDa intact cmAb U36 was used as the control mAb. cmAb U36 was premodified with Df-Bz-NCS as described by Perk et al. [22] (Fig. 1). In short, 5 mg cmAb U36 (33 nmol) reacted with 20 µl Df-Bz-NCS (100 nmol) in dimethyl sulphoxide (DMSO) for 30 min at 37°C at pH 9 in a shaker, in a total volume of 1 ml. Nonconjugated chelate was removed by size exclusion chromatography using a PD-10 column (GE Healthcare Life Science) with 0.25 M NaOAc pH 5.5 as eluant. The flow through and the first 1.5 ml were discarded. The next 2 ml containing the premodified mAb were stored.

Ga-Df complex chelate formation conditions were selected by varying pH and protein concentration. As a result, the following procedure was developed; to 10 - 200 µl (=a) ^{68}Ga and/or ^{67}Ga in deionized water, (3x a µl) 3 M NH_4OAc buffer pH 7.2 were added and mixed for 5 min at room temperature. Subsequently, the premodified cmAb U36 (100–1000 µg) in 0.25 M NaOAc pH 5.5 was added; final reaction volume was 2 ml. The reaction was stopped after 5 min at room temperature by the addition of 50 µl 50

mM ethylenediaminetetraacetate acid (EDTA), followed by PD-10 column purification using 0.25 M NaOAc with 5 mg.ml^{-1} gentisic acid, pH 5.5, as eluant. The flow through and the first 1 ml were discarded. The next 2 ml containing the $^{68/67}$Ga-labelled cmAb U36 were collected and used for further experiments.

Preparation of $^{68/67}$Ga-Df-Bz-NCS-7D12

The same protocol was applied for the modification and radiolabelling of the αEGFR Nanobody 7D12. In short, two mg 7D12 (125 nmol) was conjugated with 375 nmol Df-Bz-NCS and after PD-10 column purification the premodified 7D12 (200-1000 µg) was labelled with $^{68/67}$Ga as described for cmAb U36.

Preparation of ^{89}Zr-Df-Bz-NCS-7D12

The 7D12 nanobody was premodified as described above with a threefold molar excess of Df-Bz-NCS chelate. After PD-10 column purification the premodified 7D12 was labelled with ^{89}Zr as described by Perk et al. [22]. In short, Df-Bz-NCS-7D12 (100-1000 µg) was labelled with ^{89}Zr (37 MBq) in 0.25 M HEPES buffer pH 7.0 at room temperature in a total volume of 2 ml. The ^{89}Zr-Df-Bz-NCS-7D12 was purified by PD-10 column using 0.25 M NaOAc with 5 mg ml^{-1} gentisic acid, pH 5.5, as eluant. After discarding the flow through and the first 1 ml, the next 2 ml containing the ^{89}Zr-labelled 7D12 was collected for further experiments.

Determination of Df to 7D12 molar ratio

The Df-Bz-NCS to 7D12 molar ratio was determined following a general method using a known nanomolar excess of $GaCl_3$ spiked with ^{67}Ga. In short, 250 nmol $GaCl_3$ (in 4 M ultra pure HCl) was mixed with ~37 MBq ^{67}Ga and purified according to aforementioned method using the anion Chromafix column. Thereafter, 500 µg of premodified Df-Bz-NCS-7D12 was labelled according to the developed protocol with 20-60 nmol of the above prepared ^{67}Ga-$GaCl_3$, and the Df to 7D12 molar ratio was calculated. For comparison the Df to 7D12 molar ratio was also determined with the use of zirconium oxalate spiked with ^{89}Zr.

Analysis

^{68}Ga was measured using E_γ = 511 KeV and ^{67}Ga with E_γ = 185 KeV. When dual isotope labelling products were produced, ^{67}Ga radioactivity measurements were performed at least 20 h after production (after decay of ^{68}Ga). Each $^{68/67}$Ga-labelled product was analysed by instant thin layer chromatography (ITLC) to determine the radiochemical

labelling efficiency and radiochemical purity. The integrity of the Nanobody and mAb was analysed by high performance liquid chromatography (HPLC) and sodium dodecyl sulphate-polyacrylamide gel electrophoresis (SDS-PAGE) followed by phosphor imaging (Storm820, GE Healthcare). Immunoreactivity was determined by a cell-binding assay, 3 h at 37°C or overnight at 4°C. ITLC analysis of the $^{68/67}$Ga-labelled products was performed on chromatography strips (Biodex, Shirley, NY, USA); 2 µl were spotted on an ITLC strip with 50 mM EDTA in Milli-Q as mobile phase. HPLC analysis was performed on a Jasco HPLC system using a Superdex™ peptide size exclusion column (GE Healthcare Life Sciences) when a labelled Nanobody was injected, or a Superdex™ 200 10/300 GL size exclusion column when labelled cmAb U36 was injected, with a mixture of 0.05 M sodium phosphate and 0.15 M sodium chloride (pH 6.8) as eluent at a flow rates of 1.0 and 0.5 ml min^{-1}, respectively. Gel electrophoresis was performed on a Phastgel System (GE Healthcare Life Sciences) using high density SDS-PAGE gels when a labelled Nanobody was applied or 7.5% SDS-PAGE gels when labelled U36 was applied, under non-reducing conditions. Immunoreactivity was determined by measuring the binding of the $^{68/67}$Ga-7D12 or $^{68/67}$Ga-cmAb U36 to a serial dilution of 2% paraformaldehyde fixed A431 cells or 0.2% glutaraldehyde fixed UM-SCC-11B cells, respectively, essentially as described by Lindmo et al. [30].

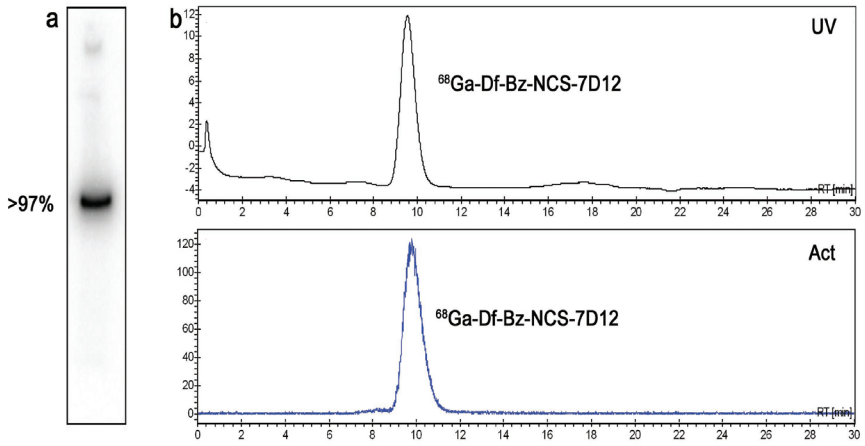

Figure 2. SDS-PAGE followed by phosphor imaging analysis (a) and HPLC chromatogram (b) of purified ^{68}Ga-Df-Bz-NCS-7D12, where the upper panel represents the UV profile at 280 nm the lower panel the radioactivity profile.

In vitro stability

To determine the in vitro stability of the gallium-labelled Nanobodies, 500 µg $^{68/67}$Ga-labelled 7D12 product was stored at 4°C up to 24 h in 0.25 M NaOAc pH 5.5, containing 5 mg ml^{-1} gentisic acid as antioxidant, and compared with ^{89}Zr-7D12. Amounts of activity at the start of storage were 120 MBq of ^{68}Ga, 20 MBq of ^{67}Ga and 20 MBq of ^{89}Zr. After 5 and 24 h storage aliquots were taken and analyzed by ITLC, HPLC and SDS-PAGE.

Stability of $^{68/67}$Ga-labeled 7D12 was also tested in freshly prepared human serum and compared with ^{89}Zr-7D12. Activity amounts at the start of storage were 80 MBq ^{68}Ga, 18 MBq ^{67}Ga and 18 MBq ^{89}Zr. The labelled 7D12 (300 µg) was incubated at 37°C, in a CO_2-enriched atmosphere (5% CO_2) with freshly prepared human serum (1:4) in the presence of 0.02 % NaN_3. Aliquots were taken after 5 and 24 h storage and analyzed by ITLC and HPLC.

Biodistribution study

The distribution of ^{68}Ga-Df-Bz-NCS-7D12 was examined using nude mice (HSD:Athymic Nude-Foxn1^{nu}, 20-30 g; Harlan) bearing subcutaneously implanted human xenografts of the vulvar tumour cell line A431 at two lateral sides. All animal experiments were done according to NIH Principles of Laboratory Animal Care and Dutch national law ("Wet op de dierproeven", Stb 1985, 336).

In this experiment mice bearing A431 xenografts were injected with 0.35 MBq ^{68}Ga-Df-Bz-NCS-7D12 (6 µg) via the retro-orbital plexus. As reference compound, 0.35 MBq ^{89}Zr-Df-Bz-NCS-7D12 (6 µg) was used. Unlabelled 7D12 was added to the injection mixture to obtain a final dose of 50 µg per mouse. At 1, 2 and 3 h post injection (p.i.) four mice were anesthetized, bled, killed and dissected. Blood, tumour and normal tissues were weighed and radioactivity was measured in a gamma counter (Wallac, Turku, Finland). Radioactivity uptake for each sample was calculated as the %ID/g.

PET study

PET imaging was performed on a HRRT PET scanner (Siemens/CTI [31]), a dedicated human brain scanner. Three A431 xenograft-bearing mice were anaesthetized by inhalation of 2% isoflurane, injected with 5 MBq ^{68}Ga-Df-Bz-NCS-7D12 (85 µg) via the retro-orbital plexus, and scanned for 3 h. In addition, three mice were injected with 2.5 MBq ^{89}Zr-Df-Bz-NCS-7D12 (85 µg). Unlabeled 7D12 was added to the injection mixture to obtain a final dose of 100 µg per mouse. Transmission scans for attenuation and scatter correction were routinely obtained with each emission scan. Three-dimensional emission scans were

acquired in list mode during 180 min. A single frame static image was reconstructed using ordinary Poisson ordered subsets expectation maximization (OP-OSEM). For visualization of the images, the freely available Amide's A Medical Imaging Data Examiner (AMIDE) program was used [32].

Statistical analysis

Differences in tissue uptake between injected conjugates were statistically analysed for each different time point with SPSS 15.0 software using Student's t-test for unpaired data. Two-sided significance levels were calculated and $p < 0.01$ was considered statistically significant.

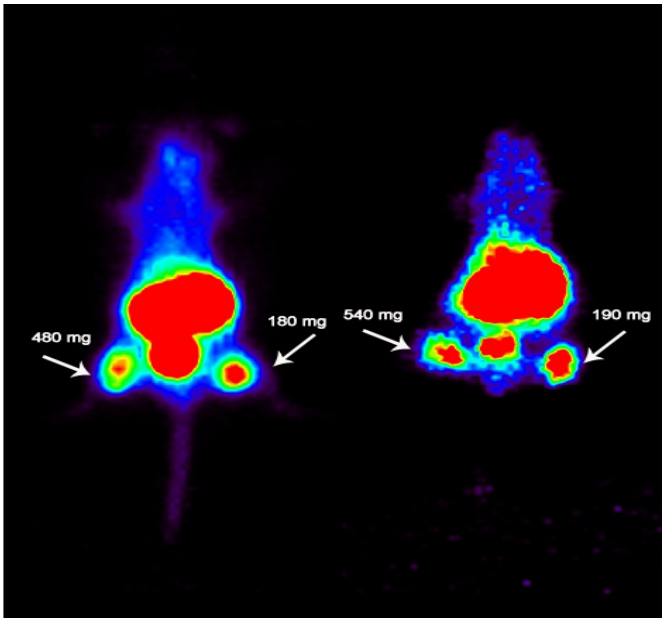

Figure 4. Static PET image of A431 tumour-bearing mice obtained 2-3 h after injection of ^{68}Ga-Df-Bz-NCS-7D12 (left mouse) or ^{89}Zr-Df-Bz-NCS-7D12 (right mouse). Images demonstrate similar uptake of both tracers. Tumours are indicated by arrows. Image planes have been chosen where both tumours were visible.

Results

Preparation of $^{68/67}$Ga-Df-Bz-NCS-cmAb U36

The Ga-Df formation conditions were investigated by performing experiments with premodified Df-Bz-NCS-cmAb U36. The Df-Bz-NCS chelate was coupled at pH 9 to the lysine groups in a 3 fold molar excess via a 30-min incubation at 37°C.

When a labelling was performed for 5 min in a 2 ml acetate solution at a pH in

the range 5.0 – 6.5 and an activity level of 200 MBq ^{68}Ga (2 pmol) and 37 MBq ^{67}Ga (25 pmol), the labelling yield was consistently >90% provided the amount of mAb was >200 µg (measured up to 1000 µg) i.e. >0.7 nmol bound Df-groups. For 100 µg (i.e. 0.35 nmol bound Df-groups) a labelling yield of 80% was obtained. When using a naked cmAb U36 under these conditions, <1% of Ga was co-eluted with the PD-10 protein fraction.

After PD-10 purification the labelled cmAb U36 was stored in 2 ml 0.25 M NaOAc with 5 mg ml^{-1} gentisic acid, pH 5.5, and analysed. The radiochemical purity was always 96-99%, as determined with ITLC and HPLC. The immunoreactive fraction was determined by an overnight immunoreactivity assay (when using ^{67}Ga) and was 81-86%. The integrity of the labelled cmAb U36 was optimal as determined with SDS-PAGE and HPLC analysis (data not shown). The radiation dose derived from labelling with 200 MBq ^{68}Ga and its subsequent full decay did not affect the integrity and immunoreactivity of the $^{68/67}$Ga product, which means that our chosen 0.25 M NaOAc with 5 mg ml^{-1} gentisic acid, pH 5.5 buffer protected adequately against radiation damage. Dilution of the $^{68/67}$Ga-cmAb U36 product with human serum to a solution containing 70 pmol/ml Df showed <1% loss of label. Upon storage of this solution at 37°C, the radiochemical purity of cmAb U36 decreased during 5 h an additional 2% and during 24 h an additional 10%, as determined by ITLC and confirmed with HPLC.

Preparation of $^{68/67}$Ga-Df-Bz-NCS-7D12 and ^{89}Zr-Df-Bz-NCS-7D12

Aforementioned conditions applied to Nanobody 7D12 gave 0.2 desferal groups per Nanobody molecule. Labelling (200-1000 µg) of the Df-Bz-NCS-7D12 with $^{68/67}$Ga resulted in overall radioactivity yields of 55-70% (not corrected for decay). Radiochemical purity was always 96-99%, as determined by HPLC and ITLC. Immunoreactivity was 40-60% for the 3 h incubation assay at 37°C while the overnight assay at 4°C using ^{67}Ga showed 80-85%. The integrity of the Nanobody was preserved as determined with SDS-PAGE and HPLC analysis (see Figure 2).

For the ^{89}Zr-Df-Bz-NCS-7D12 the overall radioactivity yield was 59-73%, radiochemical purity was always 97-99%, and the immunoreactivity was 80-85% (determined with the overnight assay at 4°C).

In vitro stability

In vitro stability of $^{68/67}$Ga-Df-Bz-NCS-7D12 was compared with ^{89}Zr-Df-Bz-NCS-7D12. Radiochemical purity of $^{68/67}$Ga-Df-Bz-NCS-7D12 was 98±1% at the start and only slightly decreased during 5 h incubation in buffer at 4°C (1.5–2.0% release of $^{68/67}$Ga); after 24 h

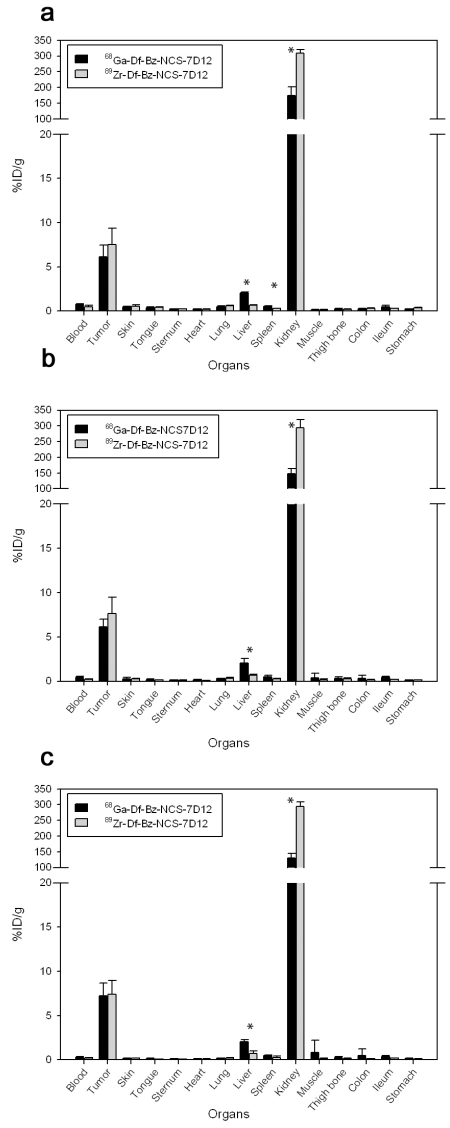

Figure 3. Biodistribution of 7D12 labelled with ^{68}Ga (black bars) or ^{89}Zr (grey bars) in A431 tumour-bearing nude mice at 1 h (a), 2 h (b), and 3 h (c) p.i. Significant differences in uptake are marked with an asterisk. Data is presented as average of four mice and standard deviation.

the decrease was 6-7% as determined with ITLC and confirmed with HPLC. For ^{89}Zr-Df-Bz-NCS-7D12 the radiochemical purity was also 98±1% at the start, which decreased to 97±1% after 24 h at 4°C. The integrity of both labelled 7D12 Nanobodies was not affected after 24 h at 4°C, as determined with SDS-PAGE and HPLC.

In human serum at 37°C, radiochemical purity of both labelled 7D12 Nanobodies slightly decreased during 5 h in human serum (1-2% release of for both compounds) and after 24 h the percentage of $^{68/67}$Ga that was dissociated was 7–8%, and 1-2% for ^{89}Zr as determined by ITLC and confirmed with HPLC.

Biodistribution study

For the biodistribution study nude mice bearing A431 xenografts were injected with either 0.35±0.05 MBq ^{68}Ga-Df-Bz-NCS-7D12 or 0.35±0.01 MBq ^{89}Zr-Df-Bz-NCS-7D12 as control group. After 1 h high uptake was seen in tumour tissue for both radioisotopes (6.1±1.3 %ID/g for ^{68}Ga and 7.5±1.9 %ID/g for ^{89}Zr), a level which remained constant up to 3 h post injection (6.1±0.9 and 7.6±1.9 %ID/g at 2 h, and 7.2±1.5 and 7.4±1.6 %ID/g at 3 h post injection for ^{68}Ga and ^{89}Zr, respectively). High radioactivity uptake was found in the kidneys, urine and bladder. Except for some liver uptake (2.1±0.1 and 0.7±0.1 %ID/g at 1 h post injection for ^{68}Ga and ^{89}Zr, respectively) all other organs showed low uptake at all time points (< 0.5±0.2 %ID/g for ^{68}Ga and < 0.3±0.1 %ID/g for ^{89}Zr). For both radioisotopes tumour to blood ratios increased at later time points. At 1 h the tumour to blood ratio for ^{68}Ga was 8.2 and increased to 14.4 at 2 h and 25.7 at 3 h post injection, while the tumour to blood ratios for ^{89}Zr were 14.8, 35.2 and 42.4 at 1, 2 and 3 h, respectively. In general, the overall biodistribution of both radioisotopes was very similar. For all time points significant differences between ^{68}Ga and ^{89}Zr were seen in liver and kidney, and at 1 h post injection significant difference was also observed for spleen ($p<0.001$).

PET study

To exclude possible radioactivity uptake in non-evaluated tissues in the biodistribution studies a PET imaging study was performed. In Figure 4 representative PET images are shown; a static PET image obtained 2-3 h after injection of ^{68}Ga-Df-Bz-NCS-7D12 is seen in the left image while the right image represents a mouse 2-3 h after injection of ^{89}Zr-Df-Bz-NCS-Df. In both images the tumours are clearly visible, with good tumour to background contrast. High accumulation in the kidney and bladder was observed.

Discussion

In this present study, we describe a method for labelling of αEFGR Nanobody 7D12 with ^{68}Ga using the novel bifuntional desferal chelate (Df-Bz-NCS) which was previously introduced for the coupling of ^{89}Zr to intact mAbs [22, 23]. Using this method, stable ^{68}Ga-7D12

radioimmunoconjugates were produced as demonstrated by stability testing in storage buffer as well as in human serum with only slightly less stability as compared with the reference compound ^{89}Zr-Df-Bz-NCS-7D12. In addition, high and selective tumour uptake was observed in biodistribution and PET imaging experiments in nude mice bearing A431 xenografts, which was similar for ^{68}Ga-7D12 and the reference conjugate ^{89}Zr-7D12. The latter indicates that Df-Bz-NCS is equally well suited for immuno-PET imaging, irrespective whether the short-lived positron emitter ^{68}Ga or the long-lived positron emitter ^{89}Zr is used. ^{89}Zr-Df-antibodies have been extensively evaluated in clinical immuno-PET studies [33].

Crucial in the labelling procedures described herein are (1) the use of ultra pure HCl, to keep the ^{nat}Ga concentrations as low as possible and also to minimize the amounts of Al, Fe and Zr, being strong competitors for complexation with Df, (2) the purification and concentration of ^{68}Ga by use of an anion exchange column, to further minimize the amounts of Al, Fe and Zr, to get rid of contaminating metals originating from the generator and to keep [$^{68}GaCl_4^-$] volumes for labelling small [16, 34], (3) the addition of a highly concentrated NH_4OAc solution to the [$^{68}GaCl_4^-$]-solution for efficient radiolabelling and stable complex formation (avoidance of the formation of gallium-oxo-chloro intermediates), (4) the use of a commercially available desferrioxamine B chelate that has been applied clinically in a safe way for many years [23], (5) radiolabelling at room temperature within a relatively wide pH range of 5.0–6.5, and (6) the use of 0.25 M NaOAc with 5 mg ml^{-1} gentisic acid, pH 5.5 for protection during storage of the purified ^{68}Ga-labelled conjugate. These procedures appeared efficient and mild, thus avoiding denaturation of protein, and resulted in optimal quality conjugates at an overall radiochemical yield of 55-70% (not corrected for decay). Therefore, these generic procedures seem suitable for GMP compliant labelling, irrespective the intrinsic stability of the biomolecule.

The only chelate that has been used for ^{68}Ga-labelling of mAbs or mAb-like molecules for clinical purposes is DOTA [35]. With DOTA the best labelling kinetics were obtained in sodium acetate buffers at low pH [36]. Tolmachev et al. evaluated the ^{68}Ga labelling kinetics of the DOTA containing anti-HER2 Affibody ABY-002. Labelling at room temperature for 5 minutes appeared inefficient (decay-corrected yield of less than 5%). Only after elevation of the temperature to 60°C or 90°C the yield increase to ~30 and ~90%, respectively. The binding and pharmacokinetic characteristics of this particular Affibody did not become affected upon labelling, but it is open to question whether other proteins can resist the harsh labelling conditions of low pH and high temperature [35, 37]. The same holds true for microwave heating that has been used for labelling of DOTA-

bioconjugates with ^{68}Ga [16, 38]. In our initial studies, using DOTA-Bz-NCS, less than 60% labelling was obtained after 20 min at 45°C, while the thus obtained labelled product was unstable. We postulate that at lower temperature no full N-coordination occurs. This means that the ^{68}Ga-atom becomes ligated to the carboxyl functions of the DOTA molecule with still having water molecules in its coordination sphere instead of N, and that only concordant heating at elevated temperatures [37, 39] creates the additional N-coordination of the DOTA molecule leading to the ^{68}Ga-DOTA-complex that is suitable for in vivo applications. This important aspect of complex formation is fully analogous to what has been shown by us for the synthesis of the ^{186}Re-MAG3-complex [40].

NOTA and its derivatives as well as the recently introduced HBED-CC chelates might have advantages over DOTA, since labelling with these chelates can be performed at room temperature and modest pH [19-21, 41]. These chelates, however, have not been clinically evaluated yet, and for us this was the reason to evaluate the desferrioxamine B derivative. Some controversy exists about the conditional stability constant of the Ga-Df complex at neutral pH. The in vitro stability we found corresponds well with the earlier findings of Smith-Jones et al. [25], Fani et al. [27], and Furukawa et al. [24], but seems to be rather in contrast with the findings of Caraco et al. [42] and Govindan et al. [26]. We feel that this is only an apparent controversy because the conditions under which Caraco et al. produced their Ga-Df-complex are completely different. We observed that a product formed at pH = 7.4 indeed suffered from instability indicating that at this pH a certain amount of weak complexes are formed containing partly hydrolyzed Ga ions and so being only mono- or bidentate bound to the three hydroxamate functions. With respect to the findings of Govindan et al. [26], they already suggested themselves that their findings are most probably mixed up by the fact that the linkages between their mAb and Df are intrinsically instable.

EGFR, a tyrosine kinase receptor, is highly expressed in many epithelial cancer cells and is a prime target for detection and therapeutic applications. Nuclear imaging techniques have a proven advantage over immunohistological techniques since nuclear imaging is noninvasive and whole-body scans can be obtained [43]. The use of Nanobodies as imaging moiety might have advantages over the use of intact mAbs, since a molecular weight of only 15 kDa allows for faster kinetics than intact mAbs in vivo. To our knowledge, Nanobodies have never been used for immuno-PET applications. In this study, ^{68}Ga-labelled Nanobody 7D12 showed high and selective uptake in A431 tumours, ranging from 6.1 to 7.2 %ID/g at 1-3 h p.i., which was comparable to the reference compound ^{89}Zr-7D12 (7.5 to 7.4 %ID/g at 1-3 h). Significant differences in liver and kidney uptake were observed

between the ^{68}Ga-7D12 and ^{89}Zr-7D12 conjugates. These differences most probably reflect the slightly lower stability observed in the in vitro stability experiments. Maybe metabolite analyses might provide further insight.

Huang et al. and Gainkam et al. [44, 45] studied the same (αEGFR) Nanobody 7D12 in the same A431 xenograft model, but labelled with technetium-99m (^{99m}Tc) for SPECT applications. Tumour uptake of ^{99m}Tc-7D12 was 4.9 %ID/g at 1 h p.i. (assessed by quantitative analysis of SPECT images) and 6.1 %ID/g at 1.5 h p.i. (assessed by radioactivity counting of dissected tumours). Like ^{68}Ga-7D12, ^{99m}Tc-7D12 showed high kidney uptake. However, uptake of ^{99m}Tc-7D12 in lung and spleen was higher than that of ^{68}Ga-7D12: 2.1 and 1.4 %ID/g versus 0.5 and 0.6 %ID/g, at 1 h p.i.. Given the superior properties of PET in comparison to SPECT for clinical quantitative imaging, these data suggests that ^{68}Ga-7D12 is the more attractive Nanobody-based probe for assessment of EGFR expression [46, 47].

^{68}Ga-7D12 allowed high contrast imaging at relatively early time points (1 h p.i.) in comparison with radiolabelled conventional intact mAbs used in other preclinical imaging studies. For example, in recent immuno-PET studies with ^{64}Cu- and ^{89}Zr-labelled anti-EGFR mAb cetuximab tumours could only be clearly delineated 16-24 h p.i. [7, 9, 48]. Another interesting small molecular protein was introduced for imaging of EGFR, namely the 8-kDa Affibody $Z_{EGFR:2377}$ [49]. PET imaging studies in A431-bearing nude mice showed higher tumour contrast when 50 μg of ^{111}In-labeled $Z_{EGFR:2377}$ was injected in comparison to 5 μg, whereas for both doses high liver uptake was observed. For the 50 μg ^{111}In-$Z_{EGFR:2377}$ group, tumour and liver uptake at 4 h p.i. was 2.4 and 5.1 %ID/g, respectively. In comparison, tumour uptake of ^{68}Ga-7D12 in the present study was substantially higher (7.2 %ID/g at 3 h p.i.), while liver uptake was lower (2.0 %ID/g at 3 h p.i.). These interesting differences in uptake can be ascribed to differences in reactivity with murine EGFR. Both probes can bind to human EGFR expressed in human xenografts, but only ^{111}In-$Z_{EGFR:2377}$ can also bind to the murine EGFR in the liver. In accordance, initial clinical imaging studies with ^{111}In-labeled anti-EGFR mAb 225 showed high liver uptake, requiring relatively high mAb doses for imaging of EGFR expression [50].

Aforementioned data indicate ^{68}Ga-7D12 Nanobody has potential for assessment of EGFR tumour expression; however, for clinical application thorough dose optimization might be needed to obtain optimal imaging results. The latter will be easier for ^{68}Ga-labelled Nanobodies directed against targets that show predominantly expression in the tumour, as was recently illustrated in PET imaging studies with ^{68}Ga-labelled Affibody ABY-002 directed against the HER2 receptor [35].

Conclusion

The newly developed GMP-compliant two-step procedure for coupling desferal to a Nanobody allows efficient and rapid preparation of ^{68}Ga-Nanobodies for clinical use with high labelling yields, high radiochemical purity and preservation of immunoreactivity. The anti-EGFR ^{68}Ga-Df-Bz-NCS-7D12 Nanobody showed high accumulation in A431 xenografts in nude mice in biodistribution studies as well as in immuno-PET, which indicates that this conjugate can be a promising fast kinetic noninvasive imaging probe for the detection of EGFR expression in tumours.

Acknowledgements

This project was financially supported by the Dutch Technology Foundation (STW, grant 10074) and partly performed within the framework of CTMM, the Center for Translational Molecular Medicine (www.ctmm.nl), project AIRFORCE number 030-103. The authors thank Leo van Rooij and Peter Schollema of the radionuclide center for their assistance with ^{68}Ga/^{68}Ge generator and Marc Huisman for PET analysis.

References

1. Yarden Y, Sliwkowski MX. Untangling the ErbB signalling network. Nat Rev Mol Cell Biol 2001;2:127-37.

2. Lurje G, Lenz HJ. EGFR signaling and drug discovery. Oncology 2009;77:400-10.

3. Dadparvar S, Krishna L, Miyamoto C, Brady LW, Brown SJ, Bender et al. Indium-111-labeled anti-EGFr-425 scintigraphy in the detection of malignant gliomas. Cancer 1994;73:884-89.

4. Vallis KA, Reilly RM, Chen P, Oza A, Hendler A, Cameron R, et al. A phase I study of 99mTc-hR3 (DiaCIM), a humanized immunoconjugate directed towards the epidermal growth factor receptor. Nucl Med Commun 2002;23:1155-64.

5. Schechter NR, Wendt RE, Yang DJ, Azhdarinia A, Erwin WD, Stachowiak AM, et al. Radiation dosimetry of 99mTc-labeled C225 in patients with squamous cell carcinoma of the head and neck. J Nucl Med 2004;45:1683-7.

6. Niu G, Li Z, Xie J, Le QT, Chen X. PET of EGFR antibody distribution in head and neck squamous cell carcinoma models. J Nucl Med 2009;50:1116-23.

7. Cai W, Chen K, He L, Cao Q, Koong A, Chen X. Quantitative PET of EGFR expression in xenograft-bearing mice using 64Cu-labeled cetuximab, a chimeric anti-EGFR monoclonal antibody. Eur J Nucl Med Mol Imaging 2007;34:850-8.

8. Ping Li W, Meyer LA, Capretto DA, Sherman CD, Anderson CJ. Receptor-binding, biodistribution, and metabolism studies of 64Cu-DOTA-cetuximab, a PET-imaging agent for epidermal growth-factor receptor-positive tumors. Cancer Biother Radiopharm 2008;23:158-71.

9. Aerts HJ, Dubois L, Perk L, Vermaelen P, van Dongen GA, Wouters BG, et al. Disparity between in vivo EGFR expression and 89Zr-labeled cetuximab uptake assessed with PET. J Nucl Med 2009;50:123-31.

10. Roovers RC, van Dongen GA, van Bergen en Henegouwen PM. Nanobodies in therapeutic applications. Curr Opin Mol Ther 2007;9:327-35.

11. Tijink BM, Laeremans T, Budde M, Stigter-van Walsum M, Dreier T, de Haard HJ, et al. Improved tumor targeting of anti-epidermal growth factor receptor Nanobodies through albumin binding: taking advantage of modular Nanobody technology. Mol Cancer Ther 2008;7:2288-97.

12. Kolkman JA, Law DA. Nanobodies - from llamas to therapeutic proteins. Drug Discov Today: Technol 2010; 7:e139-46.

13. Hamers-Casterman C, Atarhouch T, Muyldermans S, Robinson G, Hamers C, Songa EB, et al. Naturally occurring antibodies devoid of light chains. Nature 1993;363:446-8.

14. Roovers RC, Laeremans T, Huang L, De Taeye S, Verkleij AJ, Revets H, et al. Efficient inhibition of EGFR signaling and of tumour growth by antagonistic anti-EFGR Nanobodies. Cancer Immunol Immunother 2007;56:303-17.

15. Els Conrath K, Lauwereys M, Wyns L, Muyldermans S. Camel single-domain antibodies as modular building units in bispecific and bivalent antibody constructs. J Biol Chem 2001;276:7346-50.

16. Velikyan I, Beyer GJ, Långström B. Microwave-supported preparation of (68)Ga bioconjugates with high specific radioactivity. Bioconjug Chem 2004;15:554-60.

17. Hoffend J, Mier W, Schuhmacher J, Schmidt K, Mitrakopoulou-Strauss A, Strauss LG, et al. Gallium-68-DOTA-albumin as a PET blood-pool marker: experimental evaluation in vivo. Nucl Med Biol 2005;32:287-92.

18. Blom E, Långström B, Velikyan I. 68Ga-labeling of biotin analogues and their characterization. Bioconjug Chem 2009;20:1146-51.

19. Ferreira CL, Lamsa E, Woods M, Duan Y, Fernando P, Bensimon C, et al. Evaluation of bifunctional chelates for the development of gallium-based radiopharmaceuticals. Bioconjug Chem 2010;21:531-6.

20. Eder M, Wangler B, Knackmuss S, LeGall F, Little M, Haberkorn U, et al. Tetrafluorophenolate of HBED-CC: a versatile conjugation agent for 68Ga-labeled small recombinant antibodies. Eur J Nucl Med Mol Imaging 2008;35:1878-86.

21. Eder M, Knackmuss S, Le GF, Reusch U, Rybin V, Little M, et al. (68)Ga-labelled recombinant antibody variants for immuno-PET imaging of solid tumours. Eur J Nucl Med Mol Imaging 2010;37:1397-1407.

22. Perk LR, Vosjan MJ, Visser GW, Budde M, Jurek P, Kiefer GE, et al. p-Isothiocyanatobenzyl-desferrioxamine: a new bifunctional chelate for facile radiolabeling of monoclonal antibodies with zirconium-89 for immuno-PET imaging. Eur J Nucl Med Mol Imaging 2009;37:250-9.

23. Vosjan MJ, Perk LR, Visser GW, Budde M, Jurek P, Kiefer GE, van Dongen GA. Conjugation and radiolabeling of monoclonal antibodies with zirconium-89 for PET imaging using the bifunctional chelate p-isothiocyanatobenzyl-desferrioxamine. Nat Protoc 2010;5:739-43.

24. Furukawa T, Fujibayashi Y, Fukunaga M, Saga T, Endo K, Yokoyama A. An approach for immunoradiometric assay with metallic radionuclides: gallium-67-deferoxamine-dialdehyde starch-IgG. J Nucl Med 1991;32:825-9.

25. Smith-Jones PM, Stolz B, Bruns C, Albert R, Reist HW, Fridrich R, et al. Gallium-67/gallium-68-[DFO]-octreotide--a potential radiopharmaceutical for PET imaging of somatostatin receptor-positive tumors: synthesis and

radiolabeling in vitro and preliminary in vivo studies. J Nucl Med 1994;35:317-25.

26. Govindan SV, Michel RB, Griffiths GL, Goldenberg DM, Mattes MJ. Deferoxamine as a chelator for 67Ga in the preparation of antibody conjugates. Nucl Med Biol 2005;32:513-9.

27. Fani M, Andre JP, Maecke HR. 68Ga-PET: a powerful generator-based alternative to cyclotron-based PET radiopharmaceuticals. Contrast Media Mol Imaging 2008;3:67-77.

28. Schrijvers AH, Quak JJ, Uyterlinde AM, van Walsum M, Meijer CJ, Snow GB, et al. MAb U36, a novel monoclonal antibody successful in immunotargeting of squamous cell carcinoma of the head and neck. Cancer Res 1993;53:4383-90.

29. Welters MJ, Fichtinger-Schepman AM, Baan RA, Hermsen MA, van der Vijgh WJ, Cloos J, et al.: Relationship between the parameters cellular differentiation, doubling time and platinum accumulation and cisplatin sensitivity in a panel of head and neck cancer cell lines. Int J Cancer 1997;71:410-5.

30. Lindmo T, Boven E, Cuttitta F, Fedorko J, Bunn PA. Determination of the immunoreactive fraction of radiolabeled monoclonal antibodies by linear extrapolation to binding at infinite antigen excess. J Immunol Methods 1984;72:77-89.

31. De Jong HW, van Velden FH, Kloet RW, Buijs FL, Boellaard R, Lammertsma AA. Performance evaluation of the ECAT HRRT: an LSO-LYSO double layer high resolution, high sensitivity scanner. Phys Med Biol 2007;52:1505-26.

32. Loening AM, Gambhir SS. AMIDE: a free software tool for multimodality medical image analysis. Mol Imaging 2003;2:131-7.

33. Van Dongen GA, Vosjan MJ. Immuno-Positron Emission Tomography: Shedding Light on Clinical Antibody Therapy. Cancer Biother Radiopharm 2010;25:375-85.

34. Gebhardt P, Opfermann T, Saluz HP. Computer controlled 68Ga milking and concentration system. Appl Radiat Isot 2010;68:1057-9.

35. Baum RP, Prasad V, Muller D, Schuchardt C, Orlova A, Wennborg A, et al. Molecular imaging of HER2-expressing malignant tumors in breast cancer patients using synthetic 111In- or 68Ga-labeled affibody molecules. J Nucl Med 2010;51:892-7.

36. Tolmachev V, Stone-Elander S. Radiolabelled proteins for positron emission tomography: Pros and cons of labelling methods. Biochim Biophys Acta 2010;1800:487-510.

37. Tolmachev V, Velikyan I, Sandström M, Orlova A. A HER2-binding Affibody molecule labelled with (68)Ga for PET imaging: direct in vivo comparison with the (111)In-labelled analogue. Eur J Nucl Med Mol Imaging 2010;37:1356-67.

38. Velikyan I, Sundberg AL, Lindhe O, Hoglund AU, Eriksson O, Werner E, et al. Preparation and evaluation of (68)Ga-DOTA-hEGF for visualization of EGFR expression in malignant tumors. J Nucl Med 2005;46(11):1881-8.

39. Ren G, Zhang R, Liu Z, Webster JM, Miao Z, Gambhir SS, et al. A 2-helix small protein labeled with 68Ga for PET imaging of HER2 expression. J Nucl Med 2009;50:1492-9.

40. Visser GW, Gerretsen M, Herscheid JD, Snow GB, van Dongen G. Labeling of monoclonal antibodies with rhenium-186 using the MAG3 chelate for radioimmunotherapy of cancer: a technical protocol. J Nucl Med 1993;34:1953-63.

41. Riss PJ, Kroll C, Nagel V, Rösch F. NODAPA-OH and NODAPA-(NCS)n: synthesis, 68Ga-radiolabelling and in

vitro characterisation of novel versatile bifunctional chelators for molecular imaging. Bioorg Med Chem Lett 2008;18:5364-7.

42. Caraco C, Aloj L, Eckelman WC. The gallium-deferoxamine complex: stability with different deferoxamine concentrations and incubation conditions. Appl Radiat Isot 1998;49:1477-9.

43. Weissleder R. Molecular imaging in cancer. Science 2006;312:1168-71.

44. Huang L, Gainkam LO, Caveliers V, Vanhove C, Keyaerts M, De Baetseliers P, et al. SPECT Imaging with (99m)Tc-Labeled EGFR-Specific Nanobody for In Vivo Monitoring of EGFR Expression. Mol Imaging Biol 2008;10:167-75.

45. Gainkam LO, Huang L, Caveliers V, Keyaerts M, Hernot S, Vaneycken I, et al. Comparison of the biodistribution and tumor targeting of two 99mTc-labeled anti-EGFR Nanobodies in mice, using pinhole SPECT/Micro-CT. J Nucl Med 2008;49:788-95.

46. Verel I, Visser GW, van Dongen GA. The promise of immuno-PET in radioimmunotherapy. J Nucl Med 2005;46 Suppl 1:164S-71S.

47. Börjesson PK, Jauw YW, de Bree R, Roos JC, Castelijns JA, Leemans CR, et al. Radiation dosimetry of 89Zr-labeled chimeric monoclonal antibody U36 as used for immuno-PET in head and neck cancer patients. J Nucl Med 2009;50:1828-36.

48. Perk LR, Visser GW, Vosjan MJ, Stigter-van Walsum M, Tijink BM, Leemans CR, et al. (89)Zr as a PET surrogate radioisotope for scouting biodistribution of the therapeutic radiometals (90)Y and (177)Lu in tumor-bearing nude mice after coupling to the internalizing antibody cetuximab. J Nucl Med 2005;46:1898-906.

49. Tolmachev V, Rosik D, Wållberg H, Sjöberg A, Sandström M, Hansson M et al. Imaging of EGFR expression in murine xenografts using site-specifically labelled anti-EGFR 111In-DOTA-Z EGFR:2377 Affibody molecule: aspect of the injected tracer amount. Eur J Nucl Med Mol Imaging 2010;37:613-22.

50. Divgi CR, Welt S, Kris M, Real FX, Yeh SD, Gralla R, et al. Phase I and imaging trial of indium 111-labeled anti-epidermal growth factor receptor monoclonal antibody 225 in patients with squamous cell lung carcinoma. J Natl Cancer Inst 1991;83:97-104.

Chapter 5:

A biparatopic anti-EGFR Nanobody efficiently inhibits solid tumour growth

5

Rob C. Roovers

Maria J.W.D. Vosjan

Toon Laeremans

Rachid el Khoulati

Renée C.G. de Bruin

Kathryn M. Ferguson

Arie J. Verkleij

Guus A.M.S. van Dongen

Paul M. P. van Bergen en Henegouwen

International Journal of Cancer (2011) 129:2013-24

Abstract

The epidermal growth factor receptor (EGFR) has been shown to be a valid cancer target for antibody-based therapy. At present, several anti-EGFR monoclonal antibodies (mAbs) have been successfully used, such as cetuximab and matuzumab. X-ray crystallography data show that these antibodies bind to different epitopes on the ecto-domain of EGFR, providing a rationale for the combined use of these two antibody specificities. We have previously reported on the successful isolation of antagonistic anti-EGFR nanobodies. In our study, we aimed to improve the efficacy these molecules by combining nanobodies with specificities similar to both cetuximab and matuzumab into a single biparatopic molecule. Carefully designed phage nanobody selections resulted in two sets of nanobodies that specifically blocked the binding of either matuzumab or of cetuximab to EGFR and that did not compete for each others' binding. A combination of nanobodies from both epitope groups into the biparatopic nanobody CONAN-1 was shown to block EGFR activation more efficiently than monovalent or bivalent (monospecific) nanobodies. In addition, this biparatopic nanobody potently inhibited EGF-dependent cell proliferation. Importantly, in an in vivo model of athymic mice bearing A431 xenografts, CONAN-1 inhibited tumour outgrowth with an almost similar potency as the whole mAb cetuximab, despite the fact that CONAN-1 is devoid of an Fc portion that could mediate immune effector functions. Compared to therapy using bivalent, monospecific nanobodies, CONAN-1 was clearly more potent in tumour growth inhibition. These results show that the rational design of biparatopic nanobody-based anti-cancer therapeutics may yield potent lead molecules for further development.

Introduction

The epidermal growth factor receptor (EGFR) is a member of a family of four receptor tyrosine kinases (RTK), named Her- or cErbB1, -2, -3 and -4. The EGFR has an extra-cellular domain (ECD) which is composed of four sub-domains, two of which are involved in ligand binding and one of which is involved in homodimerisation and heterodimerisation[1,2] (for review, see Ref. 3). EGFR integrates extracellular signals from a variety of ligands to yield diverse intracellular responses[4,5]. The major signal transduction pathway activated by EGFR is composed of the Ras-mitogen-activated protein kinase (MAPK) mitogenic signalling cascade. Activation of this pathway is initiated by the recruitment of Grb2 to tyrosine-phosphorylated EGFR[6,7]. This leads to activation of Ras through the Grb2-bound Ras-guanine nucleotide exchange factor Son Of Sevenless. In addition, the PI3-kinase-Akt signal transduction pathway is also activated by EGFR, although this activation is much stronger in case there is co-expression of Her3[8, 9].

The EGFR is implicated in several human epithelial malignancies, notably cancers of the breast, lung, colon, head and neck and brain[10]. Activating mutations in the gene have been found, as well as over-expression of the receptor and of its ligands, giving rise to autocrine activation loops (for review, see Ref 11). This RTK has therefore been extensively used as target for cancer therapy. Both small molecule inhibitors targeting the RTK and monoclonal antibodies (mAbs) directed to the extracellular ligand-binding domains have been developed and have shown hitherto several clinical successes, albeit mostly for a select group of patients[12].

From the crystal structures of the Fab fragments of several therapeutic mAbs in complex with the ECD of EGFR[13-15], much knowledge about the working mechanisms of these antibodies has been gathered over the years (for review, see Ref. 16). Most therapeutic antibodies target the ligand-binding domain III of the EGFR. One antibody (mAb806) has been reported to recognise an unfolded region of the EGFR that is only exposed when cells either over-express EGFR or express a deletion mutant (de2-7 or variant (v) III) of the receptor[17,18]. The domain III-specific, therapeutically used antibodies, either occupy EGF contact residues directly (shown for cetuximab and panitumumab[13, 14]), or bind outside the EGF contact area and sterically inhibit the conformational change necessary for receptor activation (as was shown for matuzumab[15]). The effects of the combined use of the chimeric mAb cetuximab (derived from murine mAb 225) and humanised mAb matuzumab (derived from the murine mAb 425) on EGFR signalling has recently been investigated and this combination was indeed shown to work well in EGFR

inhibition[19].

We have previously reported the generation and use of camelid-derived single-domain antibody fragments (termed variable domain of the heavy chain of heavy chain antibodies (VHH) or Nanobody[1]) directed to EGFR in therapy of non-established tumours.[20] The single-domain nature of these fragments allows for the combination of different nanobodies with different specificities in one molecule: a biparatopic nanobody[20,21] (for review, see Ref. 22). The aim of the current study was to obtain anti-EGFR nanobodies with improved therapeutic efficacy by synthesising biparatopic molecules that would combine the specificities of the two domain III-specific anti-EGFR antibodies, i.e., cetuximab and matuzumab. We obtained antagonistic nanobodies that competed for the binding of either cetuximab or matuzumab to the receptor. When combined into one single nanobody format, together with an albumin-binding nanobody for in vivo half-life extension,[20,23,24], this nanobody CONAN-1 was shown to be a potent receptor antagonist. Importantly, our results show that in a mouse model of established A431 xenografts, this biparatopic nanobody format was very potent in inhibiting tumour outgrowth.

Materials and Methods

E.coli strain and cell lines

The bacterial strain used was TG1.[25] The epidermoid squamous carcinoma cell line A431[26] carrying an amplification of the EGFR gene[27], was purchased from the American Type Culture Collection (ATCC, cat. no. CRL-1555). Her14 cells are derived from National Institutes of Health (NIH) 3T3 fibroblasts and stably express roughly 10^5 copies of the human EGFR on their cell surface[28]. The human head and neck squamous cell carcinoma (HNSCC) cell line UM-SCC-14C (14C) was a kind gift of Dr. T.E. Carey (Ann Arbor, MI, USA). All cells were cultured in Dulbecco's modification of Eagle medium (DMEM; Gibco, Invitrogen, Paisley, UK) containing 7.5% (v/v) foetal calf serum (FCS) and 2 mM L-glutamine in a humidified atmosphere without antibiotics at 37°C under 5% CO_2.

Plasmids and constructs

The complementary DNA (cDNA)- encoding scFv 425[29], cloned as bispecific single-chain Fv antibody fragment in pSecTag,[30] was a kind gift of Dr. Van Beusechem (Department of Medical Oncology, VU University Medical Center, Amsterdam, the Netherlands). The cDNA was re-cloned from pSecTag in a bacterial expression vector identical to pUR5850[31], except lacking the C-terminal biotinylation sequence (LRSIFEAQKMEW). Induction of protein

1 The term Nanobody® is a registered trademark of Ablynx and is used with permission.

expression in E.coli and purification of scFv from the periplasmic space using Immobilise Metal ion Affinity Chromatography (IMAC) were performed as has been described.[25] The construct encoding the EGFR-ECD (amino acides 1-614) fused to a human IgG1 Fc gene was a kind gift of Prof. Dr. E.J.J. van Zoelen (Centre for Molecular Life Sciences, Radboud University, Nijmegen, the Netherlands). The construct was used to express EGFR-ECD-Fc fusion protein from an in-house developed expression vector using Hek293E cells. After 3 days of culture, cellular supernatant was collected and fusion protein was purified by means of protein G affinity chromatography.

Selection of high affinity- and of cetuximab cross-reactive anti-EGFR nanobodies

EGFR "immune" phage nanobody repertoires used for selections had been synthesised as previously described[20] and were a kind gift of Dr. E.G. Hofman (Cell Biology, Utrecht University, the Netherlands)[32]. Selections were performed on recombinant, purified and biotinylated EGFR–ECD (amino acids 1-614; Ref. 33). The protein was biotinylated using biotin amido hexanoic acid 3-sulfo-N-hydroxy succinimide ester (Sigma-Aldrich, Zwijndrecht, the Netherlands). For affinity selections, antigen concentrations used were 100, 50, 20, 10 and 1 pM. Phage (roughly 10^{10} colony-forming units) and antigen were mixed in a total volume of 100 µl phosphate buffered saline (PBS) containing 1% (w/v) casein and incubated for 3 hrs at room temperature while shaking. For off-rate selection[34], a 100-fold molar excess of non-biotinylated antigen (EGFR-ECD-Fc fusion) was added and incubated for another 3 hours at room temperature. Phage bound to biotinylated antigen were then captured in an extravidin-coated well (5 µg/ml in PBS) of a Maxisorp plate (Nunc, Rochester, NY) for 15 minutes at room tepmerature. Non-bound phage were removed by extensive washing with PBS containing 0.1% (v/v) Tween-20, and bound phage were eluted with trypsin (1 mg/ml in PBS) for 10 minutes at room temperature. Trypsin was finally inhibited by the addition of 2,2'-azino-bis(3-ethyl-benzthiazoline-6-sulphonic acid (ABTS) (1 mM), and selected phage were used to infect TG1 as described previously[35].

For the selection of cetuximab-competitive nanobodies, the method of competitive elution[36] was used. Briefly, biotinylated EGFR-ECD (4 µg/ml) was captured in a neutravidin-coated (5 µg/ml overnight in PBS at 4°C) Maxisorp plate for 1 hr at room temperature. Phage were allowed to bind for 2 hrs in PBS/0.5% (w/v) casein, and subsequently, plates were thoroughly washed (as described previousy). Phage bound to overlapping epitopes on EGFR as the one recognised by cetuximab were then eluted by incubation with 200 µg/ml cetuximab in PBS for four hours at room temperature.

Competition ELISA

Maxisorp plates were coated with a rabbit polyclonal anti-human IgG serum (1:2000 in PBS; Dako, Glostrup, Sweden) overnight at 4°C. Next day, wells were washed with PBS, blocked with 2% (w/v) bovine serum albumin (BSA) in PBS (PBS/BSA; 30 min at room temperature), and purified EGFR-ECD-Fc was captured at 0.75 µg/ml in PBS/BSA for 1 hr at room temperature. All further incubations were performed in PBS/BSA.

For EGF competition, wells were washed with PBS and a mix of nanobody [either crude periplasmic extract (50% (v/v) in PBS/BSA) or varying concentrations of purified Nanobody] in 800 pM of biotinylated EGF (Molecular probes/Invitrogen, Carlsbad, CA) was added. After incubation for 1 hr at room tempeature, wells were washed again, and bound EGF was detected with peroxidase-coupled streptavidin (1 in 5000 in PBS/BSA; Jackson ImmunoResearch Laboratories, Suffolk, England) and staining with ortho-phenylene diamine (OPD)/H_2O_2.

For cetuximab, mab 425 or nanobody competition, monoclonal phage were prepared as described.[35] Roughly 10^{10} phage were mixed with a 100-fold molar excess of either cetuximab, the 425 scFv or nanobody in 2% (w/v) Marvel (skimmed milk powder) in PBS (MPBS), and the mix was added to coated wells containing the EGFR ECD-Fc in triplicate. Bound phage was detected with a peroxidase-coupled antibody to M13 (1:10000 in MPBS; Amersham/GE Healthcare, Uppsala, Sweden) and staining with OPD/H_2O_2. Optical density was read at 490nm.

Re-cloning and expression of selected Nanobody-genes

The cDNA-encoding nanobody Alb1 was made synthetically[37] using the sequence information published in patent WO2006/122786. For the synthesis of bivalent and trivalent nanobodies, nanobody-encoding genes were PCR-amplified using the Expand High Fidelity PCR System (Roche, Mannheim, Germany) with an appropriate primer set, purified, cut with restriction enzymes and cloned into Sfi1-BstEII cut pUR 5850[31]. Linker sequences [composed of Gly4-Ser (G_4S) repeats] were encoded in the primers, making it possible to vary the length of the linker separating two nanobody genes. Constructs were sequenced[38] to verify that no mutations were introduced by PCR. Protein expression in E.coli TG1 and purification were performed as described[25].

Inhibition of EGFR signalling by selected nanobodies and test for EGFR agonism

The assays measuring the inhibition of EGF-induced EGFR activation by nanobodies and detecting possible agonistic effects of nanobodies on the receptor were performed as

described previously.[20] To demonstrate that equal amounts of cell lysate were loaded in each lane, blots were stained for either for β-actin, or for tubulin.

Inhibition of cell proliferation by nanobodies

Measurement of inhibition of cell proliferation by nanobodies or cetuximab using the sulpho-rhodamine B (SRB) assay[39] was performed as described previously[20].

Affinity measurements and pharmacokinetics

Nanobodies were ^{125}I-labelled according to the IODO-GEN method,[40] as described by Visser et al.[41].

For affinity measurements, UM-SCC-14C cells were seeded a day before the assay in 24-well tissue culture plates (Corning, Amsterdam, The Netherlands) at 100000 cells per well. ^{125}I-labelled nanobodies were diluted in binding medium [DMEM, containing 7.5 % (v/v) FCS, 25 mM 4-(2-hydroxyethyl)-1-piperazine ethanesulfonic acid (HEPES) and 2 % (w/v) Marvel] and added to cells in triplicate. After 2 hrs of incubation at 4°C, non-bound nanobody was removed by washing twice with ice-cold PBS. Bound nanobody was then quantified by lysis of the cells in 1 M NaOH and quantification of the radio-activity using a gamma counter (Wallac, Turku, Finland). Results were analysed with the Graph Pad software.

Measurement of in vivo pharmacokinetics with ^{131}I-7D12-9G8-Alb1 was performed in tumour-bearing mice essentially as described[24]. Next to a therapeutic dose of trivalent nanobody (in Group 2 in the "Therapy study" section), each mouse was injected intra-peritoneally (i.p.) with 0.33 MBq of radiolabelled nanobody (7.5 µg), and blood was drawn at 2, 6, 24, 48, and 72 hrs post injection (p.i.) to determine detailed pharmacokinetics.

Therapy study

The therapy study was performed essentially as described before[20]. However, therapy was started when tumours were established, and the average size of the tumours was approximately 100mm^3. Group 1 received PBS twice a week during 5 weeks, Group 2 received nanobody and Group 3 received cetuximab. Together with the second and seventh dose of nanobody administration, pharmacokinetics were determined in the nanobody-treated group. Anti-tumour effects were expressed by a growth delay factor (GDF), which was defined as the difference in the median time tumours needed to quadruple in the treated group and in the control group, divided by the median quadrupling time of the control group.

Results

Our study set out to improve the inhibitory capacity of anti-EGFR nanobodies by generating bi-paratopic molecules that are specific for different epitopes on domain III of the EGFR. Therefore, phage nanobody selections were performed using the purified ecto-domain of EGFR as target antigen and "immune" phage nanobody repertoires.[20,32] To obtain the different nanobody specificities, we made use of the mAbs cetuximab and matuzumab that were shown to bind to different and non-overlapping epitopes on domain III of the EGFR[13,15,16]. We first set out to obtain antagonistic nanobodies with the highest affinity possible, by performing phage selections on very low amounts of biotinylated antigen in solution, combined with "off-rate selections"[34]. When selected nanobody clones were tested for EGF competition, six clones (out of 180 clones screened) were found to inhibit the binding of EGF to the EGFR (data not shown). These were subsequently screened for their kinetic dissociation rate constant (k_{off}). Dissociation rate constants were found to vary between 2 and 150 x 10^{-4} s^{-1} (Table 1). Because of their low dissociation rate constants, clones 9G8 and 38G7 were then selected for further characterisation (the amino acid sequences of these selected nanobodies can be found in the Supporting Information).

Table 1. Kinetic dissociation rate constants of selected antagonistic anti-EGFR nanobodies as measured by SPR using BIAcore

Nanobody	k_{off} (10^{-4} s^{-1})
27H7	31.2
27E5	20.4
27C7	12.4
27E8	17.3
9G8	4.0
38G7	2.0
7C12	150
7D12	25

After protein production and purification, the IC_{50} for EGF binding to EGFR for both nanobodies was measured in enzyme-linked immuno-sorbent assay (ELISA) and found to be 6-7 nM for the 9G8 nanobody and 10 nM for the 38G7 nanobody (Fig. 1a). As the 9G8 nanobody showed a lower IC_{50} for EGF binding, expressed to a much higher level in E.coli and because the 38G7 amino acid sequence contained some very unusual

amino acids at several key positions (data not shown), the 9G8 nanobody was selected for further engineering. To gain insight into the epitope specificity of the selected anti-EGFR antagonists, selected nanobodies were tested for their competition for binding to the EGFR with the whole antibody cetuximab or the scFv of the 425 antibody (matuzumab). Surprisingly, all the selected nanobodies competed with the 425 scFv for binding, but not with cetuximab (shown for 9G8 in Fig. 1b).

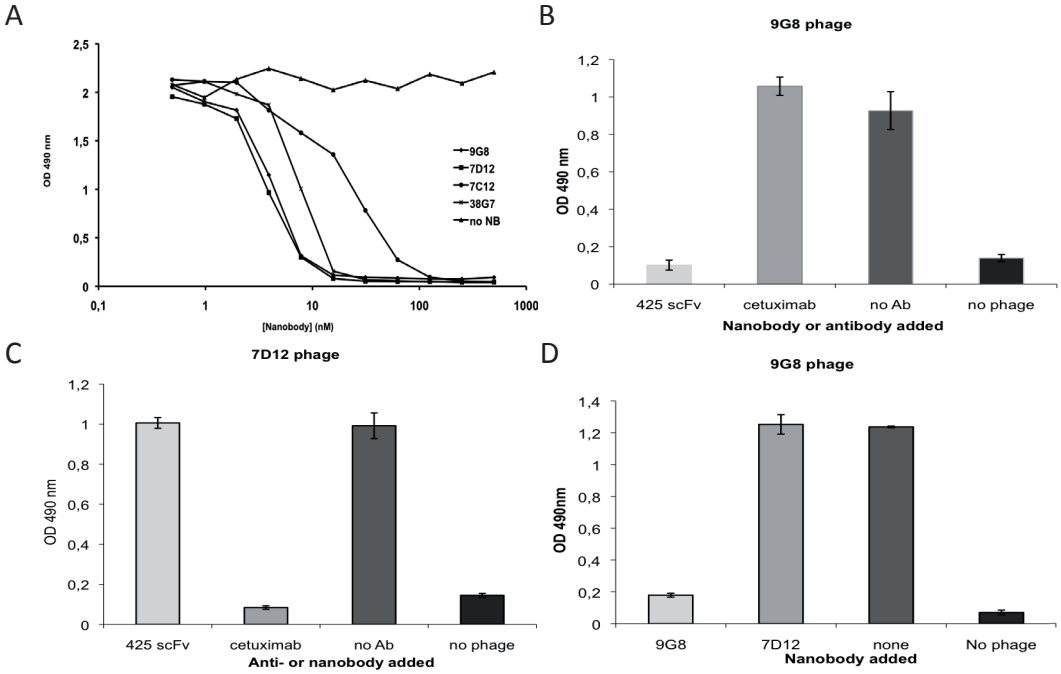

Figure 1. In vitro characterisation of selected monovalent anti-EGFR nanobodies
(a) The binding of biotinylated EGF (800 pM) to an EGFR-ECD-Fc fusion was tested in the presence of increasing amounts of the 9G8, 7D12, 7C12 or 38G7 nanobodies, or without nanobody. Receptor-bound EGF was then detected via peroxidase-coupled streptavidin and staining with OPD/H_2O_2. (b-d) The binding to EGFR of the 9G8, 7D12 and 9G8 nanobody, expressed on phage, was detected in a 100-fold molar excess of the indicated antibody (cetuximab) or antibody fragments.

We then specifically sought to select nanobodies that would recognise an epitope that overlapped with that of cetuximab by using the method of competitive elution[36] with the antibody cetuximab. Selected nanobodies were subsequently tested for EGF antagonism, as well as for competition with cetuximab for binding to EGFR in ELISA. Two nanobodies were selected (called 7C12 and 7D12) that blocked the binding of EGF to the EGFR (Fig. 1a) and indeed competed for the binding of cetuximab and not for that of the scFv of matuzumab (shown for the 7D12 nanobody in Fig. 1c). Based on its lower IC_{50} for EGF binding (8 vs 30 nM: Fig. 1a) and lower off-rate (2.5 x 10^{-3} vs 1.5 x 10^{-2} s^{-1}; Table 1), the 7D12 nanobody was then selected for further engineering. However, the fact that the 7D12 and 9G8 nanobodies competed for binding to EGFR with two mAbs that do not

block each others' binding[13,15] does not necessarily mean that they did not compete for each others' binding. To confirm that the 7D12 and 9G8 nanobodies indeed had different epitope specificities, they were tested for competitive binding to immobilised EGFR. Indeed, and as expected, 7D12 and 9G8 did not compete for each others' binding to EGFR (Fig. 1d).

The linking of two nanobody "heads" into bivalent molecules has already been shown to increase the potency of such molecules[20,42]. To find the optimal bivalent anti-EGFR nanobody combination, the 7D12 and 9G8 nanobody-encoding genes were re-formatted into bivalent molecules[21] in all possible combinations, bivalent, mono-specific, or dual-specific/bi-paratopic, using a standard flexible linker of 10 amino acids (in G_4S repeats). The affinities of the monovalent nanobodies, as well as that of the bivalent and biparatopic nanobodies were then determined by binding of ^{125}I-labelled nanobody to live cells. As expected, bivalent molecules had higher affinities than the corresponding monovalent counterparts (Table 2). The mono-specific 7D12-7D12 had the highest affinity, followed by the 7D12-9G8 biparatopic molecule.

Table 2. Affinity values of anti-EGFR nanobodies as meausred by binding of ^{125}I-labelled nanobody to live cells.

Nanobody	KD (nM) on 14C cells	KD (nM) on A431 cells
9G8	14.4	13.8
7D12	10.4	25.7
7D12-7D12	2.1	4.6
9G8-9G8	2.8	10.7
9G8-7D12	7.1	7.5
7D12-9G8	3.1	5.4

Subsequently, all constructs were tested for their capacity to inhibit EGF-induced EGFR phosphorylation and EGF-dependent cell proliferation. All nanobodies dose-dependently inhibited the EGF-induced phosphorylation of tyrosine (Y) 1068 of the EGFR (Fig. 2). As phosphorylation of Y1068 of the EGFR has been reported to be the initiation of signalling towards Ras[6], this phosphorylation site of EGFR was measured. The best inhibition was achieved with the bivalent 7D12 nanobody and biparatopic molecules 9G8-7D12 and 7D12-9G8. However, the first two showed a slight increase in receptor phosphorylation at the highest nanobody dose used (Fig. 2), a phenomenon that was not observed for the 7D12-9G8 biparatopic molecule. These results clearly show that the biparatopic anti-EGFR nanobody 7D12-9G8 performed best in inhibiting EGFR signalling.

When tested for their capacity to inhibit tumour cell proliferation, all nanobodies inhibited the growth of A431 cells (Fig. 3). For comparison, the whole mAb cetuximab was used as reference in all experiments. The biparatopic nanobody 7D12-9G8 proved as effective as cetuximab in reducing the growth of A431 cells (Fig. 3d). Both bivalent,

monospecific nanobodies 7D12-7D12 and 9G8-9G8 proved less effective in inhibiting the proliferation of A431 cells (Fig. 3a and b) than cetuximab or the 7D12-9G8 nanobody. For both bivalent, monospecific molecules increased cell proliferation was observed at higher nanobody concentrations, consistent with the observed increased level of EGFR phosphorylation (Fig. 2). Also, mixtures of monovalent 7D12 and 9G8 or of bivalent 7D12 and bivalent 9G8 were not as potent as the biparatopic 7D12-9G8 molecule in inhibiting A431 cell proliferation (Fig. 3). The biparatopic 9G8-7D12 molecule also slightly stimulated the growth of A431 cells at low nanobody concentrations, again in agreement with the increased levels of phosphorylated EGFR observed on blot (Fig. 2). These data provide strong support for the choice of the 7D12-9G8 as the most effective biparatopic nanobody combination. In addition, they show that the order of the two heads was critically important for the activity of this biparatopic nanobody. Based on these results, the 7D12-9G8 molecule was selected for further optimisation and in vivo testing.

An important characteristic of the 7D12-9G8 molecule is the linker length and linker composition connecting the two heads. This linker is supposed to provide sufficient

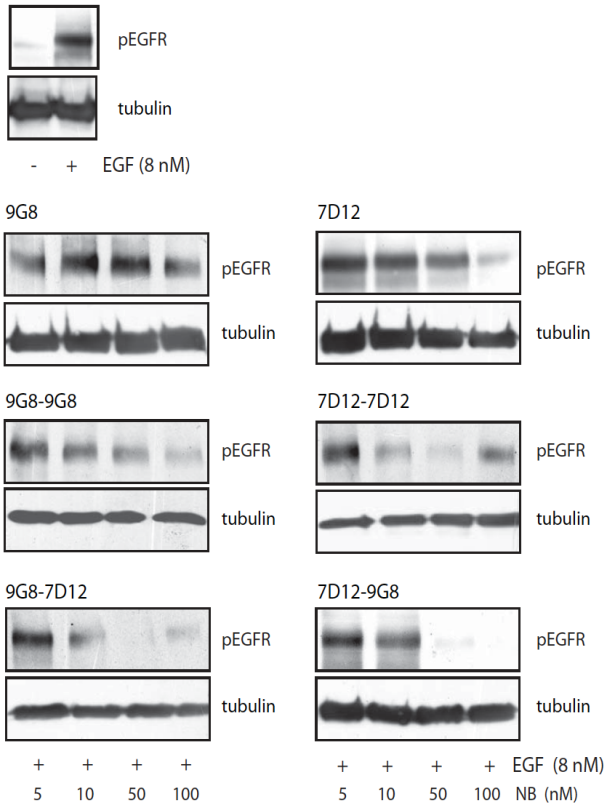

Figure 2. Inhibition of EGF-induced EGFR phosphorylation by monovalent and bivalent nanobodies EGF (8 nM) was mixed with increasing amounts of nanobody (monovalent 7D12 and 9G8; bivalent 7D12 and 9G8 and bi-paratopic nanobodies 7D12-9G8 and 9G8-7D12) and the resulting mixtures were added to Her14 cells. After stimulation for 15 min, cell lysates were prepared, and proteins were size separated and blotted to PVDF membranes. Membranes were then stained for phosphorylated EGFR (Y1068) and for the total amount of tubulin as loading control.

space/length and freedom to allow the two nanobodies to bind (chelate[43]) simultaneously to the same EGFR molecule. We therefore analysed the effect of flexible linkers consisting of G_4S repeats varying in length from 5 to 30 amino acids. The resulting bivalent constructs were then tested for their ability to inhibit A431 cell proliferation. Surprisingly, the length of the linker used between the two nanobody heads turned out to be almost inversely correlated with the efficacy of the molecule in inhibiting A431 cell proliferation, with 5- and 10- amino acids linkers being optimal (Fig. 4a). Therefore, a linker of 10 amino acids was chosen as the optimal format for the anti-EGFR 7D12-9G8 bi-paratopic nanobody.

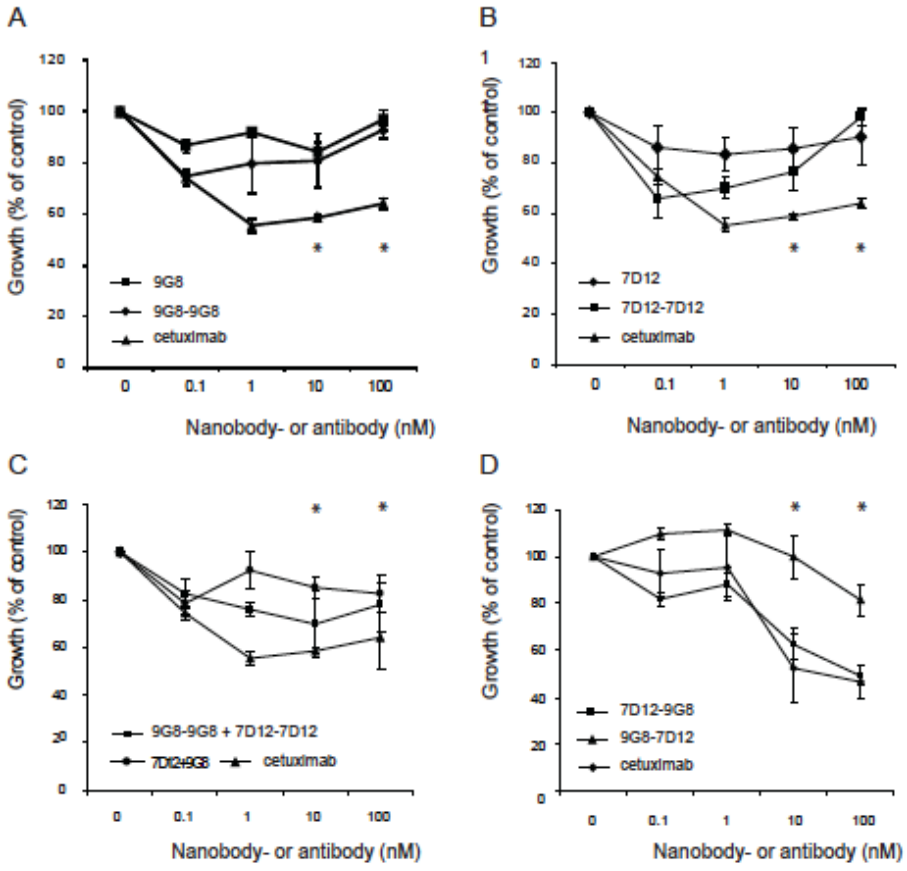

Figure 3. Inhibition of A431 tumour cell proliferation by monovalent and bivalent nanobodies (a-d) The proliferation of A431 cells in the presence of increasing amounts of nanobody [(a) monovalent and bivalent 9G8; (b) monovalent and bivalent 7D12; (c) mixtures of monovalent and bivalent 7D12 and 9G8 and (d) biparatopic molecules 7D12-9G8 and 9G8-7D12] was measured using a sulphorhodamine-based stain of total cellular protein after TCA precipitation. Proliferation is plotted as percentage of maximal growth (cells left without treatment). The whole antibody cetuximab was used as 'standard' in every test. Data points where the value of the control is statistically different from that of the nanobody-treated group are indicated by an asterix. (c) Only different between 7D12+9G8 and control; (d) only different between 9G8-7D12 and control.

Since the 7D12-9G8 nanobody has a molecular weight of roughly 30 kDa, it would be cleared very rapidly in vivo via the kidneys once injected into the blood stream of mice[44]. To prolong the in vivo half-life of small proteins, binding to albumin has been reported to be an excellent option.[20,23,24] Therefore, the gene encoding the anti-mouse serum albumin (MSA)/human serum albumin (HSA) nanobody Alb1 (this nanobody recognises both MSA as well as HSA with a equilibrium dissociation constant (KD) of 6.5 nM for MSA and 0.57 nM for HSA) was made synthetically[37] and fused C-terminally to the biparatopic 7D12-9G8 nanobody using two different linker lengths (15 or 30 amino acids in repeats of Gly_4-Ser) between the anti-EGFR nanobodies and Alb1. First, trivalent nanobodies were tested for their functionality in ELISA: the binding of biotinylated MSA to EGFR-bound 7D12-9G8 and 7D12-9G8-Alb1 was assessed and shown to depend on the presence of the Alb1 nanobody (Fig. 4b). These results show that at least one of the anti-EGFR heads together with the Alb1 nanobody present in the same trivalent molecule could simultaneously bind antigen. Since in an in vivo (therapy) situation, albumin will be abundantly present, both trivalent nanobodies (containing either a 15- or 30-amino acid linker before the Alb1 nanobody) were then tested for their capacity to inhibit A431 cell proliferation in the presence of 1 % (w/v) HSA. The construct containing a 15-amino acid linker before the Alb1 nanobody significantly lost potency in the presence of HSA (data not shown). However, for the construct containing a 30-residue linker between the anti-EGFR units and Alb1 unit, efficacy in inhibition of cell proliferation was not affected by the presence of HSA (Fig 4c). Therefore, this version was selected for further in vivo testing and was named COoperative NANobody-1 (CONAN-1).

To check whether the CONAN-1 nanobody by itself did not induce activation of the EGFR, the nanobody was given as ligand at high concentration to EGFR overexpressing cells (Her14 cells). Figure 4d shows that CONAN-1 did not cause receptor activation in the absence of EGF, whereas cells readily responded to EGF stimulation. Finally, the CONAN-1 nanobody was shown to strongly inhibit EGF induced signalling (Fig. 4e): not only receptor phosphorylation was inhibited (Fig. 2), but also the phosphorylation of MAPK reduced to background levels. These results show that the CONAN-1 nanobody functioned as a true receptor antagonist and it was therefore tested in an in vivo therapy study.

To measure blood pharmacokinetics of the CONAN-1 molecule, a trace amount of radiolabelled nanobody was injected intravenously in the tail vein of tumour-bearing mice, together with a therapeutic dose of nanobody. Blood sampling revealed an in vivo half-life of approximately 48 hrs (Fig. 5a), when fitted to a monoexponential decay. In a murine model of established A431 human xenografts in athymic mice, the administration

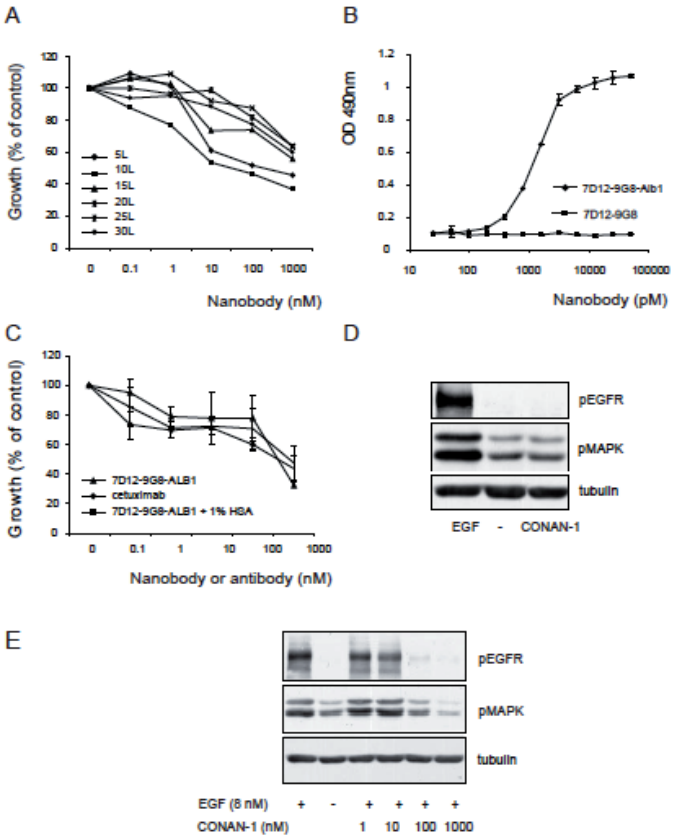

Figure 4. In vitro optimalisation and characterisation of trivalent biparatopic nanobody CONAN-1 (a) The proliferation of A431 cells in the presence of increasing amounts of biparatopic nanobody 7D12-9G8 (with linkers varying in length between the two nanobody units) was measured using a sulphorhodamine-based stain of total cellular protein after TCA precipitation. Proliferation is plotted as percentage of maximal growth (cells left without treatment). Error bars have been omitted to increase the clarity of the figure. The different linker lengths between the two nanobodies are indicated. (b) Purified EGFR-ECD-Fc fusion protein was immobilised via a coated anti-human Fc anti-serum, and a concentration range of either bivalent (7D12-9G8) or trivalent (CONAN-1) nanobody was bound. The binding of biotinylated mouse serum albumin (MSA) was subsequently detected with peroxidase-conjugated streptavidin and staining with OPD/H_2O_2. (c) The proliferation of A431 cells in the presence of increasing amounts of nanobody was measured using the sulphorhodamine B assay. The effect of the presence of human serum albumin (HSA: 1%) in the medium was assessed. (d) EGF (8 nM) or nanobody (1 µM) was added to serum-starved Her14 cells (-). After stimulation for 15 min, cell lysates were prepared, and proteins were size separated and blotted to PVDF membranes. Membranes were then stained for phosphorylated EGFR (Y1068) and for the total amount of tubulin as loading control. (e) EGF (8 nM) was mixed with increasing amounts of Nanobody, and the resulting mixture was added to Her14 cells. After stimulation for 15 minutes, cell lysates were prepared, and proteins were size separated and blotted to PVDF membranes. Membranes were then stained for phosphorylated EGFR (Y1068) and for the total amount of tubulin as loading control.

of CONAN-1 i.p. as therapy was compared to therapy using cetuximab. Based on the measured pharmacokinetics of CONAN-1 (Fig. 5a), therapy was given twice weekly. CONAN-1 had an efficacy in inhibiting the growth of established A431 tumours that was largely comparable to that of cetuximab during treatment (Fig. 5b). The mean tumour volume in the cetuximab-treated group diminished slightly after 4 days, up to 2 weeks of treatment (a phenomenon not observed in the nanobody-treated group), but then

increased at approximately the same speed as that of the nanobody-treated group. After treatment was stopped, tumours of mice in the nanobody-treated group did not regrow significantly faster than tumours of mice in the cetuximab-treated group. During therapy, CONAN-1 induced a significantly stronger effect than cetuximab during the first 6 days, but cetuximab caused a significantly stronger antitumour effect after Day 8 ($p < 0.05$; independent sample T-test). A comparison of the growth-delay factors for quadrupling of the tumour volume revealed that CONAN-1 induced a strong response in tumour growth inhibition (GDF = 1.52) but that this response was slightly stronger in the group treated with cetuximab (GDF = 2.19; Table 3). In a separate, equal experimental setup, therapy using the trivalent anti-EGFR nanobody 7D12-7D12-Alb1 was also compared to that using cetuximab. A comparison of the GDFs calculated for both nanobody treatments revealed that CONAN-1 (GDF = 1.52) induced a much stronger antitumour response than the 7D12-7D12-Alb1 nanobody (GDF = 1; Table 3). Importantly, this proves again that the combination of different paratopes and thereby different modes of EGFR inhibition into a single molecule was superior to the use of monospecific targeting for EGFR inhibition.

Discussion

Our study set out to combine nanobodies into a biparatopic format in order to improve their efficacy in tumour growth inhibition. The results show the efficacy of the optimised CONAN-1 nanobody in therapy to be better than that of monospecific 7D12-7D12-Alb1 and almost equal to that of the well-characterised anti-EGFR mAb cetuximab, although the former is devoid of immune effector functions.

To obtain anti-EGFR nanobodies that recognize non-overlapping epitopes on the ligand-binding domain 2 of EGFR (domain III), we made use of two mAbs of which the binding sites were previously shown to be different by crystallography[13,15]. First, we selected nanobodies for high affinity binding[34]. Surprisingly, these selections only resulted in clones that cross-reacted with the scFv of matuzumab (shown for the 9G8 nanobody in Fig. 1). The nanobodies Ia1, L2-3.40 and IIIa3, previously found using EGF elution,[20] were also found to compete for binding to EGFR with the 9G8 nanobody and the 425 scFv (data not shown). The high prevalence of nanobodies recognising the part of domain III also bound by matuzumab is probably a reflection of the immunogenicity of that particular part of the receptor. However, by carefully designed phage nanobody selections, cetuximab cross-reactive nanobodies were readily obtained. These results underline the power of the combination of active immunisation of Llama, nanobody repertoire cloning and phage

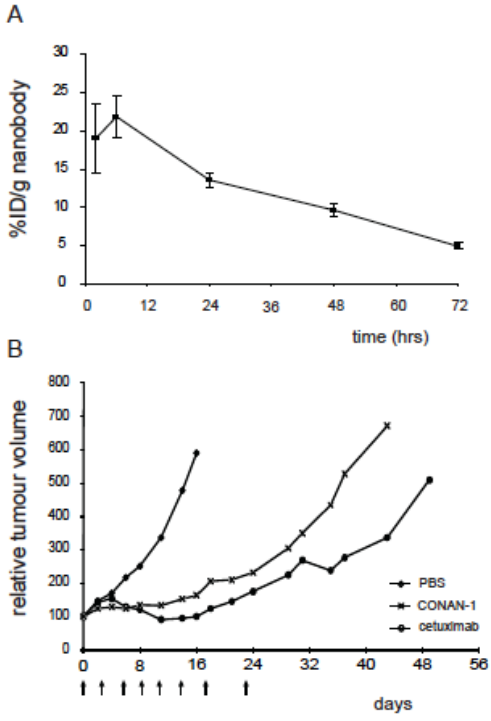

Figure 5. In vivo pharmacokinetics and therapy using CONAN-1 nanobody in athymic (nu/nu) mice bearing subcutaneous A431 xenografts (a) Together with a therapeutic dose of trivalent nanobody (1 mg), ^{131}I-labeled CONAN-1 (7.5 µg, corresponding to 0.33 MBq) was injected intraperitoneally (i.p.) in tumour-bearing athymic (nu/nu) mice to measure detailed blood pharmacokinetics. Blood pool radioactivity was measured in time and plotted as percentage of injected dose per gram of tissue as a function of time. (b) Athymic (nude) mice bearing subcutaneously implanted A431 xenografts were treated with phosphate-buffered saline (PBS; diamonds), cetuximab; barbed rounds or trivalent nanobody CONAN-1 (crosses). Treatment consisted of biweekly injections (i.p.) of 1 mg of protein (arrows).

nanobody selections to obtain nanobodies that recognise defined epitopes on a given antigen (for review, see Ref. 22).

Second, phage nanobody selections were performed in combination with specific elution using cetuximab. Only two nanobodies were found that blocked binding of EGF to EGFR and that of cetuximab to EGFR: clones 7D12 and 7C12. These nanobodies have previously been described by Gainkam et al[45]. The reported affinity of the 7D12 nanobody (2.3 nM; Ref. 45) differs from the affinity value we obtained (10 nM; Table 2). This discrepancy might well be due to the different methods used to measure the affinity. We deliberately chose for cell-binding experiments, as the affinity values obtained by this method are probably more representative for the in vivo situation. The EGFR makes numerous contacts with other receptors, integrins and lipids[32], which may shield particular epitopes on the ecto-domain that are accessible in an in vitro Surface Plasmon Resonance (SPR) setup. However, the ^{125}I-labelling of the nanobodies may have influenced their affinity, as tyrosines in the antigen binding sites may have been altered, thereby lowering the affinity.

The order in which the two nanobodies were linked together in a bivalent or biparatopic molecule was shown to be an important parameter for the efficacy of the anti-

EGFR biparatopic molecule (Figs. 2 and 3). In addition, the linker composition also strongly influenced the characteristics of the nanobody, as a hinge-derived sequence between 9G8 and 7D12 caused this biparatopic molecule to act as a receptor agonist (results not shown). The same phenomenon can slightly be observed for the 9G8-7D12 biparatopic nanobody containing a flexible linker and the 7D12-7D12 monospecific molecule (Fig. 4). The engineering and thorough testing of this type of therapeutic molecules is therefore critically important to avoid artificial receptor activation.

Table 3. Growth delay factors (GDF) for quadrupling of tumour volume after different treatment

Treatment	GDF
cetuximab	2.19
CONAN-1	1.52
7D12-7D12-Alb1	1

Surprisingly, the 7D12-7D12 bivalent nanobody had the highest affinity, yet was not the most potent in inhibiting tumour cell proliferation (Table 2 and Fig. 3). This may be explained by artificial activation of the EGFR caused by crosslinking of receptors through intermolecular binding of the nanobody. The 7D12-9G8 nanobody did not cause receptor activation (Figs. 2, 3d and 4d) and therefore functioned as true receptor antagonist. However, simultaneous binding of the two heads in the biparatopic nanobody 7D12-9G8 to one and the same EGFR molecule ("chelating" binding[43]) could not be demonstrated. Size exclusion chromatography and crosslinking experiments did not give conclusive results (data not shown). Preliminary X-ray crystallographic data confirm the predicted location of the epitopes of 7D12 and 9G8 (details of cocrystal structures of EGFR fragments with 7D12 and 9G8 will be published separately, Ferguson et al., manuscript in preparation). These structures also suggest that simultaneous binding of both heads of 7D12-9G8 may be possible with a 10-amino acids linker. However, chelating binding will be highly dependent on the linker composition. Based on the estimated locations of the C-terminus of 7D12 and N-terminus of 9G8 in these crystal structures, a linker of only 10 amino acids would have to pass very closely to the surface of EGFR. It is conceivable that such a linker does not permit the biparatopic nanobody to chelate[43] the EGFR, but that the 7D12-9G8 nanobody binds the receptor with only one head at any given time. However, the presence of the second specificity within the same molecule probably results in fast rebinding once the first nanobody unit dissociates from its epitope, thereby resulting in

increased apparent affinity (compare 7D12 and 9G8 with 7D12-9G8; Table 2) and increased potency in EGFR inhibition (Fig. 3). Also, binding of the biparatopic 7D12-9G8 to EGFR may induce some conformational change and thus an "induced fit," thereby permitting both heads to bind simultaneously. For the monospecific, bivalent 7D12-7D12 molecule, simultaneous binding of both heads would require a cluster of receptors, where domain III is available in two adjacent EGFR molecules. Predimers of EGFR in the absence of EGF have been demonstrated[46,47]. However, the EGFR in such complex will probably not be bound bivalently by 7D12-7D12, as the ligand binding domains 2 (domain III) are located on either side of the "back-to-back" dimer[2], pointing away from each other.

The in vivo half-life of the CONAN-1 nanobody was very comparable to that of a similar nanobody construct described by Tijink et al[24] and to that of directly radiolabelled MSA (data not shown). As the affinity of the Alb1 nanobody for HSA is even higher than that for MSA [6.5 nM (MSA) vs 0.57 nM (HSA)], it is expected that the CONAN-1 nanobody would circulate in humans with the same kinetics as that of HSA (its half-life being 10-14 days). The pharmacokinetics would then be very comparable to that of a whole IgG.

Treatment with cetuximab resulted in tumour regression after 4 days, which lasted until approximately day 14 (when tumour started to re-grow). This is indicative of activation of immune effector cells. Despite the fact that the CONAN-1 nanobody cannot interact with the immune system, its efficacy was largely comparable to that of cetuximab. This could be partially due to better tumour penetration[24] in combination with similar (or even better) pharmacokinetics (see Ref. 24;Fig. 5). The modular nature of nanobodies permits the addition of "effector" heads (e.g., a nanobody to recruit effector cells); it would be interesting to test such constructs in comparison with cetuximab.

The modularity of nanobodies in combination with the power and possibilities of phage display also permit the synthesis of combinations of nanobodies recognising well-defined epitopes on other receptors (e.g., the combination of nanobodies recognising the pertuzumab and trastuzumab epitopes on Her2/Neu). Additionally, it permits the synthesis of multi-specific molecules capable of inhibiting two (or even more) signal transduction pathways simultaneously, which may well lead to a higher efficacy of nanobody-mediated therapy. In conclusion, our results show that the rational design and synthesis of multivalent nanobody molecules are promising options to develop new cancer therapeutics.

Acknowledgements

The authors thank the USP/DSP team from the CMC department of Ablynx for production and purification of the CONAN-1 nanobody. They also thank Marijke Stigter-van Walsum for excellent technical assistance. R. Roovers and M. Vosjan are supported by STW grant no. 10074.

Supplemental data

Amino acid sequences of selected nanobodies; CDR regions are indicated in *italic* and underlined.

7D12*: QVKLEESGGGSVQTGGSLRLTCAASGRTSR *SYGMG* WFRQAPGKEREFVS *GISWRGDSTGYADSVKG* RFTISRDNAKNTVDLQMNSLKPEDTAIYYCAA *AAGSAWYGTLYEYDY* WGQGTQVTVSS

9G8: EVQLVESGGGLVQAGGSLRLSCAASGRTFS *SYAMG* WFRQAPGKEREFVV *AINWSSGSTYYADSVKG* RFTISRDNAKNTMYLQMNSLKPEDTAVYYCAA *GYQINSGNYNFKDYEYDY* WGQGTQVTVSS

38G7: EVQLVESGGGLVQAGGSLRLSCAASGRTFS *SYVMG* WFRQATGKEREFVA *TIAWDSGSTYYADSVKG* RFTISRDNAKNTVHLQMNSLKPEDTAVYYCAA *SYNVYYNNYYYPISRDEYDY* WGQGTQVTVSS

*The amino acid sequence of 7D12 can already be found in the paper by Gainkam et al. (J Nucl Med. 2008 May;49(5):788-795).

References

1. Garrett TP, McKern NM, Lou M, Elleman TC, Adams TE, Lovrecz GO, Zhu HJ, Walker F, Frenkel MJ, Hoyne PA, Jorissen RN, Nice EC, et al. Crystal structure of a truncated epidermal growth factor receptor extracellular domain bound to transforming growth factor alpha. Cell 2002;110:763-73.

2. Ogiso H, Ishitani R, Nureki O, Fukai S, Yamanaka M, Kim JH, Saito K, Sakamoto A, Inoue M, Shirouzu M, Yokoyama S. Crystal structure of the complex of human epidermal growth factor and receptor extracellular domains. Cell 2002;110:775-87.

3. Ferguson KM. Structure-based view of epidermal growth factor receptor regulation. Annu Rev Biophys 2008;37:353-73.

4. Yarden Y. The EGFR family and its ligands in human cancer. signalling mechanisms and therapeutic opportunities. Eur J Cancer 2001;37 Suppl 4:S3-8.

5. Jorissen RN, Walker F, Pouliot N, Garrett TP, Ward CW, Burgess AW. Epidermal growth factor receptor: mechanisms of activation and signalling. Exp Cell Res 2003;284:31-53.

6. Buday L, Downward J. Epidermal growth factor regulates p21ras through the formation of a complex of receptor, Grb2 adapter protein, and Sos nucleotide exchange factor. Cell 1993;73:611-20.

7. Gale NW, Kaplan S, Lowenstein EJ, Schlessinger J, Bar-Sagi D. Grb2 mediates the EGF-dependent activation of guanine nucleotide exchange on Ras. Nature 1993;363:88-92.

8. Soltoff SP, Carraway KL, III, Prigent SA, Gullick WG, Cantley LC. ErbB3 is involved in activation of phosphatidylinositol 3-kinase by epidermal growth factor. Mol Cell Biol 1994;14:3550-8.

9. Prigent SA, Gullick WJ. Identification of c-erbB-3 binding sites for phosphatidylinositol 3'-kinase and SHC using an EGF receptor/c-erbB-3 chimera. Embo J 1994;13:2831-41.

10. Uberall I, Kolar Z, Trojanec R, Berkovcova J, Hajduch M. The status and role of ErbB receptors in human cancer. Exp Mol Pathol 2008;84:79-89.

11. Robertson SC, Tynan J, Donoghue DJ. RTK mutations and human syndromes: when good receptors turn bad. Trends Genet 2000;16:368.

12. Patel DK. Clinical use of anti-epidermal growth factor receptor monoclonal antibodies in metastatic colorectal cancer. Pharmacotherapy 2008;28:31S-41S.

13. Li S, Schmitz KR, Jeffrey PD, Wiltzius JJ, Kussie P, Ferguson KM. Structural basis for inhibition of the epidermal growth factor receptor by cetuximab. Cancer Cell 2005;7:301-11.

14. Li S, Kussie P, Ferguson KM. Structural basis for EGF receptor inhibition by the therapeutic antibody IMC-11F8. Structure 2008;16:216-27.

15. Schmiedel J, Blaukat A, Li S, Knochel T, Ferguson KM. Matuzumab binding to EGFR prevents the conformational rearrangement required for dimerization. Cancer Cell 2008;13:365-73.

16. Schmitz KR, Ferguson KM. Interaction of antibodies with ErbB receptor extracellular regions. Exp Cell Res 2009;315:659-70.

17. Johns TG, Adams TE, Cochran JR, Hall NE, Hoyne PA, Olsen MJ, Kim YS, Rothacker J, Nice EC, Walker F, Ritter G, Jungbluth AA, et al. Identification of the epitope for the epidermal growth factor receptor-specific monoclonal antibody 806 reveals that it preferentially recognizes an untethered form of the receptor. J Biol Chem 2004;279:30375-84.

18. Garrett TP, Burgess AW, Gan HK, Luwor RB, Cartwright G, Walker F, Orchard SG, Clayton AH, Nice EC, Rothacker J, Catimel B, Cavenee WK, et al. Antibodies specifically targeting a locally misfolded region of tumor associated EGFR. Proc Natl Acad

Sci U S A 2009;106:5082-7.

19. Kamat V, Donaldson JM, Kari C, Quadros MR, Lelkes PI, Chaiken I, Cocklin S, Williams JC, Papazoglou E, Rodeck U. Enhanced EGFR inhibition and distinct epitope recognition by EGFR antagonistic MABS C225 And 425. Cancer Biol Ther 2008;7:726-33.

20. Roovers RC, Laeremans T, Huang L, De Taeye S, Verkleij AJ, Revets H, de Haard HJ, van Bergen en Henegouwen PM. Efficient inhibition of EGFR signaling and of tumour growth by antagonistic anti-EFGR Nanobodies. Cancer Immunol Immunother 2007;56:303-17.

21. Els Conrath K, Lauwereys M, Wyns L, Muyldermans S. Camel single-domain antibodies as modular building units in bispecific and bivalent antibody constructs. J Biol Chem 2001;276:7346-50.

22. Roovers RC, van Dongen GAMS, van Bergen en Henegouwen PM. Nanobodies in therapeutic applications. Curr Opin Mol Ther 2007;9:327-35.

23. Dennis MS, Zhang M, Meng YG, Kadkhodayan M, Kirchhofer D, Combs D, Damico LA. Albumin binding as a general strategy for improving the pharmacokinetics of proteins. J Biol Chem 2002;277:35035-43.

24. Tijink BM, Laeremans T, Budde M, Stigter-van Walsum M, Dreier T, de Haard HJ, Leemans CR, van Dongen GA. Improved tumor targeting of anti-epidermal growth factor receptor Nanobodies through albumin binding: taking advantage of modular Nanobody technology. Mol Cancer Ther 2008;7:2288-97.

25. Roovers RC, Henderikx P, Helfrich W, van der Linden E, Reurs A, de Bruine AP, Arends JW, de Leij L, Hoogenboom HR. High-affinity recombinant phage antibodies to the pan-carcinoma marker epithelial glycoprotein-2 for tumour targeting. Br J Cancer 1998;78:1407-16.

26. Giard DJ, Aaronson SA, Todaro GJ, Arnstein P, Kersey JH, Dosik H, Parks WP. In vitro cultivation of human tumors: establishment of cell lines derived from a series of solid tumors. J Natl Cancer Inst 1973;51:1417-23.

27. Merlino GT, Xu YH, Ishii S, Clark AJ, Semba K, Toyoshima K, Yamamoto T, Pastan I. Amplification and enhanced expression of the epidermal growth factor receptor gene in A431 human carcinoma cells. Science 1984;224:417-9.

28. Honegger AM, Dull TJ, Felder S, Van Obberghen E, Bellot F, Szapary D, Schmidt A, Ullrich A, Schlessinger J. Point mutation at the ATP binding site of EGF receptor abolishes protein-tyrosine kinase activity and alters cellular routing. Cell 1987;51:199-209.

29. Murthy U, Basu A, Rodeck U, Herlyn M, Ross AH, Das M. Binding of an antagonistic monoclonal antibody to an intact and fragmented EGF-receptor polypeptide. Arch Biochem Biophys 1987;252:549-60.

30. Haisma HJ, Grill J, Curiel DT, Hoogeland S, van Beusechem VW, Pinedo HM, Gerritsen WR. Targeting of adenoviral vectors through a bispecific single-chain antibody. Cancer Gene Ther 2000;7:901-4.

31. De Haard HJ, Bezemer S, Ledeboer AM, Muller WH, Boender PJ, Moineau S, Coppelmans MC, Verkleij AJ, Frenken LG, Verrips CT. Llama antibodies against a lactococcal protein located at the tip of the phage tail prevent phage infection. J Bacteriol 2005;187:4531-41.

32. Hofman EG, Ruonala MO, Bader AN, van den Heuvel D, Voortman J, Roovers RC, Verkleij AJ, Gerritsen HC, van Bergen En Henegouwen PM. EGF induces coalescence of different lipid rafts. J Cell Sci 2008;121:2519-28.

33. Ferguson KM, Darling PJ, Mohan MJ, Macatee TL, Lemmon MA. Extracellular domains drive homo- but not hetero-dimerization of erbB receptors. Embo J 2000;19:4632-43.

34. Hawkins RE, Russell SJ, Winter G. Selection of phage antibodies by binding affinity. Mimicking affinity maturation. J Mol Biol 1992;226:889-96.

35. Marks JD, Hoogenboom HR, Bonnert TP, McCafferty J, Griffiths AD, Winter G. By-passing immunization. Human antibodies

from V-gene libraries displayed on phage. J Mol Biol 1991;222:581-97.

36. Meulemans EV, Slobbe R, Wasterval P, Ramaekers FC, van Eys GJ. Selection of phage-displayed antibodies specific for a cytoskeletal antigen by competitive elution with a monoclonal antibody. J Mol Biol 1994;244:353-60.

37. Stemmer WP, Crameri A, Ha KD, Brennan TM, Heyneker HL. Single-step assembly of a gene and entire plasmid from large numbers of oligodeoxyribonucleotides. Gene 1995;164:49-53.

38. Sanger F, Nicklen S, Coulson AR. DNA sequencing with chain-terminating inhibitors. Proc Natl Acad Sci U S A 1977;74:5463-7.

39. Skehan P, Storeng R, Scudiero D, Monks A, McMahon J, Vistica D, Warren JT, Bokesch H, Kenney S, Boyd MR. New colorimetric cytotoxicity assay for anticancer-drug screening. J Natl Cancer Inst 1990;82:1107-12.

40. Frieden E, Lipsett MB, Winzler RJ. Methods for Labeling Thyroxine With Radioactive Iodine. Science 1948;107:353-4.

41. Visser GW, Klok RP, Gebbinck JW, ter Linden T, van Dongen GA, Molthoff CF. Optimal quality (131)I-monoclonal antibodies on high-dose labeling in a large reaction volume and temporarily coating the antibody with IODO-GEN. J Nucl Med 2001;42:509-19.

42. Coppieters K, Dreier T, Silence K, de Haard H, Lauwereys M, Casteels P, Beirnaert E, Jonckheere H, Van de Wiele C, Staelens L, Hostens J, Revets H, et al. Formatted anti-tumor necrosis factor alpha VHH proteins derived from camelids show superior potency and targeting to inflamed joints in a murine model of collagen-induced arthritis. Arthritis Rheum 2006;54:1856-66.

43. Neri D, Momo M, Prospero T, Winter G. High-affinity antigen binding by chelating recombinant antibodies (CRAbs). J Mol Biol 1995;246:367-73.

44. Cortez-Retamozo V, Lauwereys M, Hassanzadeh Gh G, Gobert M, Conrath K, Muyldermans S, De Baetselier P, Revets H. Efficient tumor targeting by single-domain antibody fragments of camels. Int J Cancer 2002;98:456-62.

45. Gainkam LO, Huang L, Caveliers V, Keyaerts M, Hernot S, Vaneycken I, Vanhove C, Revets H, De Baetselier P, Lahoutte T. Comparison of the Biodistribution and Tumor Targeting of Two 99mTc-Labeled Anti-EGFR Nanobodies in Mice, Using Pinhole SPECT/Micro-CT. J Nucl Med 2008;49:788-95.

46. Clayton A, Walker F, Orchard S, Henderson C, Fuchs D, Rothacker J, Nice E, Burgess A. Ligand-induced dimer-tetramer transition during the activation of the cell surface epidermal growth factor receptor-A multidimensional microscopy analysis. J Biol Chem 2005;280:30392-9.

47. Hofman EG, Bader AN, Voortman J, Van den Heuvel DJ, Sigismund S, Verkleij AJ, Gerritsen HC, Van Bergen en Henegouwen PM. Ligand-induced epidermal growth factor receptor (EGFR) oligomerization is kinase-dependent and enhances internalization. J Biol Chem 2010;285:39481-9.

Chapter 6:

Nanobodies targeting the hepatocyte growth factor: potential new drugs for molecular cancer therapy

Maria J.W.D. Vosjan
Jo Vercammen
Joost A. Kolkman
Marijke Stigter-van Walsum
Hilde Revets
Guus A.M.S. van Dongen

6

Molecular Cancer Therapeutics (2012) 11:1017-25

Abstract

Hepatocyte Growth Factor (HGF) and its receptor c-Met are associated with increased aggressiveness of tumors and poor prognostic outcome of patients with cancer. Here, we report the development and characterization of therapeutic anti-HGF (αHGF)-Nanobodies and their potential for positron emission tomographic (PET) imaging to assess HGF expression in vivo.

Two αHGF-Nanobodies designated 1E2 and 6E10 were identified, characterized, and molecularly fused to an albumin-binding Nanobody unit (Alb8) to obtain serum half-life extension. The resulting Nanobody formats were radiolabeled with the positron emitter zirconium-89 (^{89}Zr, $t_{½}$=78 hours), administered to nude mice bearing U87 MG glioblastoma xenografts, and their biodistribution was assessed. In addition, their therapeutic effect was evaluated in the same animal model at doses of 10, 30 or 100 µg per mouse.

The ^{89}Zr-Nanobodies showed similar biodistribution with selective tumor targeting. For example, 1E2-Alb8 showed decreased blood levels of 12.6%ID/g±0.6%ID/g, 7.2%ID/g±1.0%ID/g, 3.4%ID/g±0.3%ID/g and 0.3%ID/g±0.1%ID/g at 1, 2, 3, and 7 days after injection, whereas tumor uptake levels remained relatively stable at these time points: 7.8%ID/g±1.1%ID/g, 8.9%ID/g±1.0%ID/g, 8.7%ID/g±1.5%ID/g and 7.2%ID/g±1.6%ID/g. Uptake in normal tissues was lower than in tumor, except for kidneys.

In a therapy study, all Nanobody-treated mice showed tumor growth delay compared with the control saline group. In the 100-µg group, four of six mice were cured after treatment with 1E2-Alb8 and 73 days follow-up, and three of six mice when treated with 6E10-Alb8.

These results provide evidence that Nanobodies 1E2-Alb8 and 6E10-Alb8 have potential for therapy and PET imaging of HGF-expressing tumors.

Introduction

Hepatocycte growth factor (HGF), also known as scatter factor, is secreted as a single-chain, inactive polypeptide by mesenchymal cells, and is cleaved by serine proteases into a 69-kDa α-chain and 34-kDa β-chain (1-3). HGF is the only known ligand for the c-Met receptor. The c-Met receptor is expressed during embryogenesis and adulthood in the epithelial cells of many organs like liver, prostate, pancreas, muscle, kidney, and bone marrow. In tumor cells, c-Met activation triggers diverse series of signaling cascades resulting in cell growth, proliferation, invasion, metastasis formation, and escape from apoptosis (3). Overexpression of HGF and c-Met is associated with increased aggressiveness of tumors and poor prognostic outcome of patients with cancer (www.vai.org/vari/metandcancer and ref. 4). HGF and c-Met expression have been observed in most solid tumors. Blocking the soluble factor might be a beneficial strategy over blocking the c-Met receptor, as HGF is expected to be highly expressed in the tumor only, is easily accessible for Nanobodies, and is the only know ligand for the c-Met receptor. The possibility for success with targeting soluble factors has been illustrated with the anti-VEGF antibody bevacizumab (5).

The last decades several pharmaceutical companies have been actively involved in the development of therapeutic tyrosine kinase inhibitors and monoclonal antibodies (mAbs) that antagonize c-Met activation. At least 16 agents have been or are being evaluated in the clinic at the moment, as reviewed by Liu and colleagues (6). To their and our knowledge, 3 anti-HGF (αHGF) mAbs are under clinical development at the moment, including AMG102 (rilotumumab), a humanized anti-human HGF IgG2 from Amgen, AV-299 from Schering/Aveo, and TAK-701 from Millennium.

In the present study, we introduce αHGF-Nanobodies. Nanobodies are derived from a unique antibody format that is present in species from the family of Camelidae, including llama, camel, and dromedary. These animals contain, besides their conventional antibody repertoire, an antibody class consisting of heavy chain-only antibodies (7-9). The variable region of the heavy chain-only antibodies (VHH) represents the complete binding unit of the antibody and is also termed Nanobody®. Unique features of the Nanobody technology platform in comparison to conventional mAb technology are rapid drug development, biophysical and chemical robustness, and the potential to target intractable targets for antibodies including G-protein-coupled receptors (GPCR) and ion channels (9). Particularly attractive is the ability to design modular drugs based on 15-kDa Nanobody building blocks combined with each other, with other protein domains or with other molecules or drugs. Nanobodies have been combined in a wide range of

formats, including multivalent (multiple Nanobodies with identical-binding sites for the same antigen; refs. 10,11), biparatopic (2 Nanobodies binding to 2 different epitopes on the same antigen; refs. 12,13), and bispecific (Nanobodies binding to 2 different antigens; refs. 13,14) molecules. These formats are easy to construct and the modular proteins can often be expressed at high levels in bacteria or yeast. As a result of this formatting flexibility, the range of therapeutic applications for Nanobodies appears to be beyond that possible for conventional antibodies and antibody fragments. Nanobodies can also be tailored for a half-life varying from less than 2 hours up to a few weeks, by choosing from a wide range of half-life extension technologies. This versatility increases the number of therapeutic options available to Nanobodies ranging from acute to chronic indications where a monthly or bimonthly dosing regimen may be desirable.

Initial biodistribution studies with monospecific anti-EGFR (αEGFR)-Nanobodies in tumor-bearing mice showed, as expected, rapid blood clearance with a serum half-life time of less than an hour and low tumor uptake (15-17). Therefore, monospecific Nanobodies do not seem to be qualified for long-term blockage of growth factors and their receptors. Improvement of the pharmacokinetic and dynamic properties of otherwise short-live molecules can be achieved by fusing an anti-albumin unit (αAlb) to the Nanobody, as described by Tijink and colleagues (18). They compared the biodistribution of a bivalent αEGFR-Nanobody (αEGFR-αEGFR) with a trivalent Nanobody construct containing the αAlb-unit (αEGFR-αEGFR-αAlb) in nude mice bearing A431 tumors. Tumor uptake of αEGFR-αEGFR-αAlb was significantly higher than of αEGFR-αEGFR: 35.2%ID/g ± 7.5 %ID/g vs 5.0%ID/g ± 1.4 %ID/g. What is more, biodistribution of αEGFR-αEGFR-αAlb (50 kDa) was comparable to cetuximab (150 kDa), while it showed faster and deeper tumor penetration. The therapeutic potential of αEGFR-Nanobodies in comparison with conventional αEGFR mAbs was demonstrated by Roovers and colleagues (13).

In the present study, we developed and characterized two αHGF-Nanobodies 1E2-Alb8 and 6E10-Alb8 for their capacity to inhibit binding of HGF to the c-Met receptor and for their potential in diagnosis and therapy of cancer. After labeling with the positron emitter zirconium-89 the Nanobodies were evaluated in biodistribution studies in nude mice bearing U87 MG glioblastoma xenografts. Besides that, αHGF-Nanobodies were tested as therapeutic agents in the same animal model.

Materials and Methods

Details of production and selection of αHGF-Nanobodies are presented in the Supplementary Materials.

Selective binding of Nanobodies to human HGF in ELISA

Nanobody-containing periplasmic extracts were analyzed for their ability to bind HGF. HGF (294-HG/CF, R&D systems) was coated on ELISA plates at 2 µg/mL. Plates were washed and subsequently blocked using PBS with 1% casein. Periplasmic extracts of individual clones, prediluted 1:10 in PBS/1% casein/0.05% Tween, were added and plates were incubated at room temperature for 2 hours. Binding to immobilized HGF was detected using mouse anti-c-myc monoclonal antibody, followed by a horseradish peroxidase-conjugated rabbit-anti-mouse (human and bovine serum protein pre-absorbed) monoclonal antibody for detection. Individual clones were scored as putative HGF binders if the clones showed high optical densities in the assay. Overall, more than 90% of the clones were able to bind HGF.

Kinetic measurement Nanobody-antigen K_d values

Kinetic (k_a and k_d) and affinity constants (K_d) of individual purified Nanobodies were determined by surface plasmon resonance on a Biacore T100 instrument. Human HGF (R&D systems) was amine-coupled to a CM5 sensor chip at a density of 2,500 relative units. Remaining reactive groups were inactivated with ethanolamine. Nanobody binding was assessed at varying concentrations ranging from 500 to 15 nmol/L. Each sample was injected for 2 minutes at a flow rate of 45 µL/min to allow binding to chip-bound antigen. Next, binding buffer without Nanobody was sent over the chip at the same flow rate to allow dissociation of bound Nanobody. After 10 minutes, remaining bound analyte was removed by injecting regeneration solution (1 mol/L NaCl, 50 mmol/L NaOH). Binding-dissociation curves were used to calculate k_{off} values.

Receptor-ligand binding assay

Serial dilutions of purified Nanobodies were analyzed for their ability to block the interaction of human HGF with c-Met-Fc using the AlphaScreen™ assay (PerkinElmer). In brief, 5 µL of prediluted individual Nanobody clones were incubated with 3 nmol/L biotinylated HGF, 2 nmol/L c-Met-Fc, streptavidin-coated donor beads, and antihuman IgG1 Fc Nanobody covalently coupled Alphascreen acceptor beads. mAb clone 24612 (R&D systems) known

to inhibit the HGF/c-Met-Fc interaction was used as a positive control. Assays were read in an Envision AlphaScreen option fitted multimode reader (PerkinElmer).

Cells and culture

U87 MG (human glioblastoma), Bx-PC3 (human prostate carcinoma) and A549 (human alveolar basal epithelial cell carcinoma) cells were all obtained from the American Type Culture Collection (www.ATCC.com) and cultured according to their recommendations. Cell lines were not authenticated by the authors.

Functional cell assays: c-Met phosphorylation assay

A549 cells were plated in growth medium and after 24 hours the cells were starved for 18 to 20 hours. c-Met phosphorylation was stimulated with 5 nmol/L human HGF for 15 minutes. Each of the half-life extended Nanobodies 1E2-Alb8 and 6E10-Alb8 was prepared as a 3-point serial dilution series in the stimulation medium before adding to the cells. Following the 15-minute incubation, cells were immediately placed on ice and lysed in RIPA buffer (Cell Signaling Technology). Quantification of phosphorylated (Tyr1349) and total c-Met was performed using MSD 96-Well MULTI-SPOT® Phospho (Tyr1349)/Total c-Met Assay according to the manufacturer's instructions. IC_{50} values were calculated using the 4 Parameter Logistic equation (GraphPad Prism).

Functional cell assays: proliferation assay

BxPc3 cells were seeded in cell culture E-plates at a cell density of 10,000 cells per well and incubated overnight in culture medium at 37°C and 5% CO_2. Cells were then starved with medium containing 1% ITS (insulin, transferrin, selenium) for 4 hours after which 0.6 nmol/L HGF was added together with serial dilutions of Nanobodies 1E2-Alb8 and 6E10-Alb8. The cell growth curves were automatically recorded on the xCELLigence System (Roche Applied Sciences) in real-time. The cell index was followed for 3 days.

Preparation of ^{89}Zr-1E2-Alb8 and ^{89}Zr-6E10-Alb8

For preparation of the ^{89}Zr conjugates, the ^{89}Zr was coupled to the Nanobody by use of the bifunctional chelate p-isothiocyanatobenzyl desferrioxamine (Df-Bz-NCS, catalog # B705, Macrocyclics), essentially as described by Vosjan and colleagues (19).

Quality control of ^{89}Zr-1E2-Alb8 and ^{89}Zr-6E10-Alb8

All radioactive conjugates were analyzed by instant thin-layer chromatography (ITLC) to determine the labeling efficiency and radiochemical purity. The integrity of the

Nanobody was analyzed via size exclusion chromatography by high-performance liquid chromatography (HPLC), and sodium dodecyl sulphate-polyacrylamide gel electrophoresis (SDS-PAGE) followed by phosphor imager analysis (Storm820; GE Healthcare). Immunoreactivity was determined by a HGF-coated enzyme-linked immunosorbent assay essentially as described by Collingridge and colleagues (20).

Biodistribution study

The distribution of ^{89}Zr-labeled αHGF-Nanobodies was examined in nude mice (HSD: Athymic Nude-Foxn1^{nu}, 20-30 g; Harlan Laboratories) inoculated subcutaneously with 2 x 10^6 U87 MG cells at 2 lateral sides. These animal experiments were done according to NIH Principles of Laboratory Animal Care and Dutch national law (Wet op de dierproeven, Stb 1985, 336).

Mice bearing U87 MG xenografts (size ~100 mm^3) were injected with 0.37 MBq ^{89}Zr-Df-Bz-NCS-1E2-Alb8 or 0.37 MBq ^{89}Zr-Df-Bz-NCS-6E10-Alb8 via the retro-orbital plexus. Unlabeled Nanobody was added to the injection mixture to obtain a final dose of 30 µg per mouse. At 1, 2, 3 or 7 days post injection (p.i.) 5 mice per group were anesthetized, bled, killed and dissected. Blood, tumor, and normal tissues were weighed and radioactivity was measured in a gamma counter (Wallac). Radioactivity uptake for each sample was calculated as the percentage of the injected dose per gram of tissue (%ID/g).

In addition, a Nanobody dose-diminishing study was conducted. To this end, 5, 10, 20 and 30 µg of ^{89}Zr-labeled 1E2-Alb8 (0.23-0.83 MBq) was injected in mice bearing U87 MG xenografts, and at 3 days p.i. 5 mice per group were examined as described above.

Blood kinetics

Blood concentrations of αHGF-Nanobodies were examined in 2 groups of 2 mice. One group of tumor-bearing mice received 0.37 MBq ^{89}Zr-1E2-Alb8 (30 µg) whearas the other group received 0.37 MBq ^{89}Zr-6E10-Alb8 (30 µg). Blood was collected at 1 and 3 hours, and at 1, 2, 3 and 7 days p.i. by tail laceration and radioactivity was measured in a gamma counter. Radioactivity for each sample was calculated as %ID/g.

Therapy study

The therapeutic effectiveness of the αHGF-Nanobodies was studied in the same nude mice model as described for the biodistribution study. For this purpose, 7 groups of 6 mice with established U87 MG xenografts were used. The mean tumor size at the start of the study was ~100 mm^3, and was similar for the different treatment groups. All mice

received i.p. treatment 3 times a week for 5 weeks. Group 1 was the control group and received 200 µl of saline solution per treatment. Group 2, 3 and 4, received 10, 30 and 100 µg of Nanobody 1E2-Alb8, respectively. Group 5, 6 and 7 received 10, 30 and 100 µg of Nanobody 6E10-Alb8, respectively. Body weight and tumor volume were measured 3 times a week up to 73 days after end of treatment.

Statistical analysis

Biodistribution and therapy experiments were statistically analyzed with SPSS 15.0 software. using Student t test for unpaired data. Two-sided significance levels were calculated and P <0.01 was considered statistically significant. Survival was calculated using Kaplan-Meier curves.

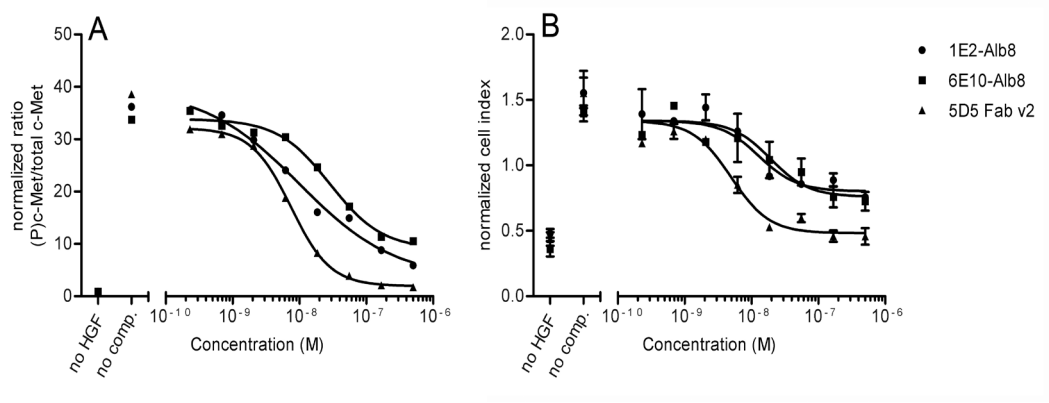

Figure 1. αHGF-Nanobodies neutralize HGF-mediated cellular functions. (A) αHGF-Nanobodies neutralize HGF-mediated c-Met phosphorylation. The percentage inhibition of c-Met phosphorylation was measured over an 8-point dose-response of each Nanobody by an enhanced chemiluminescence assay. (B) αHGF-Nanobodies inhibit HGF-dependent growth of PC3 cells. The viability of PC3 cells cultured more 3 days in the presence of 0.6 nmol/L HGF was measured over an 8-point dose-response of each Nanobody via impedance measurement. Anti-c-Met 5D5 Fab was used as a positive control.

Results

Generation and characterization of αHGF-Nanobodies 1E2 and 6E10

To obtain antagonistic Nanobodies specific for HGF, phage Nanobody repertoires were synthesized from peripheral blood lymphocytes from llamas immunized with HGF. After panning to immobilized HGF, single clones were screened as periplasmic extracts for HGF reactivity by ELISA. Approximately 90% of the clones tested were found to bind HGF. In a next step, their potential to inhibit HGF/c-Met interaction was assessed in an AlphaScreen and resulted in a final panel of 12 clones, which showed good inhibition of the HGF/c-Met interaction. Using a Biacore T100, we analyzed the affinity of the Nanobodies to HGF. On the basis of these analyses, Nanobodies 1E2 and 6E10 were selected from this panel for further characterization. These selected Nanobodies inhibited binding of HGF to c-Met with IC_{50} values in the low nanomolar range (1.8 nmol/L for 1E2 and 3 nmol/L for 6E10 Nanobody) though 100% inhibition was not achieved. The kinetic parameters of Nanobody-antigen showed that both Nanobodies displayed low nmol/L affinity constants (1.36 nmol/L for 1E2 and 1.14 nmol/L for 6E10 Nanobody).

Re-formatting of Nanobodies for in vivo use and in vitro characterization of these formats

To increase the in vivo half-life of the αHGF Nanobodies, bispecific formats were generated whereby the αHGF-Nanobodies were genetically linked to a Nanobody with specificity to serum albumin (Alb8). These bispecific Nanobodies were produced as myc-His6 tagged proteins in E. coli and analyzed for their potential to neutralize HGF-mediated c-Met phosphorylation. A549 cells do not express HGF; thus, this assay mimicked a paracrine model of ligand-mediated receptor activation. When Nanobody 1E2-Alb8 or 6E10-Alb8 was introduced into HGF-containing medium before addition to the cells, c-Met phosphorylation was inhibited in a dose-dependent manner though less efficient than control anti-c-Met 5D5 Fab (Fig. 1A).

We next measured inhibition of HGF-induced proliferation of Bx-PC3 cells. Also here, a dose-dependent inhibition was observed when the Nanobodies were added to the Bx-PC3 cells in culture, but also here inhibition was less efficient as compared to the anti-c-Met 5D5 Fab control (Fig. 1B).

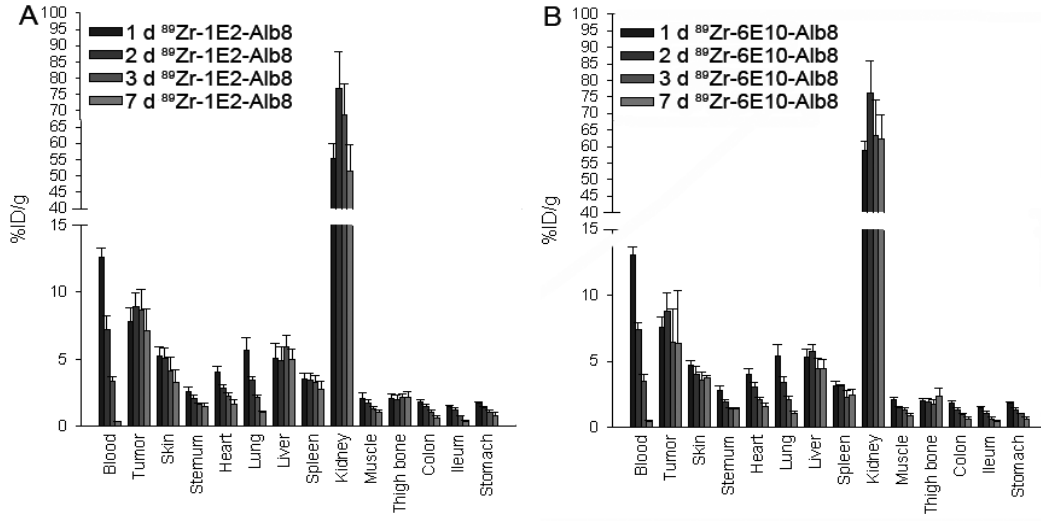

Figure 2. Biodistribution of αHGF-Nanobodies ^{89}Zr-1E2-Alb8 (A) and ^{89}Zr-6E10-Alb8 (B) in nude mice bearing U87 MG xenografts at 1, 2, 3 and 7 days p.i. Data are presented as average of 5 animals and SDs. No significant differences in uptake between both Nanobodies were observed (P<0.01).

Radiolabeling and quality control of ^{89}Zr-1E2-Alb8 and ^{89}Zr-6E10-Alb8

Labeling of both Nanobodies with ^{89}Zr resulted in overall labeling yields of 75 to 90%, after PD-10 column purification. Radiochemical purity was always more than 97%. Integrity of the Nanobodies was optimal as determined by HPLC and SDS-PAGE. Immunoreactivity of ^{89}Zr-1E2-Alb8 and ^{89}Zr-6E10-Alb8 was similar to that of the reference ^{131}I-labeled αHGF-Nanobodies (~50%).

Biodistribution study

For biodistribution studies nude mice bearing U87 MG xenografts were injected with either ^{89}Zr-1E2-Alb8 or ^{89}Zr-6E10-Alb8. Biodistributions at 1, 2, 3, or 7 days p.i. are shown in Fig. 2. Both αHGF-Nanobodies showed similar biodistributions with selective tumor uptake, no significant differences were observed (P>0.01). Whereas blood levels gradually decreased over time, tumor uptake remained relatively stable. Blood levels were 12.6%ID/g ± 0.7%ID/g, 7.2%ID/g ± 1.0%ID/g, 3.4%ID/g ± 0.3%ID/g and 0.3%ID/g ± 0.1%ID/g for ^{89}Zr-1E2-Alb8 and 13.1±0.6, 7.4±0.6, 3.5±0.5, and 0.5±0.1 %ID/g for ^{89}Zr-6E10-Alb8 at 1, 2, 3, and 7 days p.i., respectively. Tumor uptake at these time points was 7.8%ID/g ± 1.1%ID/g, 8.9%ID/g ± 1.0%ID/g, 8.7%ID/g ± 1.5%ID/g, and 7.2%ID/g ± 1.6%ID/g for ^{89}Zr-1E2-Alb8, and 7.5%ID/g ± 0.8%ID/g, 8.8%ID/g ± 1.3%ID/g, 6.5%ID/g ± 2.5%ID/g, and 6.3%ID/g ± 4.0%ID/g at 1, 2, 3, and 7 days p.i., respectively, for ^{89}Zr-6E10-Alb8. Tumor uptake was higher than in normal organs, except for kidneys. The latter is typical for small proteins, which are rapidly cleared via the kidneys.

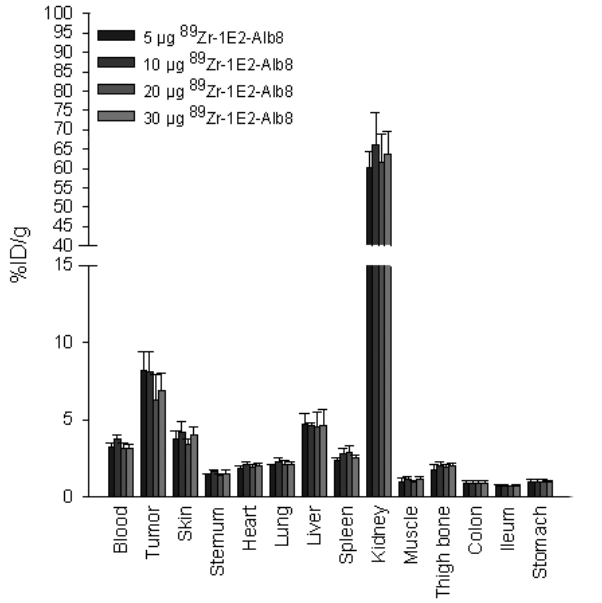

Figure 3. Biodistribution of αHGF-Nanobody ^{89}Zr-1E2-Alb8 in nude mice bearing U87 MG xenografts at 3 days p.i. with different amounts of Nanobody. Data are presented as average of 5 animals and SD. No significant differences were observed between the dose groups (P<0.01).

Dose-diminishing study

A dose-diminishing study was conducted with ^{89}Zr-1E2-Alb8 to determine the optimal Nanobody dose for in vivo imaging. Nude mice bearing U87 MG xenografts were injected with 0.32 ± 0.01, 0.47 ± 0.01, 0.47 ± 0.01, or 0.83 ± 0.01 MBq ^{89}Zr-1E2-Alb8, containing 5, 10, 20 or 30 µg 1E2-Alb8, respectively. Three days p.i., similar biodistribution was seen for all dose groups (Fig. 3). No significant differences were observed in tumor uptake, being 8.2%ID/g ± 1.2%ID/g, 8.1%ID/g ± 1.3%ID/g, 6.3%ID/g ± 1.7%ID/g, and 6.9%ID/g ± 1.1%ID/g for the 5, 10, 20, and 30 µg dose groups, respectively. High uptake in kidneys was observed for all dose groups. Also no significant differences were observed between the different dose groups (P > 0.01).

Blood kinetics in mice

Blood kinetics of ^{89}Zr-1E2-Alb8 (30 µg) and ^{89}Zr-6E10-Alb8 (30 µg) appeared to be similar (Fig. 4). Blood levels of Nanobody constructs were 41.7%ID/g ± 0.6%ID/g and 35.1%ID/g ± 1.48%ID/g 1 hour after injection for ^{89}Zr-1E2-Alb8 and ^{89}Zr-6E10-Alb8, respectively, and slowly decreased from 4.3%ID/g ± 0.1%ID/g to 0.3%ID/g ± 0.1%ID/g between 72 and 168

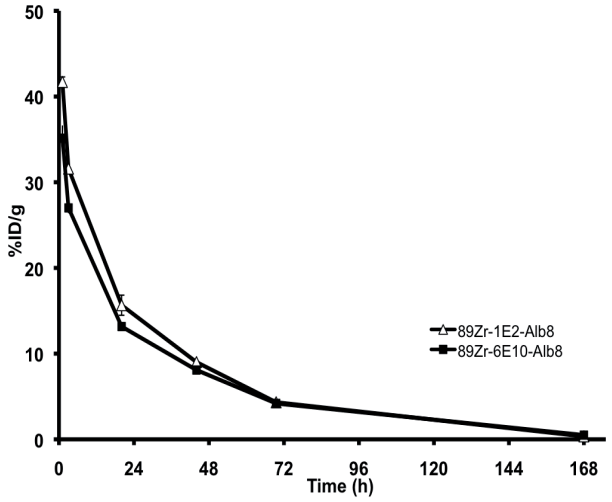

Figure 4. Blood kinetics of ^{89}Zr labeled 1E2-Alb8 and 6E10-Alb8 in nude mice bearing U87 MG xenografts (n=2 per group) up to 7 days after injection. Total administered dose, 30 µg.

hours p.i. for ^{89}Zr-1E2-Alb8 and from 4.2%ID/g ± 0.1%ID/g to 0.5%ID/g ± 0.1%ID/g for ^{89}Zr-6E10-Alb8.

Therapy study

Mice receiving Nanobodies showed tumor growth delay in comparison to the control PBS-group, while no toxicity was observed (Fig. 5A). Within the treatment period of 35 days all control mice were sacrificed because of the large volumes of the tumors. Mice receiving the lowest dose (10 µg) had minimal benefit whereas the intermediate and highest dose groups (30 µg and 100 µg) showed extensive tumor growth delay.

At the end of treatment (day 35) only mice in the intermediate and highest dose groups were alive, and followed till day 108 after start of treatment. At the end of the study 4 of 6 mice (7 of 11 tumors) were cured in the group receiving 100 µg 1E2-Alb8, and 3 of 6 mice (6 of 11 tumors) in the group receiving 100 µg 6E10-Alb8, while 3 of 6 mice (5 of 11 tumors) were cured in the group receiving 30 µg 1E2-Alb8. In contrast, all mice in the group receiving 30 µg 6E10-Alb8 faced regrowth of tumors during follow up (Fig. 5B and 5C).

Discussion

Targeting of the HGF/c-Met pathway is considered to be a promising approach for treatment of cancer. Activation of c-Met by its ligand HGF can lead to multiple cellular responses, including invasion, proliferation, and motility. In this study, we described the development of 2 Nanobodies designated 1E2 and 6E10, with low nanomolar affinity for HGF, that have the capacity to inhibit binding of HGF to the c-Met receptor. By genetically linking these αHGF-Nanobodies to a Nanobody unit with specificity for serum albumin (Alb8; refs.13,18,21), 1E2-Alb8 and 6E10-Alb8 were obtained. Nanobodies were radiolabeled

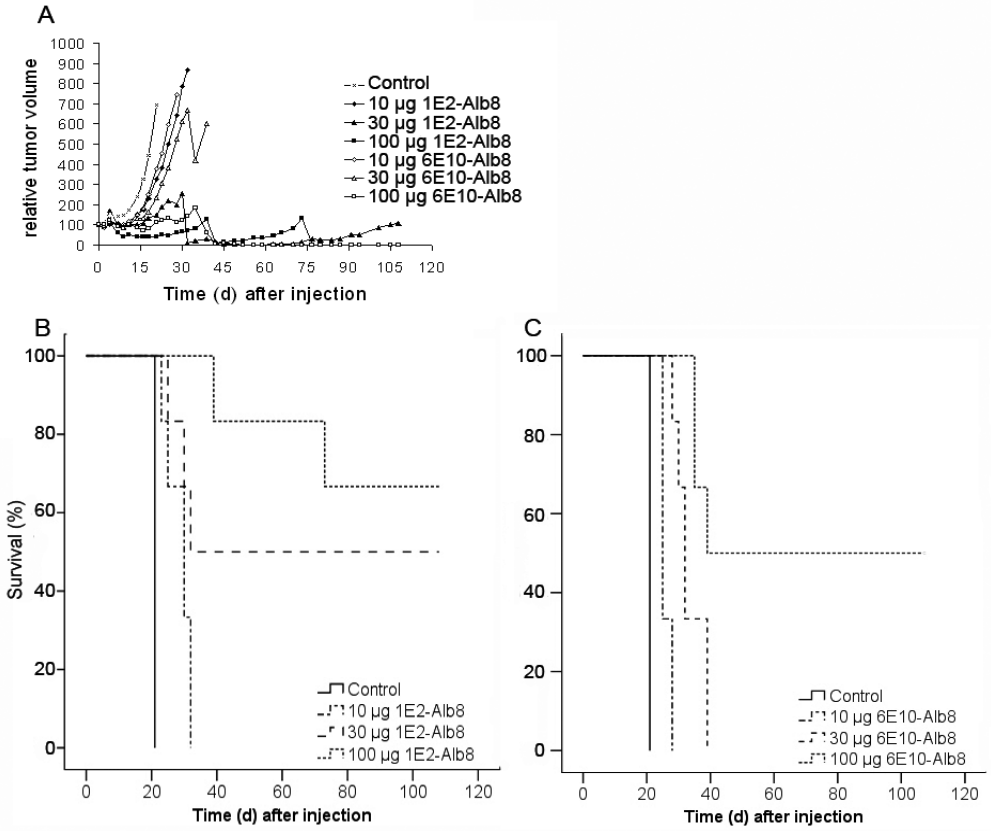

Figure 5. Therapy study with αHGF-Nanobodies 1E2-Alb8 and 6E10-Alb8 in nude mice bearing U87 MG glioblastoma xenografts (A). Treatment was 3 times a week for 5 weeks. Kaplan-Meier survival curves of nude mice treated with different amounts of 1E2-Alb8 (B) or 6E10-Alb8 (C). Treatment with all Nanobody concentrations caused significant tumor growth delay of the established tumors after day 6 ($P < 0.01$), and curative responses after treatment with 30 or 100 µg 1E2-Alb8, or 100 µg 6E10-Alb8.

with ^{89}Zr to enable accurate assessment of in vivo biodistribution either by taking biopsies as carried out herein or alternatively by noninvasive PET imaging as is foreseen in future clinical trials. ^{89}Zr-1E2-Alb8 and ^{89}Zr-6E10-Alb8 showed a similar extended serum half-life as has been previously described for αEGFR-Nanobodies (18), with blood levels of 10%ID/g to 15%ID/g at 24 hours after injection. Biodistribution studies also showed selective accumulation of ^{89}Zr-1E2-Alb8 and ^{89}Zr-6E10-Alb8 in HGF-producing U87 MG xenografts. Besides this, both αHGF-Nanobodies were able to inhibit tumor growth in U87 MG tumor-bearing nude mice, and upon treatment by 100 µg i.p. injections, 3 times a week for 5 weeks, cures were observed in 4 of 6 mice with 1E2-Alb8 and in 3 of 6 mice with 6E10-Alb8.

Several therapy studies with αHGF mAbs have been performed in U87 MG tumor-bearing mice in the past, and this allows ranking of the potency of the αHGF-Nanobodies described herein. In 2001, Cao and colleagues (22) reported for the first time on HGF-neutralizing mAbs capable for exerting antitumor activity. A mixture of 3 antibodies (200 µg per mouse every day until day 20; i.p. or intratumoral injection) was used for therapy in mice that had been injected one day earlier with C-127 or U118 cells. C-127 are mouse breast tumor cells transformed with human HGF and mouse Met, whereas U118 are human glioblastoma cells showing autocrine HGF production. Inhibition of tumor outgrowth was observed for both cell lines. The same mAb mixture (200 µg per mouse every 2 days until day 10; i.p. or intratumoral injection) also caused tumor growth inhibition in mice bearing established U118 xenografts (average size of 100 mm^3), however, no tumor regression or cures were observed. In these studies a mixture of 3 mAbs was used for therapy, because in vitro studies had shown that no single mAb appeared capable of neutralizing the activity of HGF. The authors, therefore, postulated that a minimum of 3 HGF epitopes have to be blocked to prevent c-Met tyrosine kinase activation and to exert anti-tumor activity.

In 2006, Burgess and colleagues (23) introduced fully human mAbs directed to an epitope in the β-chain of HGF, mAb AMG102 included, which showed inhibition of HGF-driven c-Met phopshorylation and of tumor growth as single agents. For their in vivo experiments they used established xenografts with an average size of 180 mm^3 derived from the glioblastoma cell lines U87 MG and U118, both expressing human HGF and c-Met. The most potent mAb showed significant growth inhibition and tumor regression when administered at a dose of 10 or 30 µg twice a week, and 7 of 10 animals in the 30-µg dose group had no measurable tumor mass at the end of the experiment. Because of the very short follow-up time of 17 days after start of therapy, and the lack of withdrawal from therapy, it did not become clear from these studies whether cures could be obtained like

in our studies with the same Nanobody dose in the same xenograft model.

In later studies, the group of Burgess showed the potential of using αHGF therapy in combination approaches for treatment of glioblastoma (24). In the above described U87 MG xenograft model, low doses of AMG102 (3 µg twice a week) enhanced the efficacy of temozolomide or docetaxel. What is more, a first in human phase I trial in patients with advanced solid tumors showed that AMG102 is safe and well tolerated, with a linear pharmacokinetic profile within the investigated dose range (up to 20 mg/kg i.v. every 2 weeks) (25). Despite the fact that the maximum-tolerated dose was not reached, 16 of 23 evaluable patients had a best response of stable disease with a progression-free survival ranging from 7.9 to 40 weeks. Above data indicate that αHGF-based therapy has clinical potential. Recently, indication was made that the HGF/c-Met pathway is also a therapeutic target in metastatic renal cell carcinoma. Nevertheless, Schöffski and colleagues showed that no significant growth inhibition occurred with AMG102 (26). Similarly, HGF and its receptor c-Met have been implicated in the pathogenesis of glioblastoma, but Wen (27) and colleagues showed in a phase II study that AMG102 monotherapy treatment at doses up to 20 mg/kg was not associated with significant antitumor activity in the selected patient groups.

Besides these mAbs, studies were conducted with the murine mAb L2G7 in 3 different established tumor models among which U87 MG (28,29). Treatment with 50 or 100 µg L2G7, i.p. twice weekly, was started when tumor volume reached approximately 50 mm^3 and resulted in inhibited tumor growth and regressions. Because of the short follow-up period (till day 40 after injection of cells) and the continuation of therapy during that time period, it is impossible to draw conclusions about cure rates in these studies. L2G7 efficacy was also examined in mice bearing pre-established intracranial U87 MG glioma xenografts. L2G7 (100 µg, i.p., twice weekly) given from days 5 to 52, significantly prolonged animal survival. In control mice, median survival was 39 days and all mice died from progressive tumors by day 41. In contrast, all mice treated with L2G7 survived to day 70 and 80% survived to day 90. At day 91 animals remaining alive were sacrificed and examined for tumor burden. All mice were found to have brain tumors left, which appeared to be consistent with tumor regrowth after withdrawal of L2G7 therapy.

Despite the fact that the αHGF-Nanobodies evaluated in this study did not fully inhibit c-Met-mediated phosphorylation and cell growth in vitro, in vivo these Nanobodies were found capable to give cures. These data indicate that in vitro functional assays are not fully predictive for assessment of the in vivo therapeutic potential of αHGF-targeting ligands. One aspect in favor of Nanobodies in comparison to traditional full-lengths mAbs

is their faster and deeper tumor penetration as was previously observed for the αEGFR-Nanobody formats (18).

On the basis of the achievements described herein we think clinical evaluation of either 1E2-Alb8 or 6E10-Alb8 is justified. In such studies, the use of ^{89}Zr-immuno-PET might be of added value. Taking the complexity of signal transduction routes into account, it is uncertain whether a relationship between imaging uptake and response will be seen in patients. What might be seen, however, is a good negative predictive value of imaging, which means that there will most probably be no response when there is no Nanobody uptake in the tumor. In such way imaging might be of value to enrich the patient population that might benefit from αHGF treatment. In addition, imaging might be of value to assess the Nanobody dosage for optimal tumor targeting, the optimal schedule of Nanobody administration and cross reactivity with normal tissues to anticipate toxicity.

The potential of ^{89}Zr-immuno-PET in mAb development and applications has been shown for several mAbs directed against membrane receptors (30-33), the c-Met receptor included (34), but also for a mAb directed against a growth factor, that is, bevacizumab directed against VEGF. Like the ^{89}Zr-αHGF Nanobodies, ^{89}Zr-bevacizumab showed selective uptake in VEGF-producing xenografts in mice (35), whereas uptake decreased when VEGF expression was inhibited by treatment with HSP90 inhibitors (36,37), indicating a relationship between ^{89}Zr-bevacizumab tumor uptake and VEGF expression. What is more, ^{89}Zr-bevacizumab biodistribution could be imaged quantitatively and at excellent resolution, and in the mean time clinical trials have been started with ^{89}Zr-bevacizumab, as a follow up of single-photon emission computed tomography (SPECT) studies with ^{111}In-bevacizumab in patients with melanoma (38). Although the performance of immuno-SPECT is less optimal than of immuno-PET, in these latter studies all known melanoma lesions were detected with VEGF-SPECT. In analogy, ^{89}Zr-immuno-PET might be supportive in the clinical development of the αHGF-Nanobodies.

To further improve the therapeutic potential of αHGF-Nanobodies, formatting into multi-targeting Nanobodies might be an appealing option. Among others, linking αHGF-Nanobodies to our recently described αEGFR-Nanobody 7D12 might be promising (17). Like other researchers postulated; combination therapies are needed to overcome acquired resistance to inhibitors of signal transduction pathways. For instance, as recently described in lung tumors, resistance to the small-molecule EGFR inhibitors gefitinib and erlotinib might be achieved through amplification of the c-Met gene (39). By combining αHGF and αEGFR units within one Nanobody construct, simultaneous blockage of both the EGFR and c-Met/HGF signal transduction pathways might result in improved therapeutic

effects.

In summary, the results presented in this study showed that the Nanobodies 1E2-Alb8 and 6E10-Alb8 are capable of selective targeting HGF-producing tumors. Furthermore, treatment of U87 MG-bearing mice with these Nanobodies resulted in inhibition of tumor growth and ultimately caused cures, indicating the therapeutic potential of αHGF-Nanobodies as cancer therapeutics in humans.

Disclosure of Potential Conflicts of Interest

J. Vercammen and H. Revets are Ablynx NV employees. J.A. Kolkman was a former employee of Ablynx NV and is presently an employee of Crucell. No potential conflicts of interest were disclosed by the other authors.

Supplementary materials

Production and selection of αHGF-Nanobodies

Anti-HGF Nanobodies were generated at Ablynx NV (Ghent, Belgium). Two Llama glama were immunized with 100 and 50 µg human HGF (Peprotech, cat# 100-39) in Stimmune adjuvant (Cedi Diagnostics) and blood was collected. These animal experiments were conducted with the approval of the Ethical Committee of the Faculty of Veterinary Medicine, University of Ghent, Belgium.

Anti-HGF Nanobodies were isolated using phage display. To this end, 2 libraries were constructed and panned on human HGF. Principles in short; peripheral blood mononuclear cells were prepared from blood samples using Ficoll-Hypaque according to the manufacturer's instructions. Next, total RNA was extracted from these cells and used as starting material for RT-PCR to amplify Nanobody encoding gene fragments. These fragments were cloned into phagemid vector pAX50. Phage was prepared according to standard methods and stored after filter sterilization at 4°C for further use. Phage library size from both animals was 0.7 x 10^8 and 2.1 x 10^8, and percentages of insert 100 and 91.3%, respectively. Phage libraries were used for selection on immobilized human HGF, and the best selections, with the highest enrichment factor, were chosen for further analysis. Bound phage was eluted by addition of trypsin and rescued via infection of E. coli. Individual colonies were picked and grown in 96 deep well plates (1 mL).

Nanobody expression was induced by addition of IPTG and periplasmic extracts (80 µL) were prepared according to standard methods. Alternatively, selected Nanobodies were expressed in the periplasmic space of E. coli as c-myc and His6 tagged proteins in

a culture volume of 50 mL and purified via immobilized metal affinity chromatography (IMAC). Nanobodies were eluted from the column with 250 mM imidazole followed by gel filtration and buffer exchange to PBS.

Selected human HGF–specific Nanobodies were converted into a bispecific format by genetic fusion to the albumin-binding Nanobody Alb8 using a flexible Gly-Ser linker (Gly4-Ser-Gly3-Ser).

References

1. Cooper CS, Park M, Blair DG, Tainsky MA, Huebner K, Croce CM et al. Molecular cloning of a new transforming gene from a chemically transformed human cell line. Nature 1984;311:29-33.

2. Bottaro DP, Rubin JS, Faletto DL, Chan AM, Kmiecik TE, Vande Woude GF et al. Identification of the hepatocyte growth factor receptor as the c-met proto-oncogene product. Science 1991;251:802-4.

3. Birchmeier C, Birchmeier W, Gherardi E, Vande Woude GF. Met, metastasis, motility and more. Nat Rev Mol Cell Biol 2003;4:915-25.

4. Boccaccio C, Comoglio PM. Invasive growth: a MET-driven genetic programme for cancer and stem cells. Nat Rev Cancer 2006;6:637-45.

5. Hurwitz H, Fehrenbacher L, Novotny W, Cartwright T, Hainsworth J, Heim W et al. Bevacizumab plus irinotecan, fluorouracil, and leucovorin for metastatic colorectal cancer. N Engl J Med 2004;350:2335-42.

6. Liu X, Newton RC, Scherle PA. Development of c-MET pathway inhibitors. Expert Opin Investig Drugs 2011;20:1225-41.

7. Hamers-Casterman C, Atarhouch T, Muyldermans S, Robinson G, Hamers C, Songa EB et al. Naturally occurring antibodies devoid of light chains. Nature 1993;363:446-8.

8. Muyldermans S. Single domain camel antibodies: current status. J Biotechnol 2001;74:277-302.

9. Van Bockstaele F, Holz JB, Revets H. The development of nanobodies for therapeutic applications. Curr Opin Investig Drugs 2009;10:1212-24.

10. Conrath EK, Lauwereys M, Wyns L, Muyldermans S. Camel single-domain antibodies as modular building units in bispecific and bivalent antibody constructs. J Biol Chem 2001;276:7346-50.

11. Ulrichts H, Silence K, Schoolmeester A, de Jaegere P, Rossenu S, Roodt J et al. Antithrombotic drug candidate ALX-0081 shows superior preclinical efficacy and safety compared with currently marketed antiplatelet drugs. Blood 2011;118:757-65.

12. Jähnichen S, Blanchetot C, Maussang D, Gonzalez-Pajuelo M, Chow KY, Bosch L et al. CXCR4 nanobodies (VHH-based single variable domains) potently inhibit chemotaxis and HIV-1 replication and mobilize stem cells. Proc Natl Acad Sci U S A 2010;107:20565-70.

13. Roovers RC, Vosjan MJWD, Laeremans T, El Khoulati R, de Bruin RC, Ferguson KM et al. A bi-paratopic anti-EGFR nanobody efficiently inhibits solid tumour growth. Int J Cancer 2011;129:2013-24.

14. Pant N, Marcotte H, Hermans P, Bezemer S, Frenken L, Johansen K et al. Lactobacilli producing bispecific llama-derived anti-rotavirus proteins in vivo for rotavirus-induced diarrhea. Future Microbiol 2011;6:583-93.

15. Huang L, Gainkam LO, Caveliers V, Vanhove C, Keyaerts M, De Baetselier P et al. SPECT imaging with ^{99m}Tc-labeled EGFR-specific nanobody for in vivo monitoring of EGFR expression. Mol Imaging Biol 2008;10:167-75.

16. Gainkam LO, Huang L, Caveliers V, Keyaerts M, Hernot S, Vaneycken I et al. Comparison of the biodistribution and tumor targeting of two ^{99m}Tc-labeled anti-EGFR nanobodies in mice, using pinhole SPECT/Micro-CT. J Nucl Med 2008;49:788-795.

17. Vosjan MJWD, Perk LR, Roovers RC, Visser GWM, Stigter-van Walsum M, van Bergen en Henegouwen P et al. Facile labelling of an anti-epidermal growth factor receptor Nanobody with ^{68}Ga via a novel bifunctional desferal chelate for immuno-PET. Eur J Nucl Med Mol Imaging 2011;38:753-63.

18. Tijink BM, Laeremans T, Budde M, Stigter-van Walsum M, Dreier T, de Haard HJ et al. Improved tumor targeting of anti-epidermal growth factor receptor Nanobodies through albumin binding: taking advantage of modular Nanobody technology. Mol Cancer Ther 2008;7:2288-97.

19. Vosjan MJWD, Perk LR, Visser GWM, Budde M, Jurek P, Kiefer GE et al. Conjugation and radiolabeling of monoclonal antibodies with zirconium-89 for PET imaging using the bifunctional chelate p-isothiocyanatobenzyl-desferrioxamine. Nat Protoc 2010;5:739-43.

20. Collingridge DR, Carroll VA, Glaser M, Aboagye EO, Osman S, Hutchinson OC et al. The development of [^{124}I] iodinated-VG76e: a novel tracer for imaging vascular endothelial growth factor in vivo using positron emission tomography. Cancer Res 2002;60:5912-9.

21. Coppieters K, Dreier T, Silence K, de Haard H, Lauwereys M, Casteels P et al. Formatted anti-tumor necrosis factor alpha VHH proteins derived from camelids show superior potency and targeting to inflamed joints in a murine model of collagen-induced arthritis. Arthritis Rheum 2006;54:1856-66.

22. Cao B, Su Y, Oskarsson M, Zhao P, Kort EJ, Fisher RJ et al. Neutralizing monoclonal antibodies to hepatocyte growth factor/scatter factor (HGF/SF) display antitumor activity in animal models. Proc Natl Acad Sci U S A 2001;98:7443-8.

23. Burgess T, Coxon A, Meyer S, Sun J, Rex K, Tsuruda T et al. Fully human monoclonal antibodies to hepatocyte growth factor with therapeutic potential against hepatocyte growth factor/c-Met-dependent human tumors. Cancer Res 2006;66:1721-9.

24. Jun HT, Sun J, Rex K, Radinsky R, Kendall R, Coxon A et al. AMG 102, a fully human anti-hepatocyte growth factor/scatter factor neutralizing antibody, enhances the efficacy of temozolomide or docetaxel in U-87 MG cells and xenografts. Clin Cancer Res 2007;13:6735-42.

25. Gordon MS, Sweeney CS, Mendelson DS, Eckhardt SG, Anderson A, Beaupre DM et al. Safety, pharmacokinetics, and pharmacodynamics of AMG 102, a fully human hepatocyte growth factor-neutralizing monoclonal antibody, in a first-in-human study of patients with advanced solid tumors. Clin Cancer Res 2010;16:699-710.

26. Schöffski P, Garcia JA, Stadler WM, Gil T, Jonasch E, Tagawa ST et al. A phase II study of the efficacy and safety of AMG 102 in patients with metastatic renal cell carcinoma. BJU Int 2011;108:679-86.

27. Wen PY, Schiff D, Cloughesy TF, Raizer JJ, Laterra J, Smitt M et al. A phase II study evaluating the efficacy and safety of AMG 102 (rilotumumab) in patients with recurrent glioblastoma. Neuro Oncol 2011;13:437-46.

28. Kim KJ, Wang L, Su YC, Gillespie GY, Salhotra A, Lal B et al. Systemic anti-hepatocyte growth factor monoclonal antibody therapy induces the regression of intracranial glioma xenografts. Clin Cancer Res 2006;12:1292-8.

29. Lal B, Goodwin CR, Sang Y, Foss CA, Cornet K, Muzamil S et al. EGFRvIII and c-Met pathway inhibitors synergize against PTEN-null/EGFRvIII+ glioblastoma xenografts. Mol Cancer Ther 2009;8:1751-60.

30. Perk LR, Visser OJ, Stigter-van Walsum M, Vosjan MJWD, Visser GWM, Zijlstra JM et al. Preparation and evaluation of ^{89}Zr-Zevalin for monitoring of ^{90}Y-Zevalin biodistribution with positron emission tomography. Eur J Nucl Med Mol Imaging 2006;33:1337-45.

31. Börjesson PKE, Jauw YWS, Boellaard R, de Bree R, Comans EFI, Roos JC et al. Performance of immuno-positron emission tomography with zirconium-89-labeled chimeric monoclonal antibody U36 in the detection of lymph node metastases in head and neck cancer patients. Clin Cancer Res 2006;12:2133-40.

32. Dijkers EC, Oude Munnink TH, Kosterink JG, Brouwers AH, Jager PL, de Jong JR. et al. Biodistribution of ^{89}Zr-trastuzumab and PET imaging of HER2-positive lesions in patients with metastatic breast cancer. Clin Pharmacol Ther 2010;87:586-92.

33. Van Dongen GAMS, Vosjan MJWD. Immuno-Positron Emission Tomography: Shedding light on clinical antibody therapy. Cancer Biother Radiopharm 2010;25:375-85.

34. Perk LR, Stigter-van Walsum M, Visser GWM, Kloet RW, Vosjan MJWD, Leemans CR et al. Quantitative PET imaging of Met-expressing human cancer xenografts with ^{89}Zr-labelled monoclonal antibody DN30. Eur J Nucl Med Mol Imaging 2008;35:1857-67.

35. Nagengast WB, de Vries EG, Hospers GA, Mulder NH, de Jong JR, Hollema H et al. In vivo VEGF imaging with radiolabeled bevacizumab in a human ovarian tumor xenograft. J Nucl Med 2007;48:1313-9.

36. Holland JP, Caldas-Lopes E, Divilov V, Longo VA, Taldone T, Zatorska D et al. Measuring the pharmacodynamic effects of a novel Hsp90 inhibitor on HER2/neu expression in mice using Zr-DFO-trastuzumab. PLoS One 2010;5:e8859.

37. Nagengast WB, de Korte MA, Oude Munnink TH, Timmer-Bosscha H, den Dunnen WFA, Hollema H et al. ^{89}Zr-bevacizumab PET of early antiangiogenic tumor response to treatment with HSP90 inhibitor NVP-AUY922. J Nucl Med 2010;51:761-7.

38. Nagengast WB, Hooge MNL, van Straten EME, Kruijff S, Brouwers AH, den Dunnen WFA et al. VEGF-SPECT with ^{111}In-bevacizumab in stage III/IV melanoma patients. Eur J Cancer 2011;47:1595-1602.

39. Engelman JA, Zejnullahu K, Mitsudomi T, Song Y, Hyland C, Park JO et al. MET amplification leads to gefitinib resistance in lung cancer by activating ERBB3 signaling. Science 2007;316:1039-43.

Chapter 7:

Summary, discussion, and future perspectives

7

Summary, discussion, and future perspectives

Currently, therapeutic monoclonal antibodies (mAbs) gain attention, due to their excellent potential for diagnosis and systemic treatment of cancer. Hundreds of mAbs and mAb fragments are under clinical development. To date, the U.S. Food and Drug Administration (FDA) has approved 30 mAbs, mostly for systemic treatment of cancer[1-3]. Despite the economic recession the annual mAb sales have grown till $48 billion in 2010[4]. The top 5 mAbs had sales over $5 billion each in 2010[1].

Unfortunately, efficacy of current mAbs is still limited, with clinical benefit for only a small group of patients. Ideally, the best drug candidates should be identified early in drug development, whereas patient populations most likely to benefit from treatment should be well defined. Molecular imaging can be of great help in fulfilling these tasks. One of the upcoming techniques is positron emission tomography (PET), which is suitable for quantitative whole body imaging with high resolution. PET can be of use in selecting patient populations, assessing target expression, and determining optimal mAb dosages (to minimize the side effects). The last decade PET imaging with use of mAbs (immuno-PET) showed valuable improvement at several stages of mAb development and clinical applications. Besides full-sized intact mAbs also mAb-fragments (e.g. Nanobodies) and third generation, non-traditional mAb-like scaffolds are gaining more attention. Immuno-PET can play a crucial role in early development of each of these targeting drugs.

For immuno-PET guided therapy with intact mAbs two approaches exist. The first approach is based on the same-day imaging with fast kinetic mAb-based PET probes. This results in a quick procedure to assess target expression in patients and a low radiation burden, especially when radionuclides with half-lives between 1-15 h are used e.g., gallium-68 (^{68}Ga, $t_{½}$ = 1.13 h)[5,6]. In a second approach, the therapeutic intact mAbs themselves are radiolabeled and imaged in a pre-therapy scouting setting or early during the course of therapeutic treatment. This gives a better insight in the *in vivo* behavior and efficacy of the particular mAbs in individual patients. In the latter approach, therapeutic intact mAbs are radiolabeled with long-lived PET isotopes like zirconium-89 (^{89}Zr, $t_{½}$ = 78.4 h) or iodine-124 (^{124}I, $t_{½}$ = 100.3 h) and imaged prior or during the course of mAb therapy.

Very recent insights showed that selective targeting of just one single tumor target might be insufficient for optimal therapeutic efficacy. Cancer cells appear to have the inherent ability to use several growth factor (receptor) systems for growth advantage and survival. This means that other receptor systems can take over the signaling and therefore tumors are still able to survive after blockade of just one growth factor

(receptor) system. The potential of dual-specificity antibody therapy has already been demonstrated in several studies in which mAbs or tyrosine kinase inhibitors affecting different anti-cancer targets, e.g., EGFR, HER2, IGF-IR, VEGF or VEGF-R2 were combined[7-14]. Nanobody technology might be better suited for blockade of growth factor (receptor) systems. Nanobodies are smaller than intact traditional IgG mAbs and can therefore better penetrate in a tumor. Furthermore, Nanobody technology enables easy construction of so-called "dual specific" or "multi-specific" Nanobodies (targeting several tumor targets simultaneously). For preclinical and clinical evaluation of the targeting potential of such new antibody fragments immuno-PET can be of great help.

Chapter 1 described the current role and future potential of immuno-PET, and introduced a novel class of antibody-fragments: Nanobodies. With the introduction of Nanobodies, a new dimension might possibly be added to development of new anti-cancer drugs as well as improved assessment of target expression in tumors. In this chapter also commonly upregulated, overexpressed and/or activated tumor targets which play a crucial role in malignant growth were described.

In **chapter 2**, the novel *p*-isothiocyanatobenzyl-desferal (Df-Bz-NCS) was introduced. This novel bifunctional Df-Bz-NCS chelator allows a labeling procedure that consists of two steps. In comparison, in the old procedure the synthesis of the tetrafluorophenyl ester of succinylated Fe-desferrioxamine B (*N*-suc-Df-Fe-TFP) takes three steps, and the labeling procedure another three steps[15]. In both methods the Df-chelate is conjugated to the lysines of a mAb in about 50 min. An important difference in the new conjugation procedure compared to the old one is the absence of a second step at a low pH (pH 4.5) to remove Fe from the Df-chelate. Avoiding this low pH step is a major improvement when pH-sensitive proteins are used, as has been recently shown for ^{89}Zr-Nanocolloidal albumin[16]. By omitting this step the whole procedure is speeded up by approximately 40 min. In the new procedure as described in this thesis, conjugation was carried out with a 3-fold molar excess of Df-Bz-NCS chelator, resulting in a chelate:mAb-ratio of 1.5:1. With this conjugate, ^{89}Zr-labeling was almost quantitative after 30 minutes of labeling at room temperature at pH 6.8-7.2. After PD-10 column purification the ^{89}Zr-Df-Bz-NCS-mAb conjugates appeared to be optimal with respect to radiochemical purity, integrity, and immunoreactivity. A point of serious attention is the way of addition of the Df-Bz-NCS to the mAb-solution. When the Df-Bz-NCS, which is dissolved in DMSO, is added in one time without shaking or proper mixing, mAb-aggregates are easily formed. For that reason it was stated that the Df-Bz-NCS should be added stepwise to the mAb-solution. A second point of attention concerns the stability of the radiolabeled mAb upon storage.

Buffers containing Cl^- should be avoided, since those buffers cause detachment of ^{89}Zr from the mAb, due to radiation-induced formation of hypochlorite. The latter component very effectively reacts with the bis-thiourea unit of the new linker. Therefore, the use of a 0.25 M sodium acetate buffer is strongly recommended. The novel Df-Bz-NCS chelate was extensively compared with the reference *N*-suc-Df chelate. Biodistribution and imaging studies in different tumor bearing mouse models showed high and selective accumulation in tumors. Furthermore, no significant *in vivo* differences were observed between ^{89}Zr-Df-Bz-NCS-mAb and ^{89}Zr-*N*-suc-Df-mAb conjugates.

In **chapter 3** a protocol was written to provide other research groups and pharmaceutical companies with a straightforward and convenient method for the labeling of ^{89}Zr to mAbs or mAb fragments via this new Df-Bz-NCS chelate. This protocol not only can be used as a standard operating procedure, but also makes aware of critical steps.

For radiolabeling of mAb fragments (e.g. Nanobodies) ^{89}Zr is not strictly necessary, since the biological half-life of a Nanobody ($t_{½}$= 1-3 h) does not really require the 78.4 hour half-life of ^{89}Zr. An alternative PET isotope might be ^{68}Ga, with a half-life of 1.16 h. In **chapter 4** a labeling method with ^{68}Ga via the novel Df-Bz-NCS chelate was described. Crucial in optimal ^{68}Ga radiolabeling is the use of ultra pure HCl, to keep the ^{nat}Ga concentrations as low as possible and also to minimize the amounts of Al, Fe and Zr, being strong competitors for complexation with Df. Also the purification and reduction of the ^{68}Ga-generator eluate volume is important. With the use of an anion exchange column removal of contaminating metals as well as minimizing the volume of the ^{68}Ga-solution was achieved. Radiolabeling with ^{68}Ga was performed at room temperature within a relatively broad pH range of 5.0-6.5 for only 5 min. Once the labeling method was established the first objective was to test whether the novel Df-Bz-NCS chelate is also the appropriate chelator for stable incorporation of ^{68}Ga and for conjugation to mAbs or Nanobodies. The second objective in this study was to evaluate Nanobody 7D12, by use of immuno-PET and biodistribution experiments. When a 3-fold molar excess of Df-Bz-NCS was added to 2 mg 7D12, 0.2 Df-groups per Nanobody molecule were coupled. Subsequent labeling with freshly eluted and purified ^{68}Ga resulted in a radioactivity yield of 55-70% (not corrected for decay). Comparable results were shown with the reference compound ^{89}Zr-Df-Bz-NCS-7D12. Stability of both compounds was compared in a sodium acetate buffer, without Cl^--ions. The $^{68/67}Ga$-labeled Nanobody showed minimal release after 5 h (1.5 - 2.0%) in sodium acetate buffer at 4°C, but 6-7% of the ^{67}Ga was released after 24 h, whereas the ^{89}Zr-labeled Nanobody showed only 1% release after 24 h at 4°C. In human serum the radiochemical purity of both compounds was equal after 5 h incubation; however, the

percentage of dissociation of the radioisotope after 24 h in serum was more for the ^{67}Ga compound than for the ^{89}Zr compound (7-8% and 1-2 % respectively). In a mouse model both the ^{68}Ga radiolabeled and the ^{89}Zr radiolabeled Nanobody 7D12 were studied. High and selective tumor uptake was seen for both compounds. Significant higher uptake was seen in catabolic organs like, liver and spleen for the ^{68}Ga labeled 7D12. These data most probably reflect the slightly lower stability observed in the *in vitro* stability experiments. When outlining the second objective of this study, examining the anti-EGFR Nanobody 7D12 as imaging probe for immuno-PET, tumors were clearly visible with radiolabeled 7D12, and tumor-to-blood ratios were high (e.g., 25.7 for ^{68}Ga-7D12 and 42.4 for ^{89}Zr-7D12 at 3 h post injection) indicating that the anti-EGFR Nanobody might be a good imaging compound.

On the basis of aforementioned biodistribution data, there is no clear preference in the use of either ^{68}Ga or ^{89}Zr for clinical imaging with Nanobodies. Both radionuclides are nowadays commercially readily available. An advantage of using ^{89}Zr is that logistics of labeling, transportation and clinical handling are easier, due to its longer half-life. A disadvantage of ^{89}Zr might be the higher radiation burden to the patient, although this burden is expected to be lower than for ^{89}Zr-labeled intact mAbs as have extensively been used in clinical immuno-PET studies.

From the results obtained in chapter 2, 3 and 4 concerning the novel Df-Bz-NCS chelator, it can be concluded that this chelator is well suited for labeling of intact mAbs with ^{89}Zr, and for labeling of antibody fragments, like Nanobodies, with ^{89}Zr or ^{68}Ga for immuno-PET applications. The novel chelate is commercially available at Macrocyclics (www.macrocyclics.com) and can be produced in a GMP compliant way, on request. Also, in March 2012, the Fe-*N*-suc-Df-TFP-ester was added to the portfolio of ABX (www.ABX.de). With this recent input from ABX, a second chelator company showed their interest in ^{89}Zr chemistry. Furthermore, it also allows other laboratories or research groups to choose their desired labeling method. Till now the use of the procedure as described by Verel[15] was only reserved to research groups who synthesized this Fe-*N*-suc-Df-TFP ester themselves or when the ester was provided by our group. ^{89}Zr-immuno-PET imaging has now reached a matured stage, and allows global exploration.

Nanobodies are a promising novel class of antibody-based fragments for imaging. With their small molecular size, Nanobodies are fast penetrating agents allowing imaging within a few hours post injection. Therefore, Nanobodies can have great potential in tumor detection, confirmation of target expression, and selection of patients who have

the highest chance to benefit from mAb-therapy. Besides as a diagnostic tracer, another potnet application is the construction of multi-specific Nabododies by combining multiple Nanobody units within one molecule. In this way, Nanobodies targeting different receptors can be developed, and improvement in therapeutic effectiveness might be acchieved.

In **chapter 5** therapeutic applications of anti-EGFR Nanobodies were examined. To be more precise, a bi-paratopic (directed to two different epitopes on EGFR) Nanobody, called CONAN-1, was developed and characterized. In earlier studies, bi-valent Nanobodies directed against EGFR had showed their potency in a mouse model[17]. Hereto mice subcutaneously injected with 10^7 A431 cells one day before treatment, were treated twice weekly with three different bi-valent anti-EGFR Nanobody constructs for 4 weeks. Significant delay of A431 xenograft outgrowth was observed during treatment for all three Nanobody constructs compared to a control group. However, in this study no established xenografts were used and no comparison with cetuximab was made. In our study, as described in chapter 5, we hoped to improve the inhibitory effects of Nanobodies via the construction of bi-paratopic Nanobodies. To this end, we selected and constructed Nanobodies that could recognize domain III of EGFR, competing with EGF, and Nanobodies that could bind to another epitope on domain III inhibiting the dimerization of the receptor. Nanobody 7D12, the same Nanobody as described in chapter 4, was selected as the most potent Nanobody competing with EGF with an IC_{50} of 8 nM. The second selected Nanobody was 9G8 with an IC50 of 6-7 nM. After engineering these two Nanobodies *in vitro* tests were performed to select the most optimal construct. In these tests different linker lengths as well as the sequential order of the Nanobody units were examined. It turned out that 7D12-9G8 with a linker length of 10 amino acids was the optimal bi-paratopic Nanobody construct. 7D12-9G8 was more effective than 9G8-7D12 in inhibiting the phosphorylation of EGFR, and also in causing tumor cell growth inhibition in the proliferation assay. With respect to the different linker lengths for 7D12-9G8, linker lengths >10 amino acids showed less growth inhibition in the proliferation assay.

Because Nanobody 7D12-9G8 has a molecular weight of about 35 kDa, it is excreted very rapidly via the kidneys *in vivo*. To extend the half-life of the Nanobodies *in vivo,* binding to albumin has been reported as an excellent option[17-19]. Therefore, an anti-albumin Nanobody (called Alb1) was C-terminally fused to the bi-paratopic Nanobody. The thus constructed Nanobody, 7D12-9G8-Alb1 was studied in a mouse study and compared with the monoclonal antibody cetuximab (Erbitux®). Treatment of mice bearing A431 tumors with cetuximab resulted in tumor regression after 4 days till approximately day 14. Despite the fact that 7D12-9G8-Alb1 cannot interact with the immune system (like

intact mAbs can via their Fc part) its efficacy was largely similar to that of cetuximab. This is most probably due to the better tumor penetration of Nanobodies amidst the similar pharmacokinetics.

These data demonstrate the flexibility of Nanobody technology for the formation of constructs that show optimal binding characteristics even when several units are coupled to each other, like a bead chain. These findings encourage further exploration of the Nanobody toolbox, for the development of bi- and multi-specific Nanobodies, targeting two or more critical tumor targets. With respect to head and neck squamous cell carcinomas (HNSCC) overexpression of both EGFR and HGF/c-Met has been observed, while expression was correlated to bad prognosis[20]. Possible new Nanobody constructs may be bi-specific Nanobodies consisting of a unit targeting EGFR and another unit targeting c-Met or HGF (e.g., αEGFR-αc-Met-αAlb1 or αHGF-αEGFR-αAlb1).

In **chapter 6**, we described two monospecific Nanobodies (1E2 and 6E10) targeting HGF. Targeting the HGF/c-Met pathway is considered to be a promising approach for treatment of cancer. HGF is the only known ligand for c-Met. c-Met is overexpressed in various tumor types. Also in this study the earlier described method was used to elongate the half-life of these Nanobodies *in vivo*: genetic fusion of an anti-albumin Nanobody to the anti-HGF unit. Both anti-HGF Nanobodies were radiolabeled with ^{89}Zr via the novel method as developed and described in chapter 2 and 3, to enable accurate assessment of *in vivo* biodistribution. This can be achieved by taking biopsies as performed in this study, or alternatively by non-invasive PET imaging, as might been foreseen in future clinical trials. Biodistributions showed selective accumulation of both ^{89}Zr-labeled anti-HGF Nanobodies in mice bearing U87 MG xenografts. In addition, both αHGF-Nanobodies were able to inhibit tumor growth in the same mouse model, and upon treatment with 100 µg, three times a week up to 5 weeks, cures were observed in 4 of 6 mice with 1E2-Alb8 and in 3 of 6 mice with 6E10-Alb8.

On the basis of the achievements described above, we decided to use the remaining time to explore the potential of bi- and multi-specific Nanobodies for therapy. Blocking two or more critical tumor targets e.g., EGFR, HGF/c-Met, VEGF, IGF-1R, HER2, by one single Nanobody construct might give better therapeutic results. Our first attempt to test this hypothesis was with a bi-specific Nanobody targeting EGFR as well as IGF-1R. To this end, we developed and tested several Nanobody constructs. After *in vitro* evaluation, Nanobody 7D12 targeting EGFR and Nanobody 11C6 targeting IGF-1R were selected, and Nanobodies 7D12-11C6-Alb1, 7D12-7D12-Alb1 and 11C6-11C6-Alb1 were constructed. In a preclinical therapy study in nude mice bearing the head and neck xenograft FaDu the

bi-specific Nanobody 7D12-11C6-Alb1 was found to show a better efficacy than the mono-specific Nanobodies 7D12-7D12-Alb1, and 11C6-11C6-Alb1, see figure 1.

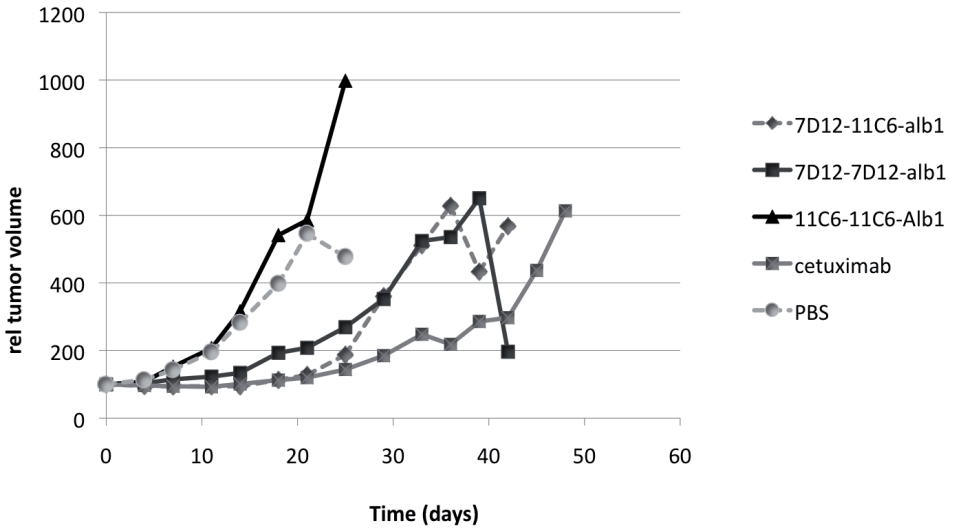

Figure 1. Therapy study with bi-specific Nanobody 7D12-11C6-Alb1, mono-specific Nanobodies 7D12-7D12-Alb1 and 11C6-11C6-Alb1 and cetuximab (αEGFR mAb) in nude mice bearing FaDu HNSCC xenografts. 7D12 is targeting EGFR, whereas 11C6 is targeting IGFR. Treatment was given 2 times a week: 330 µg Nanobody or 1000 µg mAb for 5 weeks. Treatment with bi-specific Nanobody 7D12-11C6-Alb1 caused significant tumor growth delay of the established tumors after day 5 ($P < 0.05$) that lasted till day 25 compared to the mono-specific Nanobodies and the control saline group. N=6 mice per group, SD bars are omitted for clarity.

Besides this, during the first 25 days after start of treatment 7D12-11C6-Alb1 caused the same tumor growth delay as cetuximab. Ultimately, after 25 days, tumors in the Nanobody treated mice group started to grow more rapidly than the tumors in the cetuximab group. This is most probably due to the fact that Nanobodies lack the Fc-region, and immune responses are absent. These first promising *in vivo* results, however, could not be confirmed in another tumor model. In nude mice bearing the human lung cancer xenograft line A549 no tumor growth delay was observed upon treatment with 7D12-11C6-Alb1. So, it can be concluded that the construction of multi-specific Nanobodies directed at different tumor targets is possible, though the first results are somewhat variable. EGFR is known to be a promising tumor target, but in several studies IGF-1R was reported not to be a promising target for therapy[21]. This might explain the observed poor tumor growth delay in our studies.

Notwithstanding the preliminary results with these bi-specific Nanobodies our

findings might very well be a prelude to further development of more promising bi-specific and multi-specific Nanobodies. As EGFR and HGF/c-Met are frequently overexpressed in tumors, HNSCC included, a promising candidate might be a Nanobody that targets both receptors, e.g., 7D12-1E2-Alb8. Furthermore, it is also known that VEGF is an important target in many carcinomas. VEGF is involved in angiogenesis, and blocking of this ligand causes tumor growth inhibition. It is already known that inhibition of EGFR with cetuximab results in anti-angiogenic effects like a decrease in VEGF synthesis[22]. VEGF expression was elevated in αEGFR-resistant colon cancer[22]. Therefore, bi-specific αEGFR-αVEGF Nanobodies might be an interesting combination. A potential advantage of using bi-specific Nanobodies for simultaneous blockade of a receptor and neutralization of a growth factor is that sterical aspects and therefore also Nanobody linker length might be less critical for optimal efficacy.

In conclusion: With the new Df-Bz-NCS chelate a less laborious procedure is available for assessment of tumor targeting using immuno-PET. Nanobodies showed their potential as fast and convenient diagnostic tools for assessment of target expression. In addition, Nanobodies might become successful agents in cancer therapy. Further improvement of multi-specific Nanobodies allows for multi-targeted therapies by targeting several tumor targets, blocking different critical signaling routes and improving therapy results.

References

1 Reichert JM. Monoclonal antibodies as innovative therapeutics. Curr. Pharm. Biotechnol. 2008; 9: 423-30.

2 Reichert JM, Valge-Archer VE. Development trends for monoclonal antibody cancer therapeutics. Nat. Rev. Drug Discov. 2007; 6: 349-56.

3 Scolnik PA. mAbs: a business perspective. MAbs. 2009; 1: 179-84.

4 Maggon K. Top Ten Monoclonal Antibodies. Knol 2012.

5 Olafsen T, Wu AM. Antibody vectors for imaging. Semin. Nucl. Med. 2010; 40: 167-81.

6 McCabe K, Wu AM. Positive progress in immunoPET - Not just a coincidence. Cancer Biother. Radiopharm. 2010; 25:253-81.

7 Tonra JR, Deevi DS, Corcoran E et al. Synergistic antitumor effects of combined epidermal growth factor receptor and vascular endothelial growth factor receptor-2 targeted therapy. Clin. Cancer Res. 2006; 12: 2197-207.

8 Goetsch L, Gonzalez A, Leger O et al. A recombinant humanized anti-insulin-like growth factor receptor type I antibody (h7C10) enhances the antitumor activity of vinorelbine and anti-epidermal growth factor receptor therapy against human cancer xenografts. Int. J. Cancer 2005; 113: 316-28.

9 Jung YD, Mansfield PF, Akagi M et al. Effects of combination anti-vascular endothelial growth factor receptor and anti-epidermal growth factor receptor therapies on the growth of gastric cancer in a nude mouse model. Eur. J. Cancer 2002; 38: 1133-40.

10 Shaheen RM, Ahmad SA, Liu W et al. Inhibited growth of colon cancer carcinomatosis by antibodies to vascular endothelial and epidermal growth factor receptors. Br. J. Cancer 2001; 85: 584-9.

11 Reid A, Vidal L, Shaw H, de Bono J. Dual inhibition of ErbB1 (EGFR/HER1) and ErbB2 (HER2/neu). Eur. J. Cancer 2007; 43: 481-9.

12 Larbouret C, Robert B, Navarro-Teulon I et al. In vivo therapeutic synergism of anti-epidermal growth factor receptor and anti-HER2 monoclonal antibodies against pancreatic carcinomas. Clin. Cancer Res. 2007; 13: 3356-62.

13 van der Veeken J, Oliveira S, Schiffelers RM, Storm G, van Bergen En Henegouwen PMP, Roovers RC. Crosstalk between epidermal growth factor receptor- and insulin-like growth factor-1 receptor signaling: implications for cancer therapy. Curr. Cancer Drug Targets. 2009; 9: 748-60.

14 Xu H, Stabile LP, Gubish CT, Gooding WE, Grandis JR, Siegfried JM. Dual blockade of EGFR and c-Met abrogates redundant signaling and proliferation in head and neck carcinoma cells. Clin. Cancer Res. 2011;17:4425-38.

15 Verel I, Visser GWM, Boellaard R, Stigter-van Walsum M, Snow GB, van Dongen GAMS. ^{89}Zr immuno-PET: comprehensive procedures for the production of 89Zr-labeled monoclonal antibodies. J. Nucl. Med. 2003; 44: 1271-81.

16 Heuveling DA, Visser GWM, Baclayon M et al. ^{89}Zr-nanocolloidal albumin-based PET/CT lymphoscintigraphy for sentinel node detection in head and neck cancer: preclinical results. J. Nucl. Med. 2011; 52: 1580-4.

17 Roovers RC, Laeremans T, Huang L et al. Efficient inhibition of EGFR signaling and of tumour growth by antagonistic anti-EGFR Nanobodies. Cancer Immunol. Immunother. 2007; 56: 303-17.

18 Dennis MS, Zhang M, Meng YG et al. Albumin binding as a general strategy for improving the pharmacokinetics of proteins. J. Biol. Chem. 2002; 277: 35035-43.

19 Tijink BM, Laeremans T, Budde M et al. Improved tumor targeting of anti-epidermal growth factor receptor Nanobodies through albumin binding: taking advantage of modular Nanobody technology. Mol. Cancer Ther. 2008; 7: 2288-97.

20 Knowles LM, Stabile LP, Egloff AM et al. HGF and c-Met participate in paracrine tumorigenic pathways in head and neck squamous cell cancer. Clin. Cancer Res. 2009; 15: 3740-50.

21 Pollak M. The insulin and insulin-like growth factor receptor family in neoplasia: an update. Nat. Rev. Cancer 2012; 12: 159-69.

22 Bianco R, Rosa R, Damiano V et al. Vascular endothelial growth factor receptor-1 contributes to resistance to anti-epidermal growth factor receptor drugs in human cancer cells. Clin. Cancer Res. 2008; 14: 5069-80.

Hoofdstuk 8:

Nanobody constructen, voor het blokkeren van groeifactoren en hun receptoren: mogelijke toepassing in PET imaging en kankertherapie

Nederlandse samenvatting

Nederlandse Samenvatting

Therapeutische monoklonale antilichamen (mAbs) staan op dit moment erg in de belangstelling. Zo wordt er veel onderzoek gedaan naar hun mogelijke toepassingen zowel in de diagnostiek als bij de behandeling van kanker. Meer dan 100 mAbs en mAb-fragmenten worden er op dit moment klinisch getest. Tot op heden zijn er 30 mAbs goedgekeurd door de "US Food and Drugs Administration" (FDA), waarvan de meeste voor de systemische behandeling van kanker[1-3]. Ondanks de economische crisis groeide de jaarlijkse verkoop van mAbs in 2010 tot 48 miljard dollar[4]. De omzet van de mAbs die in 2010 in de top 5 stonden bedroeg meer dan 5 miljard dollar[1].

Helaas is de effectiviteit van de huidige mAbs vaak nogal beperkt en heeft slechts een klein gedeelte van de patiënten die mAbs krijgen baat bij deze behandeling. Idealiter zouden al tijdens een vroege fase van ontwikkeling de beste medicijnen geselecteerd moeten worden en snel duidelijk zou moeten zijn welke patiëntengroepen waarschijnlijk het meeste baat zullen hebben van de behandeling met het medicijn. Moleculaire beeldvorming kan hieraan een bijdrage leveren. Een veelbelovende techniek is positron emissie tomografie (PET) waarbij kwantitatieve moleculaire beeldvorming van het gehele lichaam mogelijk is. PET kan een bijdrage leveren bij de selectie van patiëntengroepen, het bepalen van de targetexpressie in de tumor, en het bepalen van de optimale dosis (om bijwerkingen beperkt te houden). De laatste jaren is gebleken dat PET scans met behulp van mAbs (immuno-PET) een toegevoegde waarde hebben tijdens verschillende fasen van mAb-ontwikkeling en klinische toepassingen. Naast intacte mAbs staan ook mAb-fragmenten (zoals Nanobodies) en derde generatie mAb-achtige verbindingen in de belangstelling. Immuno-PET kan een cruciale rol spelen tijdens de vroege fase van ontwikkeling van deze medicijnen.

Er bestaan twee manieren om de ontwikkeling van therapie met intacte mAbs met behulp van immuno-PET te ondersteunen. Bij de eerste methode wordt er een snelklarend radioactief gelabeld mAb-fragment toegediend en een PET scan gemaakt op dezelfde dag. Op deze manier wordt het snel duidelijk of het mAb kan binden aan de tumor en is de stralingsbelasting voor de patiënt gering, zeker als het gebruikte radionuclide een korte halveringstijd heeft (tussen 1-5 uur) zoals bijvoorbeeld het geval is bij gallium-68 (^{68}Ga, halveringstijd ($t_{½}$)= 1.13 uur)[5,6]. Bij de tweede methode wordt het therapeutische mAb zelf radioactief gelabeld en wordt er een PET scan gemaakt voor aanvang van de therapie (scouting procedure) of kort nadat de behandeling gestart is. Op deze manier kan er beter gekeken worden hoe het mAb zich gedraagt en hoe de biodistributie is bij

de individuele patiënt. Bij deze laatste toepassing wordt het therapeutische mAb gelabeld met een langlevend PET isotoop zoals zirconium-89 (^{89}Zr, $t_{½}$=78.4 uur) of jodium-124 (^{124}I, $t_{½}$=100.3 uur) en worden de patiënten gescand net voor of tijdens hun behandeling met het therapeutische mAb.

Recent is vastgesteld dat het selectief blokkeren/uitschakelen van één tumortarget waarschijnlijk niet voldoende is om een optimaal therapeutisch effect te bereiken. Tumorcellen kunnen namelijk voor hun snelle groei en overleving gebruik maken van meerdere groeifactoren of groeireceptor-systemen. Dit betekent dat als er één systeem wordt uitgeschakeld een ander groeireceptor-systeem de groei en overleving kan overnemen. Daarom wordt er op dit moment ook veel onderzoek gedaan naar mAb-therapie waarbij zgn. bispecifieke mAbs en tyrosine kinase remmers worden gebruikt die twee tumortargets gelijktijdig kunnen blokkeren, bijv. EGFR, HER2, IGF-1R, VEGF of VEGF-R2[7-14]. Nanobody technologie kan nog geschikter blijken voor het blokkeren/uitschakelen van groeifactor (receptor) systemen. Nanobodies zijn namelijk kleiner dan traditionele intacte mAbs en kunnen daarom beter in de tumor doordringen. Daarnaast is het met behulp van de Nanobody technologie relatief eenvoudig om bispecifieke of multispecifieke Nanobody constructen te maken die meerdere tumortargets tegelijk kunnen blokkeren. Immuno-PET kan een grote bijdrage leveren bij de preklinische en klinische evaluatie van deze nieuwe mAb-fragmenten.

In **hoofdstuk 1** werd de huidige en de toekomstige rol van immuno-PET beschreven. Ook werd er een nieuwe klasse mAb-fragmenten geïntroduceerd: Nanobodies. Met het introduceren van Nanobodies wordt er wellicht een nieuwe wereld geopend in de ontwikkeling van nieuwe antikanker medicijnen en voor het vaststellen van tumortarget-expressie. Er werden tevens in dit hoofdstuk verschillende tumortargets beschreven waarvan bekend is dat ze veelal opgereguleerd en/of geactiveerd zijn bij kanker.

In **hoofdstuk 2** werd het nieuwe p-isothiocyanatobenzyl-desferal (Df-Bz-NCS) geïntroduceerd. Met behulp van dit nieuwe bifunctionele Df-Bz-NCS chelaat kan de positron emitter ^{89}Zr in twee stappen aan een mAb gekoppeld worden. Ter vergelijking, in de oude procedure vergt de synthese van de tetrafluorfenyl ester van gesuccinyleerd Fe-desferrioxamine B (N-suc-Df-Fe-TFP) drie stappen, waarna nog drie stappen nodig zijn om ^{89}Zr aan een mAb te koppelen[15]. In beide methoden wordt het Df-chelaat in ongeveer 50 min geconjugeerd aan de lysines van een mAb. Een belangrijk verschil is echter dat met de nieuwe conjugatieprocedure geen tweede stap nodig is waarin bij een lage pH (pH 4.5) het Fe verwijderd wordt. Door het vermijden van deze stap bij lage pH kunnen ook pH-gevoelige eiwitten succesvol geconjugeerd worden zoals recent is beschreven voor ^{89}Zr-

Nanocolloidaal albumine[16]. Door het weglaten van deze stap wordt de totale procedure ook nog versneld met zo'n 40 minuten. In de nieuwe procedure zoals in dit proefschrift beschreven werd de conjugatie uitgevoerd met een drievoudige molaire overmaat van Df-Dz-NCS chelaat wat resulteerde in een chelaat:mAb ratio van 1.5:1. Met dit conjugaat was de ^{89}Zr-koppeling na 30 minuten bij kamertemperatuur met een pH tussen 6-8 en 7.2 bijna kwantitatief. Na zuivering over een PD-10 kolom bleek het geproduceerde ^{89}Zr-Df-Bz-NCS-mAb conjugaat optimaal, het was radiochemisch zuiver, en de integriteit en immunoreactiviteit van het mAb waren behouden gebleven. Een punt van aandacht was het toevoegen van het Df-Bz-NCS aan de mAb-oplossing. Het Df-Bz-NCS was opgelost in DMSO en als dit in één keer zonder mengen toegevoegd werd aan de mAb-oplossing ontstonden er precipitaties en aggregaten. Daarom wordt dringend aangeraden het Df-Bz-NCS stapsgewijs toe te voegen aan de mAb-oplossing. Het tweede punt dat aandacht vraagt is de stabiliteit van het radioactief gelabelde mAb tijdens het bewaren. Het gebruik van Cl^- bevattende buffers moet vermeden worden omdat deze er voor zorgen dat het ^{89}Zr kan loslaten van het mAb. Dit komt omdat er t.g.v. stralingsschade hypochloriet gevormd wordt. Dit hypochloriet reageert specifiek met het bis-thiourea gedeelte van het nieuwe chelaat. Daarom wordt er aangeraden om een 0.25 M natrium acetaat buffer te gebruiken bij het bewaren van het radioactief gelabelde mAb. Het nieuwe Df-Bz-NCS chelaat werd uitgebreid vergeleken met het oude N-suc-Df chelaat. In diverse biodistributie- en PET-studies werden hoge en selectieve tumoropnames met beide mAb conjugaten gevonden. Er werden geen significante verschillen gemeten tussen beide mAb conjugaten.

In **hoofdstuk 3** werd een protocol geschreven om andere onderzoeksgroepen en farmaceutische bedrijven een eenvoudige en gemakkelijke methode te geven voor de koppeling van ^{89}Zr aan mAbs of mAb-fragmenten via het nieuwe Df-Bz-NCS chelaat. In dit protocol wordt ook gewezen op de kritische stappen in deze methode.

Voor het imagen van mAb-fragmenten (zoals Nanobodies) is ^{89}Zr niet strikt noodzakelijk omdat de biologische halveringstijd van een Nanobody ($t_{½}$ = 1-3 uur) niet echt een langlevend isotoop als ^{89}Zr nodig heeft ($t_{½}$ = 78.4 uur). Een mogelijk alternatief PET isotoop zou ^{68}Ga kunnen zijn, dat een $t_{½}$ van 1.16 uur heeft. In **hoofdstuk 4** werd een koppelingsmethode van ^{68}Ga via het nieuwe Df-Bz-NCS chelaat beschreven. Heel belangrijk bij deze koppeling is het gebruik van ultra zuivere HCl om het natuurlijke Ga (^{nat}Ga) en de hoeveelheden Al, Fe en Zr zo laag mogelijk te houden. Deze metalen competeren namelijk sterk voor de complexatie met het Df-chelaat. Verder zijn ook de zuivering en het verkleinen van het ^{68}Ga-generator eluaatvolume van belang. Door gebruik te maken van een anion-uitwisselingskolom werden de ongewenste metalen verwijderd en werd

het volume van de ^{68}Ga-oplossing geminimaliseerd. Het koppelen van ^{68}Ga vond plaats bij kamertemperatuur gedurende 5 minuten met een pH die lag tussen 5.0-6.5. Toen deze koppelingsreactie eenmaal opgezet was, werd eerst onderzocht of het nieuwe Df-Bz-NCS chelaat het meest geschikte chelaat is voor het stabiel koppelen van ^{68}Ga aan mAbs en Nanobodies. Vervolgens werd het in vivo gedrag van het volgens deze methode gelabelde ^{68}Ga-Nanobody 7D12 geëvalueerd door middel van immuno-PET en biodistributie studies. Door het toevoegen van een drievoudige molaire hoeveelheid Df-Bz-NCS aan 2 mg 7D12 konden 0.2 Df-groepen per Nanobody molecuul gekoppeld worden. De daarop volgende koppeling met vers geëlueerd en gezuiverd ^{68}Ga leverde 50-70% radioactiviteitopbrengst op (niet gecorrigeerd voor verval). Vergelijkbare resultaten werden verkregen met de referentieverbinding ^{89}Zr-Df-Bz-NCS-7D12. De stabiliteit van beide verbindingen werd vergeleken in een natrium acetaat buffer, zonder Cl^--ionen. Het $^{68/67}$Ga gekoppelde product bleef 5 uur stabiel na productie (1.5-2.0% vrij $^{68/67}$Ga) in natrium acetaat bij 4˚C, maar na 24 uur was 6-7% van het ^{67}Ga vrij. De referentieverbinding met ^{89}Zr bleek maar 1% vrij ^{89}Zr te bevatten na 24 uur bij 4˚C. Na 5 uur incubatie in humaan serum was de radiochemische zuiverheid nagenoeg gelijk voor beide producten, maar ook hier was na 24 uur het ^{89}Zr-gelabelde Nanobody stabieler dan het ^{67}Ga-gelabelde Nanobody (1-2% vrij ^{89}Zr en 7-8% vrij ^{67}Ga). Bij evaluatie van het ^{68}Ga-gelabelde en het ^{89}Zr-gelabelde Nanobody 7D12 in een muizenmodel werd een hoge en selectieve tumoropname waargenomen voor beide producten. Significant hogere opname van het ^{68}Ga-Nanobody werd gezien in de katabole organen zoals de lever en milt. Deze data weerspiegelen de stabiliteitsverschillen die waren gevonden bij de *in vitro* experimenten. Met betrekking tot het onderzoeken of het anti-EGFR Nanobody 7D12 gebruikt kan worden voor immuno-PET, kunnen we zeggen dat alle tumoren duidelijk zichtbaar werden gemaakt door het radioactief gelabelde 7D12. Daarnaast waren de tumor tot bloed ratio's hoog (bijv. 25.7 voor ^{68}Ga-7D12 en 42.4 voor ^{89}Zr-7D12 op 3 uur na injectie). Dit geeft aan dat het anti-EGFR Nanobody mogelijkerwijs goed gebruikt kan worden voor immuno-PET.

Op basis van de hiervoor beschreven biodistributiegegevens kan niet gezegd worden welk radioisotoop het meest geschikt is voor klinische immuno-PET met Nanobodies. Beide radionucliden zijn tegenwoordig commercieel verkrijgbaar. Een voordeel bij het gebruik van het langlevende ^{89}Zr is de gemakkelijkere logistiek bij het transport en bij klinische handelingen. Het kan echter zijn dat de stralingsbelasting voor de patiënt iets hoger is in het geval van ^{89}Zr en dit zou een nadeel betekenen. Toch zal deze stralingsbelasting naar verwachting beduidend lager zijn dan de stralingsbelasting met ^{89}Zr gelabelde intacte mAbs, die nu al veelvuldig in de kliniek gebruikt worden.

De in hoofdstuk 2, 3 en 4 beschreven resultaten geven aan dat het nieuwe chelaat zeer geschikt is voor het koppelen van ^{89}Zr aan intacte mAbs en voor het koppelen van ^{89}Zr of ^{68}Ga aan mAb-fragmenten zoals Nanobodies voor immuno-PET toepassingen. Het nieuwe chelaat is commercieel verkrijgbaar bij Macrocyclics (www.macrocyclics.com) en kan op verzoek geproduceerd worden onder GMP condities. Door eerder genoemde ontwikkelingen toonde een tweede chelaatbedrijf interesse in de ^{89}Zr chemie. In maart 2012 werd de Fe-N-suc-Df-TFP-ester toegevoegd aan het portfolio van ABX (www.ABX.de). Hierdoor kunnen andere laboratoria of researchgroepen kiezen van welke koppelingsmethode zij gebruik willen maken. Tot op heden was voor andere researchgroepen alleen de procedure Verel[15] toepasbaar, als ze zelf de Fe-N-suc-Df-TFP ester synthetiseerden of als de ester door ons verstrekt werd. ^{89}Zr-immuno-PET is nu klaar voor wereldwijde toepassingen.

Nanobodies zijn een interessante nieuwe klasse van mAb-fragmenten voor imaging. Omdat Nanobodies tamelijk klein zijn, kunnen ze zich snel in het lichaam verplaatsen waardoor er al binnen enkele uren na injectie een scan gemaakt kan worden. Daarom lijken Nanobodies zeer geschikt voor snelle tumordetectie, het bevestigen van target expressie en voor de selectie van patienten die mogelijk baat hebben bij een bepaalde mAb-therapie. Naast toepassing als diagnostische tracer, bestaat ook de mogelijkheid meerdere Nanobody-units te combineren tot één nieuw molecuul. Aldus zouden Nanobodies geconstrueerd worden die in staat zouden zijn om meer dan één receptor pathway te blokkeren en zodoende therapeutische effecten kunnen verbeteren.

In **hoofdstuk 5** werden de therapeutische toepassingen van anti-EGFR Nanobodies onderzocht. Een biparatopisch (gericht tegen twee verschillende epitopen op EGFR) Nanobody, genaamd CONAN-1, werd ontwikkeld en gekarakteriseerd. In eerdere studies hadden bivalente Nanobodies gericht tegen EGFR in een muizenmodel hun effectiviteit laten zien[17]. Hierbij werden muizen, die kort daarvoor subcutaan waren ingespoten met 10^7 A431 cellen, twee keer per week behandeld met drie verschillende bivalente anti-EGFR Nanobody-constructen gedurende 4 weken. Hierbij gaven de drie Nanobody-constructen een significante vertraging van xenograft groei, dit in vergelijking met de controle groep. In deze studie werd echter geen gebruik gemaakt van reeds uitgegroeide tumoren (xenografts) en ook werden de geteste Nanobodies niet vergeleken met cetuximab. In onze studie, zoals beschreven in hoofdstuk 5, hoopten we het remmende effect op tumorgroei te verbeteren door gebruik te maken van biparatopische Nanobodies. We selecteerden en construeerden Nanobodies die kunnen binden aan domein III van EGFR en competeren

met EGF, en Nanobodies die kunnen binden aan een ander epitoop op domein III om dimerisatie van de receptor te blokkeren. Nanobody 7D12, ook al gebruikt in hoofdstuk 4, werd geselecteerd als het meest potente Nanobody dat kan competeren met EGF met een IC_{50}-waarde van 8 nM. 9G8 was het andere Nanobody dat geselecteerd werd met een IC_{50}-waarde van 6-7 nM. Na de productie van deze twee Nanobodies werden diverse *in vitro* testen uitgevoerd om het optimale construct te selecteren. Zo werden er verschillende linkerlengtes getest alsmede de volgorde van de Nanobody-units. 7D12-9G8 met een linkerlengte van 10 aminozuren bleek het meest optimale biparatopische Nanobody-construct. 7D12-9G8 was effectiever dan 9G8-7D12 in het remmen van de fosforylering van EGFR en ook in tumorcelgroeiremming. Bij een linkerlengte >10 aminozuren werd minder groeiremming waargenomen.

Omdat Nanobody 7D12-9G8 slechts een moleculair gewicht van 35 kDa heeft wordt het *in vivo* snel via de nieren uitgescheiden. Er is in de literatuur beschreven dat door binding aan albumine de in vivo verblijftijd van de Nanobodies verlengd kan worden[17-19]. Om die reden werd een anti-albumine Nanobody (genaamd Alb1) C-terminaal gefuseerd aan het biparatopische Nanobody. Het verkregen construct, 7D12-9G8-Alb1, werd vervolgens bestudeerd in een muizenstudie en vergeleken met het mAb cetuximab (Erbitux®). De behandeling van A431 tumordragende muizen met cetuximab gaf tumorregressie van dag 4 tot ongeveer dag 14 na de start van behandeling. Ondanks het feit dat 7D12-9G8-Alb1 niet het immuunsysteem kan activeren (zoals intacte mAbs dat wel kunnen via hun Fc gedeelte) was de effectiviteit gelijk aan cetuximab. Dit komt waarschijnlijk omdat Nanobodies beter in de tumor kunnen binnendringen, ondanks hun vergelijkbare farmacokinetiek.

Deze gegevens demonstreren de grote flexibiliteit van de Nanobody-technologie bij het maken van constructen met optimale bindingskarakteristieken, zelfs als er meerdere units aan elkaar gekoppeld worden. Deze bevindingen zijn bemoedigend voor verder onderzoek naar de mogelijkheden van Nanobodies, bijvoorbeeld voor het ontwikkelen van bi- en multispecifieke Nanobodies die twee of meerdere kritische targets kunnen blokkeren. Zo zouden voor de behandeling van plaveiselcelcarcinoom in het hoofd-halsgebied nieuwe bispecifieke Nanobodies interessant kunnen zijn, die zowel EGFR als c-Met of HGF kunnen blokkeren (bijv. aEGFR-ac-Met-aAlb1 of aHGF-aEGFR-aAlb1). Het is namelijk bekend dat zowel EGFR als HGF/c-Met tot overexpressie komen in dit tumortype, en dat overexpressie gecorreleerd is aan een slechte prognose[20].

In **hoofdstuk 6** beschreven we twee monospecifieke Nanobodies (1E2 en 6E10) die aan HGF kunnen binden. Het blokkeren van de HGF/c-Met signaleringsroute wordt als een belangrijke veelbelovende benadering beschouwd voor de behandeling van kanker. HGF is het enige bekende ligand voor c-Met. c-Met komt tot overexpressie in veel verschillende tumortypes. Ook in deze studie hebben we gebruik gemaakt van eerder genoemde methodes om de *in vivo* verblijftijd van de Nanobodies te verlengen: het genetisch fuseren van een anti-albumine Nanobody aan het anti-HGF Nanobody. Aan beide anti-HGF Nanobodies werd ^{89}Zr gekoppeld met behulp van de nieuwe methode zoals ontwikkeld en beschreven in hoofdstuk 2 en 3, om accurate biodistributiegegevens te verkrijgen. In deze studie werd dat gedaan door middel van het nemen van biopten, maar een goed alternatief zou non-invasieve immuno-PET kunnen zijn, wat eventueel gebruikt zou kunnen worden in toekomstige klinische studies. De biodistributiestudie liet selectieve ophoping van beide ^{89}Zr-gelabelde anti-HGF Nanobodies zien in muizen met U87 MG tumoren. Ook bleken beide anti-HGF Nanobodies in staat om tumorgroei te remmen in hetzelfde muizenmodel. Bij de behandeling met 100 µg, drie keer per week gedurende vijf weken, werden curaties waargenomen in 4 van de 6 muizen die behandeld waren met 1E2-Alb8 en in 3 van de 6 muizen die behandeld waren met 6E10-Alb8.

Op basis van bovengenoemde resultaten besloten we de resterende promotieperiode extra inzicht te verwerven in de mogelijkheden van bi- en multispecieke Nanobodies voor therapie. Het blokkeren van twee of meerdere kritische tumortargets zoals EGFR, HGF/c-Met, VEGF, IGF-1R en HER2 door één Nanobody-construct zou wellicht veel betere therapeutische resultaten kunnen opleveren. Onze eerste poging om deze hypothese te testen was met een bispecifiek Nanobody dat zowel EGFR als IGF-1R kan blokkeren. Na in vitro evaluatie werden Nanobody 7D12 (gericht tegen EGFR) en Nanobody 11C6 (gericht tegen IGF-1R) geselecteerd en de Nanobodies 7D12-11C6-Alb1, 7D12-7D12-Alb1 en 11C6-11C6-Alb1 geproduceerd. Een preklinische therapie studie in muizen met de hoofd-hals plaveiselcelcarcinoom xenograft FaDu liet zien dat het bispecifieke Nanobody 7D12-11C6-Alb1 beter in staat is tumorgroei te remmen dan de monospecifieke Nanobodies 7D12-7D12-Alb1 en 11C6-11C6-Alb1, zie Figuur 1.

Ook was de tumorgroei gedurende de eerste 25 dagen na de start van de behandeling gelijk voor 7D12-11C6-Alb1 en cetuximab. Uiteindelijk groeiden de tumoren in de met Nanobody behandelde muizen na 25 dagen sneller dan de tumoren in de cetuximab groep. Dit kan worden verklaard door de afwezigheid van een Fc-gedeelte bij de Nanobodies waardoor immuunresponses afwezig blijven. Deze eerste veelbelovende *in*

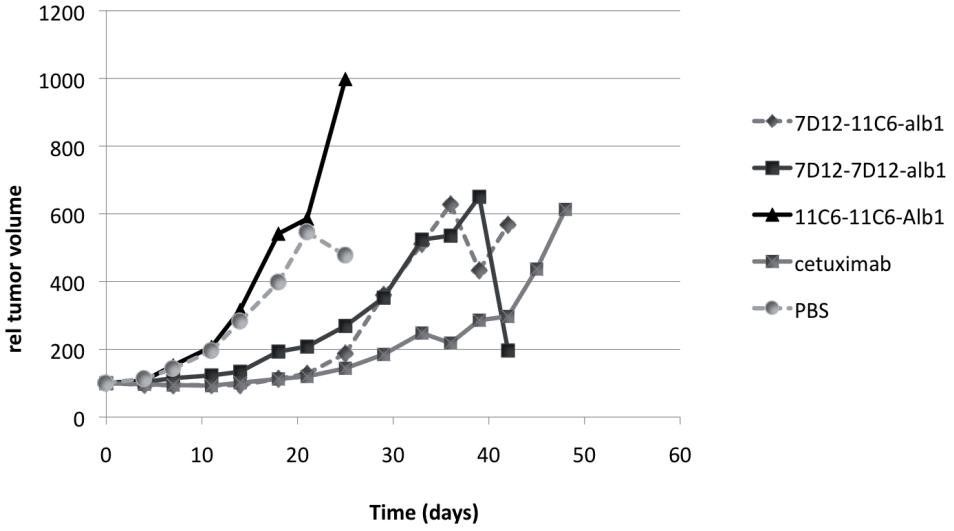

Figuur 1. Therapiestudie met het bispecifieke Nanobody 7D12-11C6-Alb1, monospecifieke Nanobodies 7D12-7D12-Alb1 en 11C6-11C6-Alb1 en cetuximab (aEGFR mAb) in muizen met de hoofd-hals plaveiselcelcarcinoom xenograft FaDu. 7D12 is gericht tegen EGFR en 11C6 tegen IGF-1R. Behandeling werd twee keer per week gegeven: 330 µg Nanobody of 1000 µg mAb gedurende 5 weken. Behandeling met het bispecifieke Nanobody 7D12-11C6-Alb1 gaf significant betere tumorgroeiremming ($p<0.05$) tussen dag 5 en dag 25 na de start van behandeling, dit ten opzichte van de monospecifieke Nanobodies en de controle groep. N=6 muizen per groep, standaarddeviaties zijn voor de duidelijkheid uit de grafiek weggelaten.

vivo resultaten konden helaas niet bevestigd worden in een tweede tumormodel. In muizen met de longkanker xenograftlijn A549 werd geen tumorgroeiremming waargenomen met 7D12-11C6-Alb1. Er kan dus geconcludeerd worden dat we in staat zijn om multispecifieke Nanobodies, gericht tegen verschillende tumortargets te construeren, maar dat de eerste resultaten nog variabel zijn. Een verklaring voor de tegenvallende tumorgroeiremming zou kunnen zijn dat de gekozen combinatie (anti-EGFR x anti-IGF-1R) niet de meest optimale was. EGFR is gebleken een goed tumortarget te zijn, maar een recente andere studie[21] toonde aan dat IGF-1R wellicht niet het meest veelbelovende target is.

Wij zijn van mening dat bovenvermelde eerste resultaten met nieuwe bispecifieke Nanobodies een gerede aanleiding vormen om andere veelbelovende bispecifieke en multispecifieke Nanobodies te gaan ontwikkelen. Het is bijvoorbeeld bekend dat zowel EGFR als HGF/c-Met vaak tot overexpressie komen in tumoren, waaronder hoofd-hals plaveiselcelcarcinoom. Bispecifieke Nanobodies die beide receptoren blokkeren zouden zeer waardevol kunnen zijn, bijvoorbeeld 7D12-1E2-Alb8. Verder is het ook bekend

dat VEGF een belangrijk target is voor verschillende carcinomen. VEGF is betrokken bij de bloedvatvorming (angiogenese) van tumoren, en door dit ligand te blokkeren kan tumorgroeiremming optreden. Het is al bekend dat door het blokkeren van EGFR met cetuximab er anti-angiogenese effecten optreden, zoals het verlagen van de VEGF expressie[22]. Daarom zou een bispecifiek aEGFR-aVEGF Nanobody een interessante combinatie kunnen zijn. Een potentieel voordeel bij het gebruik van bispecifieke Nanobodies voor het gelijktijdig blokkeren van een receptor en het neutraliseren van een groeifactor is dat sterische hindering minder kritisch wordt voor effectiviteit, en daarmee ook de linkerlengte tussen de Nanobody-units.

Concluderend: met het nieuwe Df-Bz-NCS chelaat is er een procedure ontwikkeld die minder bewerkelijk is waardoor het bepalen van tumortargeting met behulp van immuno-PET eenvoudiger wordt. Nanobodies hebben zich bewezen als snelle en gemakkelijke diagnostische moleculen om targetexpressie te bepalen. Daarnaast zouden Nanobodies ook succesvol kunnen worden in kankertherapie. Verdere verbetering van multispecifieke Nanobodies kan leiden tot het blokkeren van meerdere tumortargets, het blokkeren van verschillende kritische routes en het effectiever maken van therapieën.

Curriculum Vitae

Maria Vosjan werd geboren op 18 juni 1977 in Ommen. Na het behalen van het MAVO-diploma aan de Groen van Prinsterer MAVO in Ommen in 1989, werd aan het Drenthe College in Emmen het middelbaar laboratorium diploma behaald, waarna een studie medisch laboratorium onderwijs, afstudeerrichting medische biochemie aan de hogeschool Enschede werd gevolgd. De afstudeeropdracht werd uitgevoerd bij de afdeling KNO Tumorbiologie aan de Vrije Universiteit Medisch Centrum in Amsterdam onder begeleiding van prof. dr. R.H. Brakenhoff en dr. B.J.M. Braakhuis. Er werd onderzoek gedaan naar moleculaire genetische markers in metastasen van hoofd-hals kanker patiënten. In september 2000 werd het diploma behaald waarna de auteur aansluitend startte als research analist bij deze afdeling onder begeleiding van prof. dr. G.A.M.S. van Dongen. In november 2001 werd zij senior research analist in dezelfde onderzoeksgroep. In mei 2008 werd begonnen met het promotieonderzoek bij dezelfde onderzoeksgroep (prof. dr. G.A.M.S. van Dongen) en in samenwerking met de afdeling Nucleaire Geneeskunde & PET research van het VU Medisch Centrum (dr. G.W.M. Visser) en de afdeling celbiologie van de Universiteit Utrecht, (dr. P.M.P. van Bergen en Henegouwen en dr. R.C. Roovers), waarvan de onderzoeksresultaten staan beschreven in dit proefschrift en werden gepresenteerd op diverse internationale wetenschappelijke congressen. Sinds mei 2012 is ze werkzaam als Radionuclide Project Manager bij BV Cyclotron VU in Amsterdam.

Publications

Vosjan MJWD, Vercammen J, Kolkman JA, Stigter-van Walsum M, Revets H, van Dongen GAMS. Nanobodies targeting the hepatocyte growth factor: potential new drugs for molecular cancer therapy. Mol. Cancer Ther. 2012 Apr;11(4):1017-25.

Rizvi SN, Visser OJ, **Vosjan MJWD,** van Lingen A, Hoekstra OS, Zijlstra JM, Huijgens PC, van Dongen GAMS, Lubberink M. Biodistribution, radiation dosimetry and scouting of (90)Y-ibritumomab tiuxetan therapy in patients with relapsed B-cell non-Hodgkin's lymphoma using (89)Zr-ibritumomab tiuxetan and PET. Eur J Nucl Med Mol Imaging. 2012 Mar;39(3):512-20.

Roovers RC, **Vosjan MJWD**, Laeremans T, El Khoulati R, de Bruin RC, Ferguson KM, Verkleij AJ, van Dongen GAMS, van Bergen En Henegouwen PMP. A biparatopic anti-EGFR nanobody efficiently inhibits solid tumour growth. Int J Cancer. 2011 Oct 15;129(8):2013-24.

Vosjan MJWD, Perk LR, Roovers RC, Visser GW, Stigter-van Walsum M, van Bergen En Henegouwen PM, van Dongen GA. Facile labelling of an anti-epidermal growth factor receptor Nanobody with (68)Ga via a novel bifunctional desferal chelate for immuno-PET. Eur J Nucl Med Mol Imaging. 2011 Apr;38(4):753-63.

van Dongen GAMS, **Vosjan MJWD**. Immuno-positron emission tomography: shedding light on clinical antibody therapy. Cancer Biother Radiopharm. 2010;25(4):375-85.

Vosjan MJWD, Perk LR, Visser GWM, Budde M, Jurek P, Kiefer GE, van Dongen GAMS. Conjugation and radiolabeling of monoclonal antibodies with zirconium-89 for PET imaging using the bifunctional chelate p-isothiocyanatobenzyl-desferrioxamine.Nat Protoc. 2010;5(4):739-43.

Perk LR, **Vosjan MJWD**, Visser GWM, Budde M, Jurek P, Kiefer GE, van Dongen GAMS. p-Isothiocyanatobenzyl-desferrioxamine: a new bifunctional chelate for facile radiolabeling of monoclonal antibodies with zirconium-89 for immuno-PET imaging. Eur J Nucl Med Mol Imaging. 2010;37(2):250-9.

Perk LR, Stigter-van Walsum M, Visser GW, Kloet RW, **Vosjan MJWD,** Leemans CR, Giaccone G, Albano R, Comoglio PM, van Dongen GAMS. Quantitative PET imaging of Met-

expressing human cancer xenografts with (89)Zr-labelled monoclonal antibody DN30.Eur J Nucl Med Mol Imaging. 2008; 35:1857-1867.

Perk LR, Visser OJ, Stigter-van Walsum M, **Vosjan MJWD**, Visser GW, Zijlstra JM, Huijgens PC, van Dongen GAMS.Preparation and evaluation of (89)Zr-Zevalin for monitoring of (90) Y-Zevalin biodistribution with positron emission tomography.Eur J Nucl Med Mol Imaging. 2006;33(11):1337-45.

Börjesson PK, Jauw YW, Boellaard R, de Bree R, Comans EF, Roos JC, Castelijns JA, **Vosjan MJWD,** Kummer JA, Leemans CR, Lammertsma AA, van Dongen GAMS. Performance of immuno-positron emission tomography with zirconium-89-labeled chimeric monoclonal antibody U36 in the detection of lymph node metastases in head and neck cancer patients. Clin Cancer Res. 2006;12(7 Pt 1):2133-40.

Perk LR, Visser GW,M **Vosjan MJWD**, Stigter-van Walsum M, Tijink BM, Leemans CR, van Dongen GAMS. (89)Zr as a PET surrogate radioisotope for scouting biodistribution of the therapeutic radiometals (90)Y and (177)Lu in tumor-bearing nude mice after coupling to the internalizing antibody cetuximab. J Nucl Med. 2005;46(11):1898-906.

Verel I, Visser GWM, **Vosjan MJWD**, Finn R, Boellaard R, van Dongen GAMS. High-quality 124I-labelled monoclonal antibodies for use as PET scouting agents prior to 131I-radioimmunotherapy. Eur J Nucl Med Mol Imaging. 2004;31(12):1645-52.

Verel I, Visser GW, Boerman OC, van Eerd JE, Finn R, Boellaard R, **Vosjan MJWD**, Stigter-van Walsum M, Snow GB, van Dongen GAMS. Long-lived positron emitters zirconium-89 and iodine-124 for scouting of therapeutic radioimmunoconjugates with PET. Cancer Biother Radiopharm. 2003;18(4):655-61.

Cruz I, Snijders PJ, Van Houten V, **Vosjan MJWD**, Van der Waal I, Meijer CJ. Specific p53 immunostaining patterns are associated with smoking habits in patients with oral squamous cell carcinomas. J Clin Pathol. 2002;55(11):834-40.

Tabor MP, van Houten VM, Kummer JA, **Vosjan MJWD**, Vlasblom R, Snow GB, Leemans CR, Braakhuis BJ, Brakenhoff RH. Discordance of genetic alterations between primary head and neck tumors and corresponding metastases associated with mutational status of the TP53 gene. Genes Chromosomes Cancer. 2002;33(2):168-77.

Dankwoord

Mijn 4 jaar promotieonderzoek zit erop. Het is onmogelijk om al het onderzoek helemaal alleen te doen. Daarom wil ik proberen in dit dankwoord iedereen te bedanken die een bijdrage heeft geleverd aan het tot stand komen van dit boekje.

Allereerst wil ik mijn promotor prof. G.A.M.S. van Dongen bedanken. Beste Guus, dank voor het gestelde vertrouwen in mij. Je hebt het aangedurfd om mij als HLO-er promotieonderzoek te laten doen. Ik ben je heel dankbaar dat je me deze kans hebt gegeven. Onder jouw vleugels durfde ik het wel aan. Ik bewonder jouw optimisme en doorzettingsvermogen. En ik ben je dankbaar voor alles wat je me geleerd hebt. Je stond altijd voor me klaar en ik zal altijd met veel plezier terug denken aan de periode dat ik in jouw groep mocht werken.
Daarnaast ben ik dank verschuldigd aan mijn copromoteren, dr. G.W.M. Visser en dr. P.M.P. van Bergen en Henegouwen. Beste Gerard, ook jou ken ik al heel wat jaren. Ik wil je hartelijk bedanken voor jouw chemische hulp, vooral bij het tot stand komen van de 1e hoofdstukken in mijn boekje was jouw hulp erg gewenst. Het is gelukt, het nieuwe NCS-Df chelaat is er! Ook jouw hulp bij het schrijven, ook al waren het vaak lange sessies, is van grote waarde gebleken. Beste Paul, dank je wel voor je hulp en input in het slagen van dit STW-project. Jouw enthousiasme over Nanobodies werkt aanstekelijk.

De leden van de promotiecommissie, prof. dr. H. Revets, prof. dr. O. Boerman, prof. dr. P.H. Elsinga, prof. dr. H.M.W. Verheul, dr. N.H. Hendrikse en dr. D. Vugts wil ik hartelijk danken voor het kritisch doornemen van het manuscript en voor het zitting nemen in de promotiecommissie.

In dit dankwoord kunnen mijn collega's niet ontbreken. Het zijn er nogal wat en ik hoop dat ik niemand vergeet te bedanken. Als eerste wil ik Marijke Stigter-van Walsum bedanken. Lieve Marijke, je bent 7 jaar lang mijn 'roomie' geweest. Toen ik naar de AIO-kamer verhuisde spraken we elkaar niet meer dagelijks, maar vaak troffen we elkaar wel weer op een lab en konden we gezellig bijkletsen. Ook de bezoekjes aan Gouda waren erg gezellig. Dank voor alle hulp met de muizenstudies, in het bijzonder hulde voor alle proeven die ik precies zo wist te plannen dat jij met kerst moest werken om mijn experimenten af te maken. Zonder jouw input waren het behoorlijk lastige proeven geworden. Ik ben heel blij dat je mijn paranimf wilt zijn.

Ook wil ik iedereen van 'Groep Guus' bedanken voor hun support; Marianne, Annelies, Inge, Cindy, Ara, Kevin en Marije, dank voor jullie hulp op het lab. Het werk in de 'RNC-bunker' werd een stuk gezelliger met jullie op het lab. Dank voor het helpen met alle labelingen. Danielle en Alex, jullie chemische kennis heb ik zeer kunnen waarderen ook heb ik uiteindelijk veel opgestoken van jullie 'kippengaas' presentaties. Heel fijn om kennis te mogen delen met jullie. Ik hoop dat we in de toekomst nog blijven samenwerken, en dat ook ons kookclubje (met Hester) voort blijft bestaan.

Dr. B.J.M. Braakhuis en prof. dr. R.H. Brakenhoff, ook jullie wil ik hartelijk bedanken. Beste Boudewijn en Ruud, jullie stonden in 2000 aan de basis van mijn wetenschappelijke carrière. Bij jullie is het allemaal begonnen; waar een stage al niet toe kan leiden. Bedankt voor jullie input tijdens mijn promotietijd. Altijd mocht ik jullie mening vragen over mijn onderzoek en kon ik in discussie gaan over de verkregen resultaten. Ook zal ik onze lunchgesprekken niet snel vergeten. Ik weet ondertussen alles van verkeersboetes, auto's, Digitenne, de financiële crisis en (klus)huisjes in Frankrijk.

Collega-AIO's, Peggy, Lisa, Sanne, Marlon, Géke, Derrek, Ruth, Anne-Marie, Michelle, Sara en Annette. Ik ben de 1^{e} van ons die het boekje af heeft, maar het is een goed vooruitzicht dat er nog meer boekjes volgen. Ik heb in veel verschillende samenstellingen in PK2Y036 gezeten, maar Derrek, de enige man in dit rijtje, met jou heb ik de meeste tijd doorgebracht. Je zorgde altijd voor een vrolijke noot op de kamer en samen hebben we elkaar regelmatig gemotiveerd en bekritiseerd. Ben blij dat ik jou heb leren kennen. Voor iedereen, succes met het afronden van jullie onderzoek; ik zie uit naar jullie promotie(s)(feesten).

Alle overige collega's van KNO Tumorbiologie wil ik natuurlijk niet vergeten. Marijke B, Arjen, Thijs, Michiel en Remco, bedankt voor de gezellige tijd (lees; koekjes!) en de nuttige discussies. Ook Fred, Hanneke en Ton wil ik bedanken voor hun hulp. Daarnaast wil ik mijn enige student Robin bedanken voor zijn inzet en enthousiasme. Heel veel succes met het afronden van je studie en het vinden van een leuk AIO-project.

Alle collega's van het RNC wil ik bedanken voor hun support. In het bijzonder de instrumentatiedienst onder leiding van Leo van Rooij ben ik heel veel dank verschuldigd. Ik dacht af en toe dat jullie wegdoken als ik weer eens in de werkplaats verscheen. Maar jullie waren altijd bereid om me uit de brand te helpen. Beste Arjan, heel veel dank voor de hulp bij het automatiseren van de ^{89}Zr-producties. Beste Peter, heel veel dank voor het

ontwerpen en uitvoeren van het ^{68}Ga-automaat.

De stralingsveiligheidsdienst; Tjaard, Jan en Marcel, jullie wil ik bedanken voor al jullie hulp. Hoe vaak jullie voor mij naar de kluis zijn gelopen om een potje ^{89}Zr, ^{131}I, ^{124}I, ^{67}Ga of ^{59}Fe te halen weet ik niet meer. Greet, ik zal het “wij gaan koffie drinken” missen!

Op het RNC zijn ook nog een aantal collega AIO’s bezig met de laatste loodjes, Hans B, Joost, Pieter succes! Ik wacht met smart jullie (te) chemische boekjes af en zie uit naar jullie promoties. Ook wens ik de ‘nieuwe’ AIO’s; Dion, Bieneke, Berend en Paul veel succes.

Van de oud-collega’s die ik nog niet genoemd heb omdat ze al geruime tijd weg zijn, wil ik er hier zeker nog een aantal noemen. Lieve Hester, je bent een heel bijzondere oud-collega. Ten eerste omdat je verre familie van me bent, maar ook omdat ik met jou altijd kan lachen, praten of huilen. Samen naar het theater, Lowlands of gewoon gezellig thee of wijn drinken en met de mannen Catannen. Ik vind het daarom ook heel fijn dat jij mijn paranimf wilt zijn.
Beste Lars, onze samenwerking, die begon in 2003, is nooit helemaal gestopt en gaat nu weer in volle vaart verder bij BV Cyclotron VU. Ik ben blij je te kennen en hoop dat onze hernieuwde samenwerking (weer) vruchtbaar zal zijn. Beste Serge, ook jou ken ik al heel wat jaartjes, je bent namelijk altijd ongemerkt mijn ’grote voorbeeld’ geweest. Ik hoop dat we elkaar nog regelmatig blijven ontmoeten. Ook Janny, Jantien, Tieneke, Frederieke, Pontus en Bernard wil ik bedanken voor de interesse in mijn onderzoek, en de gezellige ‘ik-kom-even-aanwaaien’ -bezoekjes.

Dit STW-project werd uitgevoerd in samenwerking met de Nanobody-groep van dr. P.M.P. van Bergen en Henegouwen uit Utrecht. Dank aan alle mensen op het lab en in het bijzonder aan dr. R.C. Roovers. Beste Rob, jouw enthousiasme voor Nanobodies heeft mij mede doen beslissen in dit project te stappen. Jouw manier van werken enthousiasmeert. Je was nooit te beroerd om ’s avonds laat als koerier naar de Poortstraat te gaan om weer een pakketje nieuwe Nanobodies af te geven. Ik heb veel van je geleerd. Ook Rachid heel veel dank voor het produceren en testen van de Nanobodies. Nooit te beroerd om je handen uit je mouwen te steken als ik weer eens vroeg of je misschien nog 10 mg Nanobody voor mij kon maken.

Verder wil ik mijn vrienden bedanken; H1m-united! (ik heb het T-shirt uit 1997 nog steeds!). Als 2e van ons klasje uit Enschede ga ik ook promoveren. Ik hoop jullie allemaal te zien op mijn promotie(feestje).
Mireille, mijn snookermaatje. Aan het einde van de werkdag moest ik vaak even stoom afblazen. Dat kon op dinsdagavond samen met jou bij 'Final Touch'. Vaak heb jij klaagzangen of euforische momenten van me moeten aanhoren. Jij kon meestal alles weer relativeren en daarna maakten we er een gezellige snookeravond van. Je had me alleen wel wat vaker mogen laten winnen!

Mijn familie; Bert-Jan, Thea, Martijn, Judica, Edwin, Eduard, Bineke, Wolter, Tryntsje, Engbert, Annelies, Wouter, Ilse, Deborah, Rosan, Tamar, Linda, Mike, Sanne, Beppe, Oma Vos, ooms en tantes, hier is het boekje waar ik de afgelopen 4 jaar aan gewerkt heb. Ik hoop dat jullie er wat van snappen. Dank voor al jullie support en interesse in mijn onderzoek. Speciale dank voor Mike. Beste Mike, bedankt voor het maken van de plaatjes in mijn introductie en het ontwerpen van de voorkant van dit boekje, het is heel mooi geworden.
Lieve pa en ma, ik weet dat jullie trots op me zijn. En ik ben trots op jullie. Van jullie heb ik geleerd om in mezelf te blijven geloven en vooral niet op te geven als je iets wilt bereiken. Het is gelukt, mijn boekje is er. Ik proost vandaag op jullie gezondheid!

Tot slot, Sebastiaan. Lieve Bas, die anderhalf jaar dat jij in Groningen zat kwam ik erachter dat ik écht niet zonder jou kan. Het gaf me wel de mogelijkheid om lekker door te werken aan mijn boekje, mede daardoor is het boekje dus ook op tijd klaar. We gaan samen weer verder waar we gebleven waren. Dikke kus!

Amsterdam, November 2012

Maria Vosjan